Simulation Study of MU-MIMO for 5G-NR Millimeter-Wave Networks in ns-3

Felix Kloer

Bachelor Thesis

August 5, 2024

Examiners

Prof. Dr.-Ing. Marina Petrova
Dr. Ljiljana Simić

Supervisors

Prof. Dr.-Ing. Marina Petrova
Aron Schott, M.Sc
Aleksandar Ichkov, M.Sc.

Institute for Networked Systems
RWTH Aachen University

communicated by Prof. Dr.-Ing. Marina Petrova

The present work was submitted to the Institute for Networked Systems

Simulation Study of MU-MIMO for 5G-NR Millimeter-Wave Networks in ns-3

Bachelor Thesis

presented by
Felix Kloer

Prof. Dr.-Ing. Marina Petrova
Dr. Ljiljana Simić

Aachen, August 5, 2024

(Felix Kloer)

Acknowledgements

I would like to express my sincere gratitude to Prof. Dr.-Ing. Marina Petrova and Dr. Ljiljana Simić for providing me with the opportunity to work on this thesis and gain insights into the research at iNets. I am especially thankful to my supervisors, Aron Schott and Aleksandar Ichkov, for their unwavering support and profound knowledge of the topic. Their assistance allowed me to better understand identify and resolve problems throughout this thesis. Additionally, I would like to acknowledge the iNets staff for their efforts in providing access to the necessary computational resources.

Finally, I want to thank my family and friends for their unwavering support throughout the writing of this thesis.

Contents

ABSTRACT

To achieve the targeted data rates of several Gbps in the fifth generation of cellular networks (5G), the utilization of millimeter-wave frequencies between 24 and 71 GHz is essential due to the vast amount of unused bandwidth available in this range. However, these frequencies have challenging propagation characteristics, which necessitate directional communication to maintain robust connections. This is accomplished through beamforming with antenna arrays, which focus transmission energy into narrow beams. To ensure consistently high link quality, these beams must be precisely aligned, a process managed by continuous monitoring and transmission of control signals, known as beam management. Additionally, beams introduce space as a new dimension for transmissions, allowing multiple beams to be sent simultaneously to a single user, significantly enhancing data throughput.

In this thesis, a framework implementing realistic beam management and single-user multiple input, multiple output (SU-MIMO) capabilities for multi-user 5G-NR non-standalone millimeter-wave network simulations is presented. A comprehensive simulation study is conducted to analyze the end-to-end network performance of a 5G-NR millimeter-wave network using different SU-MIMO configurations with realistic beam management strategies, both for single and multiple users.

It has been shown that SU-MIMO significantly enhances throughput, particularly when requested data rates exceed the limits of single-stream transmissions. In highly loaded multi-user environments, SU-MIMO effectively mitigates congestion by enabling dual-stream transmissions, thereby boosting the overall data rate capacity of gNBs.

Keywords: 5G-NR, millimeter-waves, beam management, SU-MIMO, ns-3

1

INTRODUCTION

Mobile networks are crucial in today's interconnected world, enabling seamless communication and access to information anytime and anywhere. The next generation of mobile networks, 5G, promises to revolutionize our lives with its capabilities. Offering peak data rates of several Gbps and ensuring ultra-low latency of 1 ms, 5G aims to support a wide range of applications, from enhanced mobile broadband to the internet of things (IoT) and autonomous vehicles [1]. To achieve these ambitious goals, several key technologies are essential. One critical advancement is the use of millimeter-waves, which is pivotal in meeting the high data rate requirements. Because of this, 5G-NR includes a new frequency range for transmissions, spanning from 24 GHz to 71 GHz. This high-frequency range provides access to a vast amount of unused bandwidth, crucial for enabling the high data rates that 5G promises. However, millimeter-wave propagation faces challenges such as higher susceptibility to atmospheric absorption, blockage by obstacles, and limited range compared to lower frequency bands. To counter these challenges, transmission energy must be focused into narrow beams using beamforming techniques. This is achieved through antenna arrays, which can dynamically adjust the direction of the beams to maintain a strong and reliable connection. Beamforming enhances signal strength and coverage, but it requires precise alignment between the transmitter and receiver. Thus this approach not only compensates for the propagation losses of millimeter-waves but also introduces new challenges in maintaining optimal connectivity. Effective beam management is crucial for the success of 5G networks when using millimeter-waves. Beam management involves the continuous transmission and monitoring of physical control signals to maintain optimal beam alignment between the transmitter and receiver. This process, while essential for sustaining high-quality connections, consumes network resources and impacts overall performance. Additionally, the use of beams introduces space as a new dimension for communication. This allows multiple beams to be transmitted simultaneously to a user equipment (UE), significantly enhancing throughput. The ability to use multiple beams is particularly important for meeting the high data rate demands of modern applications, ensuring that 5G can deliver on its promise of unprecedented broadband.

This thesis aims to study the end-to-end network performance of a 5G millimeter-wave network of different SU-MIMO configurations when realistic beam management strategies are used. The objective was to evaluate how these technologies impact network throughput, signal-to-interference-plus-noise ratio (SINR), and overall performance in both single-user and multi-user scenarios. To simulate a network with realistic beam management and SU-MIMO configurations the 3GPP-compliant CTTC NR module [2] was extended. The simulation setup was designed to mimic a realistic urban environment. The area east of the main train station in Frankfurt am Main was chosen as the simulation environment. Realistic user walk paths were generated using the commercial pedestrian flow simulator *Viswalk*. The in the CTTC NR module incorporated statistical 3rd Generation Partnership Project (3GPP) compliant channel model was used to simulate the network. The study compared two SU-MIMO configurations, port and polarization, against a reference scenario with no SU-MIMO, and evaluated the performance under two beam management strategies.

The remainder of this thesis is organized as follows: Chapter 2 provides context, reviews existing literature, and clarifies key concepts related to millimeter-wave propagation and 5G-NR. Chapter 3 offers a detailed description of the ns-3 framework and explains the modifications made to include SU-MIMO and realistic beam management. Chapter 4 outlines the statistical channel model employed, the simulation setup, the different SU-MIMO configurations, the different beam management strategies, and the simulation scenarios used in the study. In Chapter 5, the results obtained from the simulations are evaluated and analysed. Finally, Chapter 6 presents the conclusions and offers suggestions for future work.

2

BACKGROUND

This chapter provides the theoretical and conceptual foundations necessary for understanding the topics discussed in this thesis. It begins by exploring the vision and challenges of 5G technology. Section 2.2 delves into various aspects of millimeter-wave propagation, including bandwidth, free-space path loss, atmospheric attenuation, and shadow fading. Following this, Section 2.3 discusses directional communication, focusing on key technologies such as beamforming, spatial multiplexing, and massive MIMO, along with the different MIMO architectures. Section 2.4 covers the critical topic of beam management, detailing the measurement signals required and the frameworks used for 5G beam management. The chapter also touches on network simulation tools and modules in Section 2.5, with a specific focus on ns-3, and the CTTC NR module. Finally, Section 2.6 reviews related work, situating this thesis within the broader context of current research and technological developments.

2.1 5G VISION AND CHALLENGES

Approximately every decade, mobile communication technology undergoes wide-ranging changes, increasing its performance and paving the way for new advancements. The 5G is set to meet the growing global demand for mobile data, which is predicted to reach 5 zettabytes per month by 2030 [3]. Additionally, 5G is expected to support a diverse range of innovative use cases, which can be categorized into three major groups:

- **enhanced mobile broadband (eMBB)**: This includes the services that are already implemented in 4G, with several improvements. Namely, seamless coverage over wide areas, support of high user density in hot spots and a generally very high traffic capacity [4].

- **ultra-reliable and low latency communications (URLLC)**: Some services require exceptionally reliable and low-latency connections. For instance, next generation vehicle-to-everything (V2X) communication involves the exchange of sensor data between vehicles, demanding a 3 millisecond end-to-end latency and high reliability, as noted by the authors of [5].

- **massive machine type communication (mMTC)**: This category is for use cases with a large number of connected devices, each emitting relatively small amounts of non-delay-sensitive data. Applications include machine-to-machine communication and smart cities [4].

Due to the ambiguity of the application scenarios, each subgroup requires a different key capability from the network: high data rate for eMBB, high connection density

Description	Minimum Requirement in 5G	
Peak Data Rate	DL: 20 Gbps	UL: 10 Gbps
User Plane Latency	1 ms for URLCC	4 ms for eMBB
Connection Density	1.000.000 devices/km^2	

TABLE 2.1: Some Minimum Technical Requirements of 5G by IMT 2020 [1].

for mMTC and high reliability combined with low latency for URLLC. Consequently, the minimum technical performance requirements for 5G, issued by the International Telecommunication Union (ITU), are very challenging. A few exemplary performance parameters are provided in Table 2.1. To achieve these targets, 5G must utilize several key technologies. Two of the most critical are millimeter-wave bands and massive multiple input multiple output (MIMO) antenna arrays, which are further explored in the following sections.

2.2 MILLIMETER-WAVE PROPAGATION

2.2.1 *Bandwidth*

Millimeter-wave frequencies, lying between 30 and 300 GHz, have mostly been left untouched by the previous mobile network generations. For that reason, there is a large amount of unused and continuous bandwidth available in the millimeter-wave spectrum, which could be the key contribution to achieve a peak data rate of multiple gigabits per second. The theoretical upper bound of the information rate in an additive white Gaussian noise channel is given by the Shannon-Hartley theorem:

$$C = B \cdot \ln(1 + \frac{S}{NB}), \tag{2.1}$$

where B represents the bandwidth, S the signal strength, and N the noise and interference power. The capacity of a channel can be linearly increased with the bandwidth, provided the signal power grows proportionally. However, there are practical limits to how much the signal strength can realistically be increased. Raising the transmit power results in higher power consumption, which is only feasible up to a certain degree [6]. To use this bandwidth, 5G-NR envisions the use of a novel millimeter-wave frequency range, known as frequency range 2 (FR2), which comprises frequencies from 24.25 Ghz to 71.0 Ghz, as specified in the latest release of the respective technical specification by the 3GPP [7]. The other frequency range, frequency range 1 (FR1), stretches from 410 MHz to 7125 MHz. Millimeter-wave frequencies were overlooked in past mobile networks due to the technical challenges they present, including free space path loss, atmospheric loss, shadow fading, penetration loss and reflection loss.

2.2.2 Free-Space Path Loss

Free-space propagation models predict the average received signal strength at a given distance when the transmitter and receiver have a clear, unobstructed line-of-sight path. One such model is the Friis free space equation [8]:

$$P_r = \frac{P_t G_t G_r \lambda^2}{(4\pi)^2 d^2}, \tag{2.2}$$

where P_t and P_r represent the transmitted and received power, G_t and G_r the transmitter and receiver antenna gain, λ the wavelength and d the distance between transmitter and receiver. The path loss is given by the difference between the transmitted power and the received power in dB. It represents the attenuation of the power with distance and is caused by the decreasing power density due to the conservation of energy [9]:

$$PL_{dB} = 10 \cdot \log(\frac{P_t}{P_r}) \tag{2.3}$$

$$= -10 \cdot \log(\frac{G_t G_r \lambda^2}{(4\pi d)^2}). \tag{2.4}$$

If constant antenna gains for the transmitter and receiver are assumed, the order of the path loss function in dB is given by $\mathcal{O}(PL_{dB}) = 20 \cdot \log(\frac{d}{\lambda})$. By decreasing the wavelength to millimeter frequencies, the path loss increases with the square of the frequency, which negatively affects the received signal quality.

2.2.3 Atmospheric Attenuation

In reality, a signal does not travel in a vacuum, as assumed in the free-space path model. Electromagnetic waves interact with various particles along their propagation path, resulting in energy loss due to absorption or scattering. The three most significant attenuation factors due to these interactions are caused by rain, fog and atmospheric gases [10]. In the cases of fog and rain, the absorption and scattering are caused by water droplets of various sizes within the propagation path. Fig. 2.1 depicts the attenuation at different rainfall levels over varying frequencies. It is evident that rainfall has a much bigger impact on the signal strength of higher frequencies. The traditionally used sub-6 GHz frequency range experiences attenuation levels of just under 1 dB/km for a rainfall rate of 100 mm/hr, while millimeter-wave frequencies experience attenuation of around 30 dB/km for the same rainfall rate. Even without considering weather phenomena, signal degradation still occurs due to atmospheric gases. Fig. 2.2 illustrates atmospheric gas attenuation over varying frequencies. Notably, some peaks in attenuation levels, reaching over 10 dB/km, can be found around the frequencies of 60 GHz and 180 GHz. Atmospheric gas attenuation for frequencies below 20 GHz are almost negligible.

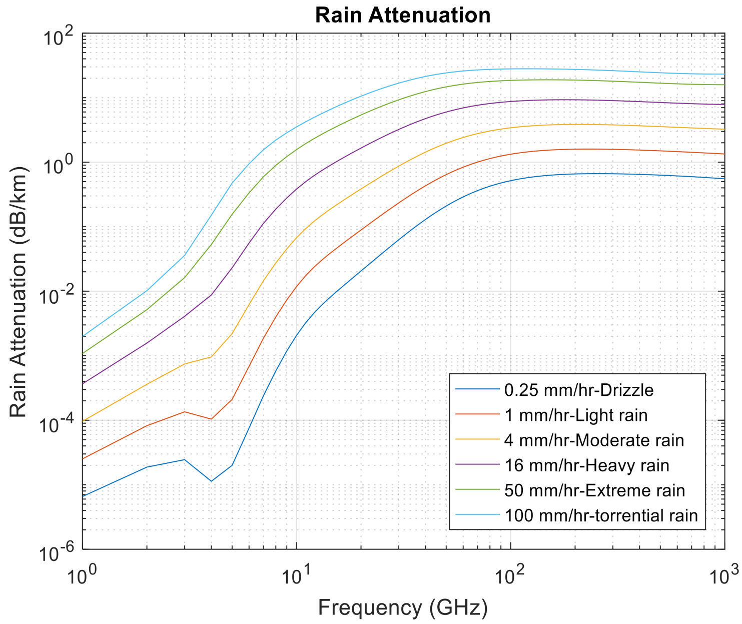

FIGURE 2.1: Rain attenuation in dB/km over the frequency in GHz at different rainfall levels [10].

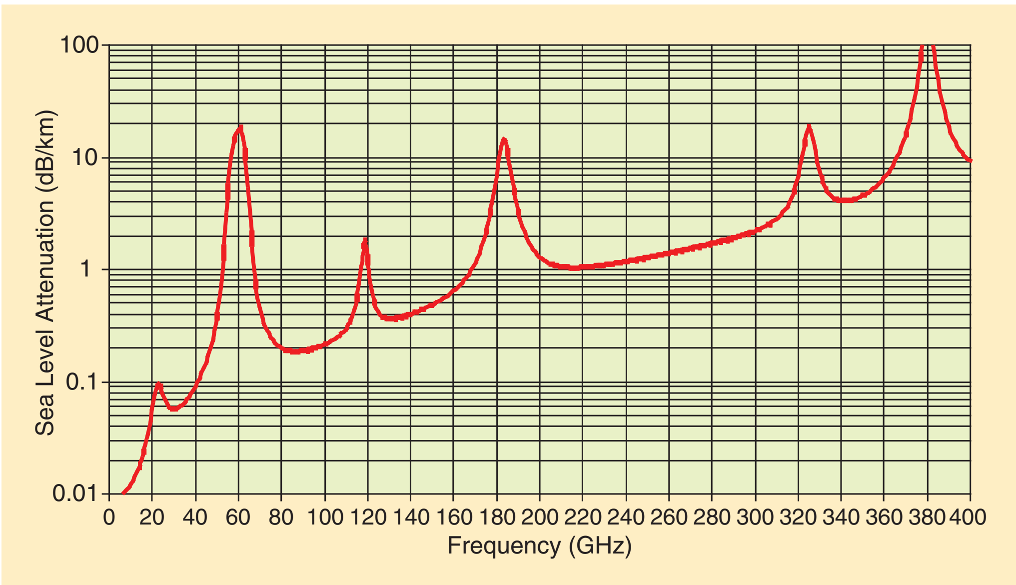

FIGURE 2.2: Atmospheric attenuation at sea level in dB/km over the frequency in GHz [11].

2.2.4 *Shadow Fading*

Shadowing describes the large-scale variation of a signal caused by obstacles of various forms between the receiver and the transmitter. These objects can absorb, reflect, scatter or diffract electromagnetic waves, thereby weakening the signal strength at the receiver. For an object to cause this type of blockage, its size needs to be larger than the wavelength, preventing the electromagnetic wave from diffracting around it [12]. By definition, millimeter-waves have a smaller wavelength than sub-6 GHz frequencies, making them more susceptible to shadowing by smaller objects, including humans. In an indoor environment, blockage by a human can deteriorate the link by 20-30 dB when using a frequency of 60 GHz [13]. Even holding a mobile phone while browsing or calling can cause significant shadowing effects. The attenuation can reach up to 22 dB and 60 dB at 28 Ghz and 60 GHz, respectively [14].

2.3 DIRECTIONAL COMMUNICATION

The previous section highlighted the major challenges associated with millimeter-wave propagation without exploring potential solutions. This section will address those solutions.

The attenuation triggered by environmental factors does not pose a significant challenge if the cell sizes are kept small. The authors in [15] remark that cell sizes in urban environments are of the order of 200 m. At this distances, atmospheric and rain attenuation is almost negligible. Additionally, 5G envisions network densification to distribute user plane traffic across multiple cells in dense urban environments, further reducing cell sizes [4]. In this case, the strong attenuation with distance of millimeter-waves could even be beneficial in reducing inter-cell interference. The attenuation caused by atmospheric gases peaks only at certain frequencies. As stated by the authors of [11], there is still large potential bandwidth available in between those peaks that can be used for millimeter-wave communication systems. One solution to leverage the bandwidth opportunities of millimeter-waves without increasing the power consumption, while also addressing the attenuation problems caused by shadowing or free-path propagation, is to use directional communication.

2.3.1 *Beamforming*

Traditionally, in mobile cellular networks, a signal is transmitted omnidirectionally from the base station. This method has the advantage of requiring no knowledge about the receiver's position and no directional adjustments between transmissions. However, this approach is not suitable for millimeter-wave transmission due to the harsher propagation environment. In omnidirectional transmissions, the energy is dispersed equally over the entire spatial domain. As the signal travels further, the energy density decreases because the emitted energy is constant while the area over which it is distributed increases. Since the receiver occupies only a fraction of the emitter's angular space, only a small portion of the emitted energy is eventually received. A natural solution would be to increase the signal power to maintain a similar signal to noise ratio (SNR) with millimeter-waves. However, this is not feasible due to regulatory limitations and higher power consumption. The key to resolving this problem is to use directional antennas. The idea is to maximise the antenna gain (G_t and G_r in 2.3) by focusing the transmit energy into the angular range where the receiver resides. This approach allows for achieving a sufficient SNR without increasing the transmit power, thus countering the propagation disadvantages of millimeter-waves [16]. One method to achieve beamforming is to use antenna arrays composed of multiple antenna elements to direct and shape the signal through spatial filtering. The vector sum of the fields radiated by these antenna elements forms the output spatial power distribution, which exhibits constructive interference in some directions and destructive interference in others. The directions of the constructive and destructive interference is controlled by the array geometry and amplitude/phase shifts applied to the antenna elements [17].

2.3.2 *Spatial Multiplexing*

Space is now usable for data transmission as a new dimension due to beamforming. With this capability, a single UE can be served with several streams simultaneously, a technique known as SU-MIMO. Additionally, the use of this spatial dimension enables multi-user multiple input, multiple output (MU-MIMO), providing a new method for multiple access where data streams can be transmitted to multiple UEs simultaneously. The idea behind spatial multiplexing (SM) is to transmit more than one data stream using multiple antennas, each having a separate radio chain, on the same time-frequency resource to a single UE. Multiple antennas at the receiver side and signal processing make it possible to suppress the interference between different spatial streams and reconstruct the data streams by utilizing the multipath scattering in the channel [18]. This method increases the communication system's throughput. SM is referred to as single-user multiple input, multiple output because it is enabled by multiple transmit and receive antennas with separate radio chains [19] [20]. To realize spatial division multiple-access (SDMA), a base station needs to transmit data streams to different UEs in the same time-frequency resource. If the principle of SU-MIMO is used, each UE needs to have knowledge about all current transmissions to suppress the interference of the other data streams [19]. To avoid this, spatial multiplexing can be combined with beamforming. If the different signal streams are spatially separated through beamforming, their interference at the devices is minimized, and no knowledge about the other transmissions is required to reconstruct the data.

2.3.3 *Massive MIMO*

The size of an antenna element is proportional to the wavelength of the transmitted waveform. Therefore, if millimeter-wave frequencies are used instead of the traditional sub-6 GHz frequencies, a higher antenna element density is achievable within the same antenna array footprint [17]. In theory, this enables the use of antenna arrays with hundreds of antennas, known as massive MIMO antenna arrays. 5G-NR envisions the use of massive MIMO at the base stations (where sufficient resources are available), with antenna arrays consisting of 256 and up to 1024 individual antenna elements for the millimeter bands [4]. The large amount of antenna elements allows for focusing energy with extreme precision into smaller regions of the angular space, resulting in improved radiated energy efficiency. Additionally, spatial multiplexing capabilities are enhanced, leading to higher capacity. This comes at a cost of increased complexity and higher energy consumption for signal processing.

2.3.4 MIMO Architectures

The previous sections outlined the advantages of using multiple antennas (MIMO systems) in a radio communication network. Array gain can be achieved through beamforming and a higher data rate can be achieved through spatial multiplexing. However, both techniques have drastically different requirements for the antenna architecture. This section will present the trade-offs between the different architectures.

1. **Fully Analog Architecture:**

   In the analog architecture, shown in Fig. 2.3, analog signal processing is used to perform the spatial filtering. A single digital base band signal is converted to an analogue signal by a digital-to-analog converter (DAC) and then upconverted to the carrier frequency. Afterwards, amplitude and phase shifts are applied for each antenna element. The advantages of analog beamforming include low cost and low power consumption, as only one radio frequency (RF) chain, analog-to-digital converter (ADC) and DAC are used. A major drawback is that only one beam can be used at a time, which prohibits spatial multiplexing [17]. UEs in close proximity can be served with the same beam via orthogonal frequency division multiple-access (OFDMA). However, UEs that require different spatial beams need to utilize time division multiple-access (TDMA).

2. **Fully Digital Architecture:**

   In the digital architecture, displayed in Fig. 2.4, each antenna element has its own RF chain, ADC and DAC. This allows each antenna element to emit a different signal, not just in terms of phase and amplitude. Several data streams can be digitally processed before multiple DACs convert specific digital signals into analog ones, forming multiple beams. This makes the technology viable for MU-MIMO, as the number of data streams equal to the number of RF chains can be transmitted in parallel to spatially separated UEs. The trade-off is higher complexity and significantly higher power consumption [17].

3. **Hybrid Architecture:**

   The hybrid architecture aims to combine the advantages of digital and analog architectures. The antenna elements are divided into subarrays, with each subarray having a dedicated RF chain, ADC and DAC. This approach limits power consumption and complexity while still allowing multiple beams to be formed.

2.4 BEAM MANAGEMENT

In contrast to omnidirectional communication, directional communication requires knowledge about the location of both the transmitter and receiver to establish and maintain a connection. This necessitates procedures to determine the directional information for transmitting and receiving antennas to form their beams correctly. The

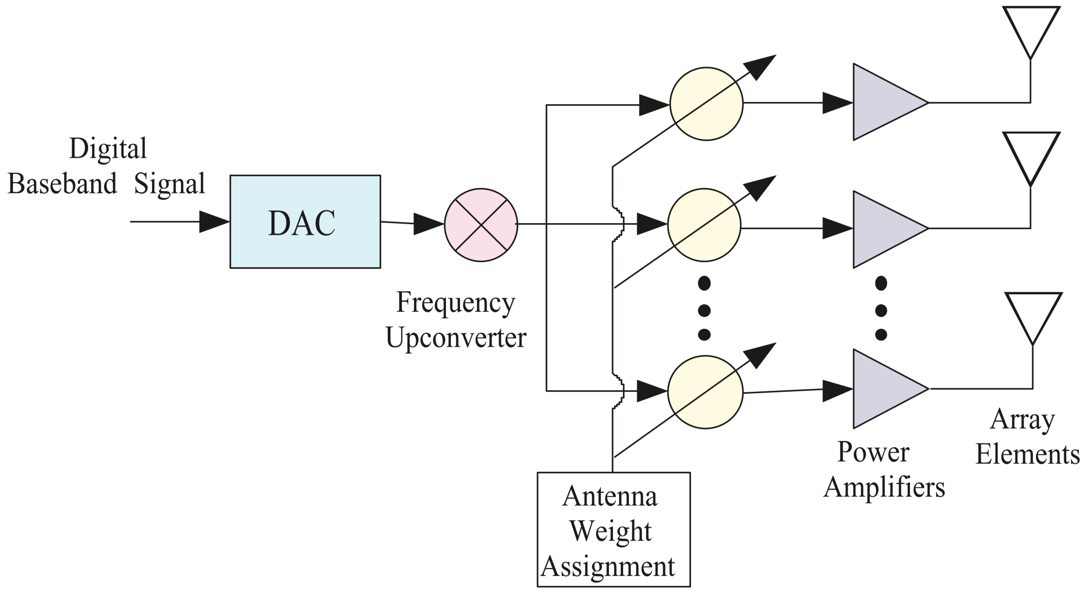

FIGURE 2.3: Analog architecture for beamforming at the transmitter [17].

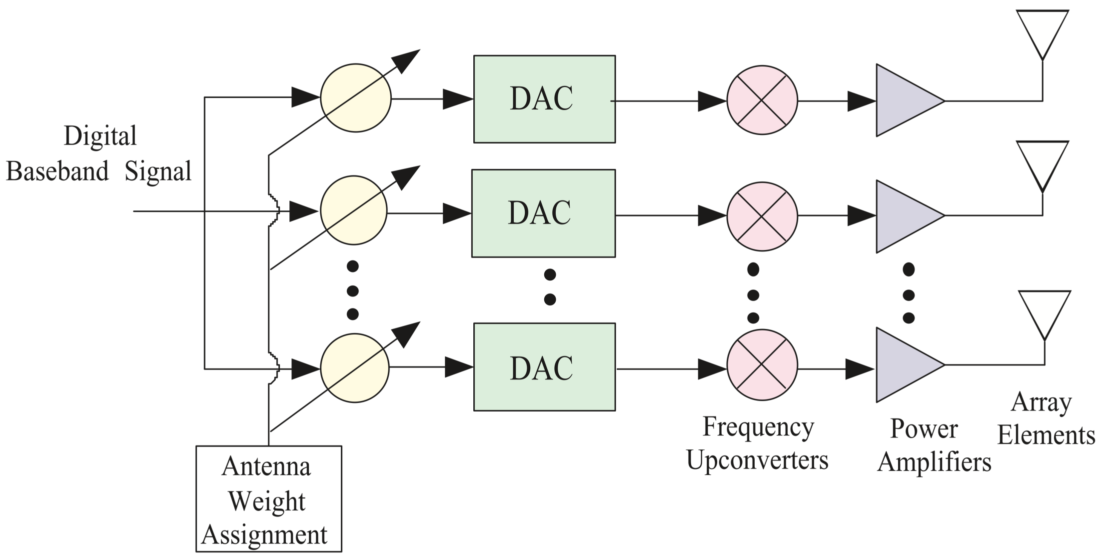

FIGURE 2.4: Digital architecture for beamforming at the transmitter [17].

process is highly dynamic as the propagation environment is constantly changing, e.g. due to UE movement. Beam management can be divided into two main categories: initial access (IA) and beam tracking. IA allows a UE to establish a connection via a physical link with a gNB [21]. Beam tracking involves the regular monitoring of the link quality between the UE and gNB, as well as making necessary beam adjustments. If the link quality deteriorates, procedures such as handovers, radio link recoveries or beam switches can be triggered in order to maintain a stable connection [22]. To accomplish beam management, a set of distinct operations can be executed [23]:

- **Beam sweeping:** Multiple reference signals are transmitted in pre-specified intervals and directions.
- **Beam measurement:** The received reference signals are evaluated in terms of quality, using metrics such as the SNR.
- **Beam determination:** The most suitable beam is selected based on the results of the beam measurement.
- **Beam reporting:** The UE sends a report to the gNB, containing the selected beams and the associated beam quality.

2.4.1 Measurement Signals for Beam Management

The presented beam management operations rely on a number of control messages that are regularly exchanged between the UE and gNB [23].

2.4.1.1 Synchronization Signal Block (SSB)

So called synchronization signal blocks (SSBs) are signals emitted by gNBs to assist with the initial synchronization of an idle UE and the beam tracking of a connected UE [24]. They consist of three components grouped into four orthogonal frequency division multiplexing (OFDM) symbols in time and 240 sub-carriers in frequency [25]. These components are:

- primary synchronization signal (PSS)
- secondary synchronization signal (SSS)
- physical broadcast channel (PBCH) and demodulation reference signal (DMRS)

With the PSS and SSS, the UE can estimate and correct frequency and time offsets. Furthermore, the cell ID, which uniquely identifies the radio cell that sent the SSB, can be obtained [26]. The PBCH and DMRS carry critical information needed to further access the network and complete the synchronization procedure. The general structure is depicted in Fig. 2.5.

So called synchronization signal bursts (SS bursts) consist of a series of SSBs grouped together. Each SSB in an SS burst can be transmitted in a different direction via a specific beam to cover a large angular space. Upon reception, the UE determines the best SSB in terms of SNR within the SS burst, which corresponds to a specific beam. SS bursts need to be transmitted periodically for idle UEs to connect to the network

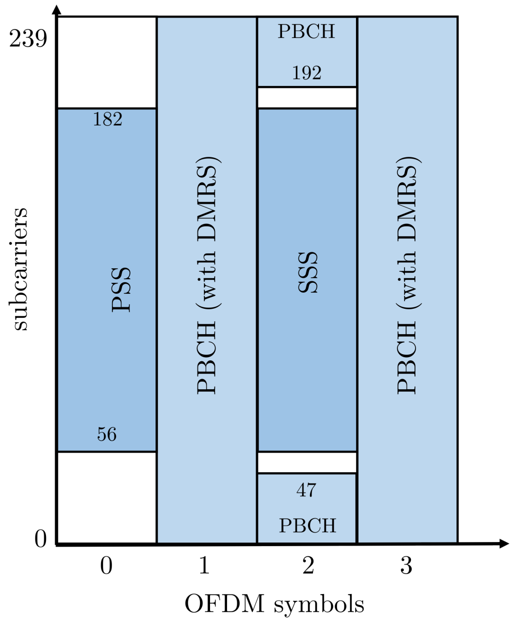

FIGURE 2.5: Structure of the synchronization signal block (SSB) [23].

at any time. The possible periods, as specified by 3GPP, are $T_{SS} \in$ {5, 10, 20, 40, 80, 160} ms [27].

2.4.1.2 Channel State Information - Reference Signal (CSI-RS)

Beam management operations require knowledge of the propagation channel, typically gained through channel sounding operations. In the downlink (DL) direction, this operation is executed by the channel state information - reference signal (CSI-RS). CSI-RSs are transmitted by gNBs and received by UEs. Upon reception, UEs can calculate the channel state information (CSI) describing the status of the DL channel. This information is then transmitted back to the gNBs in channel quality information (CQI) reports, enabling them to make accurate beamforming decisions. Similar to SSBs, CSI-RSs can be send in different directions to monitor a selection of beam pair links (BPLs) obtained from previous beam measurement operations [28]. CSI-RSs can be composed of 1, 2, or 4 OFDM symbols in the time domain with their transmission being periodic, semi-persistent, or aperiodic [29]. The supported periodicities are $T_{CSI} \in$ {5, 10, 20, 40, 80, 160, 320, 640} slots [25]. A slot is the basic time unit for scheduling and transmission, consisting of 14 OFDM symbols.

2.4.1.3 Sound Reference Signal (SRS)

In contrast to SSBs and CSI-RSs, sound reference signals (SRSs) are transmitted in the uplink (UL) direction from UEs to gNBs. Similar to the CSI-RS, the SRS accomplishes a sounding operation to gain knowledge of the UL channel quality [23]. The scheduling parameters, such as the time-frequency resources to use, the direction of transmission and the periodicity type, are configured by the gNB. The periodicity types can be periodic, semi-persistent or aperiodic. To monitor more than one beam direction,

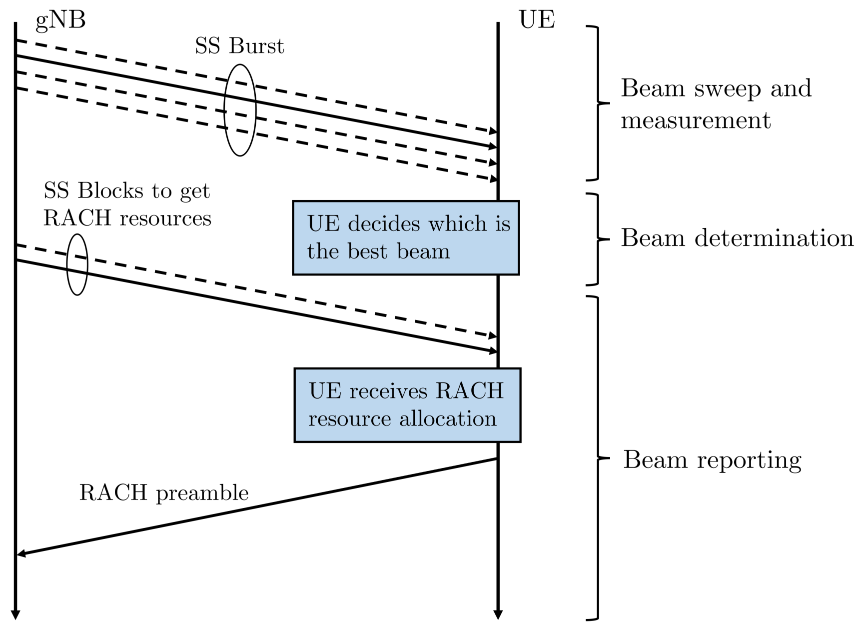

FIGURE 2.6: Exchanges between UE and gNB during IA in a SA-DL beam management framework [23].

the UE can be configured with multiple SRSs in different directions. The SRS can be composed of 1 to 4 OFDM symbols in the time domain and use some of the UE's available bandwidth in the frequency domain [25].

2.4.2 5G Beam Management Frameworks

In 5G beam management frameworks, both non-standalone (NSA) and standalone (SA) architectures are considered. In NSA, a legacy Long Term Evolution (LTE) link is used alongside a directional millimeter-wave link to support control plane transmissions. In SA, this is not the case, so all the beam management operations solely rely on the directional millimeter-wave links between the UE and gNB. NSA architectures benefit from the robustness of the legacy LTE channels while still taking advantage of the high throughput opportunities provided by millimeter-wave links [23]. Another important distinction is between UL and DL frameworks. In UL, the reference signals are sent from the UEs to the gNBs, while in DL, it is the other way around. Correspondingly, SSBs and CSI-RSs are used in DL, while SRSs are used in UL. Three resulting measurement schemes are considered by 3GPP: standalone-downlink (SA-DL), non-standalone-downlink (NSA-DL) and non-standalone-uplink (NSA-UL).

2.4.2.1 Standalone-Downlink (SA-DL)

To carry out a beam sweep in the SA-DL framework, both UEs and gNBs use a predefined codebook containing possible beam directions. The gNB sends reference signals on all its beam directions within one SS burst. Thus, for each SS burst send, the UE can receive one SSB per transmittable beam direction from the gNB. To choose the optimal

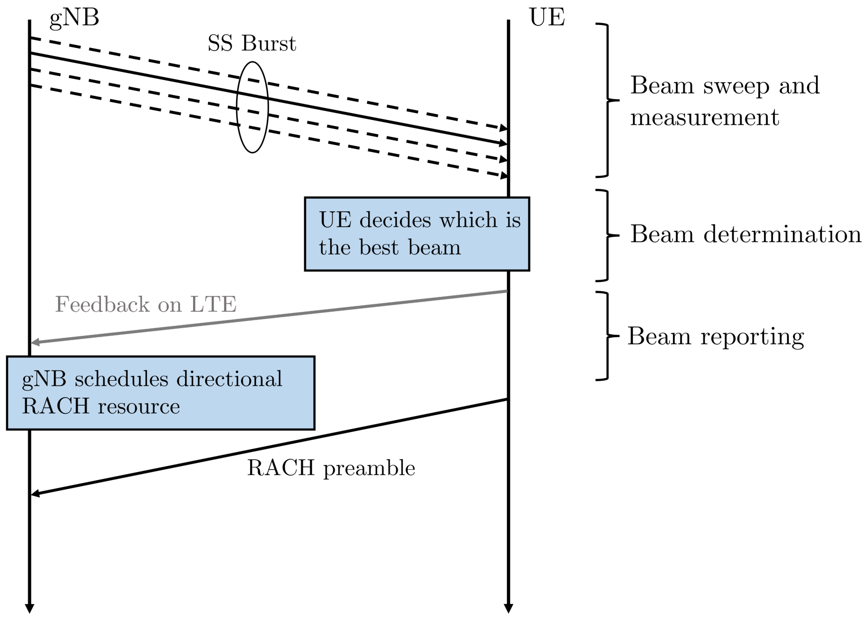

FIGURE 2.7: Exchanges between UE, gNB and eNB during IA in a NSA-DL beam management framework [23].

BPL, this process needs to repeated for all possible beam directions at the UE's side, resulting in a duration of

$$T_{beam\ sweep} = N_{UE\ beam\ directions} \cdot T_{SS\ burst}. \tag{2.5}$$

This beam sweep procedure is also referred to as exhaustive search. The optimal direction is then selected on the UE by comparing the different SNRs received through SSB measurements. For IA, the UE needs to receive a random access channel (RACH) opportunity after the beam determination to access the channel. For this purpose, the UE waits for another SS burst to receive the RACH opportunity of its chosen BPL. Once received, the UE sends a RACH preamble using the assigned frequency-time resource towards the gNB (*cf.* Fig. 2.6). During the following random access (RA) procedure, the UE informs the gNB about its chosen BPL and, in some cases, the BPLs to be monitored. CSI-RS resources can be used for this monitoring [23].

2.4.2.2 Non-Standalone-Downlink (NSA-DL)

The NSA-DL frameworks operates identically to the SA-DL in terms of beam sweeping, beam measurement and beam determination. However, the LTE connection provides some advantages during the beam reporting phase. The legacy link can be used to transfer information about BPLs from the UE to the gNB. This way the UE does not need to wait for another SS burst and a RACH can directly be scheduled (*cf.* Fig. 2.7). Another benefit is that, if a radio link failure (RLF) occurs, the LTE link can be used as a fallback for the data plane to ensure a continuous connection. For this to work, the UE must already be connected to an eNB prior to the IA [23].

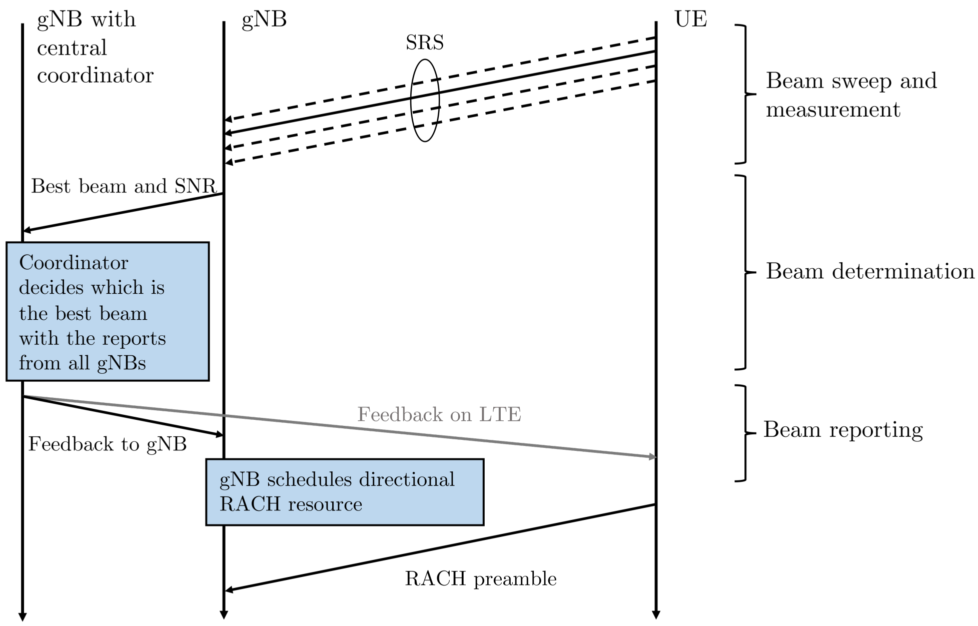

FIGURE 2.8: Exchanges between UE, gNB and eNB during IA in a NSA-UL beam management framework [23].

2.4.2.3 Non-Standalone-Uplink (NSA-UL)

For the NSA-UL framework presented in [30], the roles of the gNB and the UE are reversed. Beam management decisions are based on UL channel quality rather than DL channel quality. This means that the channel sounding signals (in this case, the SRSs) need to be send from the UE and received by the gNBs. This framework assumes that the gNBs and eNBs are roughly time-synchronized and that the propagation time within a cell is not too high [31]. For beam sweeping in NSA-UL, the UE transmits SRSs in different beam directions. The potentially serving gNBs receive these signals and through measurement procedures, build a report table monitoring the best beam directions in terms of SNR. When all gNBs complete their report table, they send them to the network coordinator (in most cases an eNB), which then finds the best BPL among all report tables. This information, along with the optimal beam direction for the specific gNB is then reported back to the UE via the legacy LTE link. The chosen gNB receives the information through a backhaul high-capacity link (*cf.* Fig. 2.8).

2.5 NETWORK SIMULATION

A crucial element in the implementation of novel network technologies is the use of simulators. Before any innovations are introduced into a network, they need to be thoroughly tested in one way or another. Compared to a hardware setup of network typologies, software programs are a cost-efficient and highly modifiable alternative for analyzing network behavior [32]. This is especially true for the technologies to be used in 5G-NR.

2.5.1 NS-3

The network simulator used throughout this thesis is ns-3, the latest successor of a discrete-event computer network simulator series. It is open-source software under the GNU GPLv2 license and is mainly used for research and educational purposes. ns-3 is programmed in C++ and Python and can be used on different operating systems like Linux or macOS. There is no graphical interface, so all operations are performed through the command line. The simulator is designed in a modular way, with each module implementing a separate functionality. This modular design allows for extending ns-3 without modifying the existing functionalities, enabling continuous development to keep up with advancements in network design. Among the already implemented communication technologies through modules are wireless local area network (WLAN), LTE, Ethernet and Bluetooth. To evaluated the key technological advancements for 5G-NR, several extensions are necessary. One of the most important ones is the support of millimeter-waves. There are two existing modules to address this gap: a millimeter-wave module by New York University (NYU) [33] and a 3GPP-compliant module by the Centre Tecnologic de Telecommunicacions de Catalunya (CTTC) [2].

2.5.2 NYU Module

The millimeter-wave module developed by NYU introduces end-to-end simulations of 5G millimeter-wave networks into ns-3. The entire architecture builds on the ns-3 LTE module (LENA) developed by the CTTC [34]. The physical layer (PHY) and media access control (MAC) layer responsible for millimeter-wave transmission and scheduling are custom implementations. A service access point (SAP) in the MAC layer classes enables the use of LTE/EPC protocols [33]. The transmissions and receptions in UL or DL direction are handled by the PHY layer classes. Each PHY instance uses one *MmWaveSpectrumPhy* instance, shared by UL and DL, to communicate over the channel. This is also where interference calculations, SINR calculations and error models for millimeter-waves are executed. Overall, the NYU module has implemented important concepts for the use of millimeter-waves in communication networks, such as beamforming, antenna gain, propagation channel models and access to the millimeter-wave spectrum. However, one issue is that its development started before all the NR 3GPP specifications were available, so the implementation is not fully compliant with the standards [2].

2.5.3 CTTC NR module

The CTTC NR module is a fork of the millimeter-wave module by the NYU, adapting it to be compliant with the 3GPP Release 15 [35]. Among the most important added features are: a flexible and automatically configured frame structure using multiple numerologies, OFDMA with variable TTIs, flexible MAC schedulers and bandwidth parts (BWP) [2]. An example of an end-to-end structure in a simulation with the CTTC NR module is shown in Fig. 2.9. A remote host connects to a service gateway (SGW) through an IP link. In turn, the SGW has an IP connection with a gNB. A packet can be send from the remote host over the IP links to the gNB, where the payload is decapsulated. After that, the packet is transferred over the radio access network

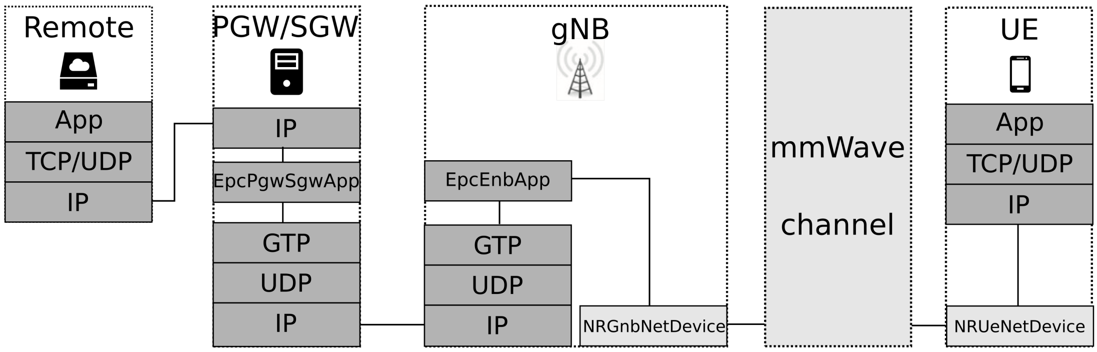

FIGURE 2.9: End-to-end class overview of the CTTC NR module [2].

(RAN) through the millimeter channel, with the *NRGnbNetDevice* and *NRUeNetDevice* acting as access points. Once received at the UE side, it can be passed to the higher layers. The following sections will go into more detail on how the 3GPP-compliant millimeter-wave module is implemented in ns-3.

2.5.3.1 *Channel Model*

One of the three channel models in the NYU module is entirely in line with 3GPP specifications and was therefore incorporated without modifications into the CTTC NR module. This 3GPP statistical channel model can be used for frequencies between 6 and 100 GHz with a bandwidth of 10 % of the carrier frequency, as described in [36]. Based on the distance between the UE and the gNB and the simulation scenario, a line of sight (LOS) probability is calculated. This LOS probability is then used to calculate pathloss, small-scale fading and shadowing in the channel.

2.5.3.2 *Physical Layer*

One of the most important changes implemented by the CTTC NR module is the introduction of flexible frame structures. Similar to LTE, the NR frame length is 10 ms and contains ten subframes of 1 ms each. The difference is that these subframes are further split in the time domain into a variable number of slots. The number of slots per subframe depends on the slot duration. A slot is composed of 12 or 14 OFDM symbols, depending on the cyclic prefix (CP) configuration [2]. In 3GPP's Release 15, a flexible numerology structure was introduced to configure OFDM symbol length and sub-carrier spacing (SCS) based on current requirements. This flexibility is essential to support the multiple use cases envisioned for 5G-NR. The following relations connect the numerology μ with the SCS and the OFDM symbol length [37]:

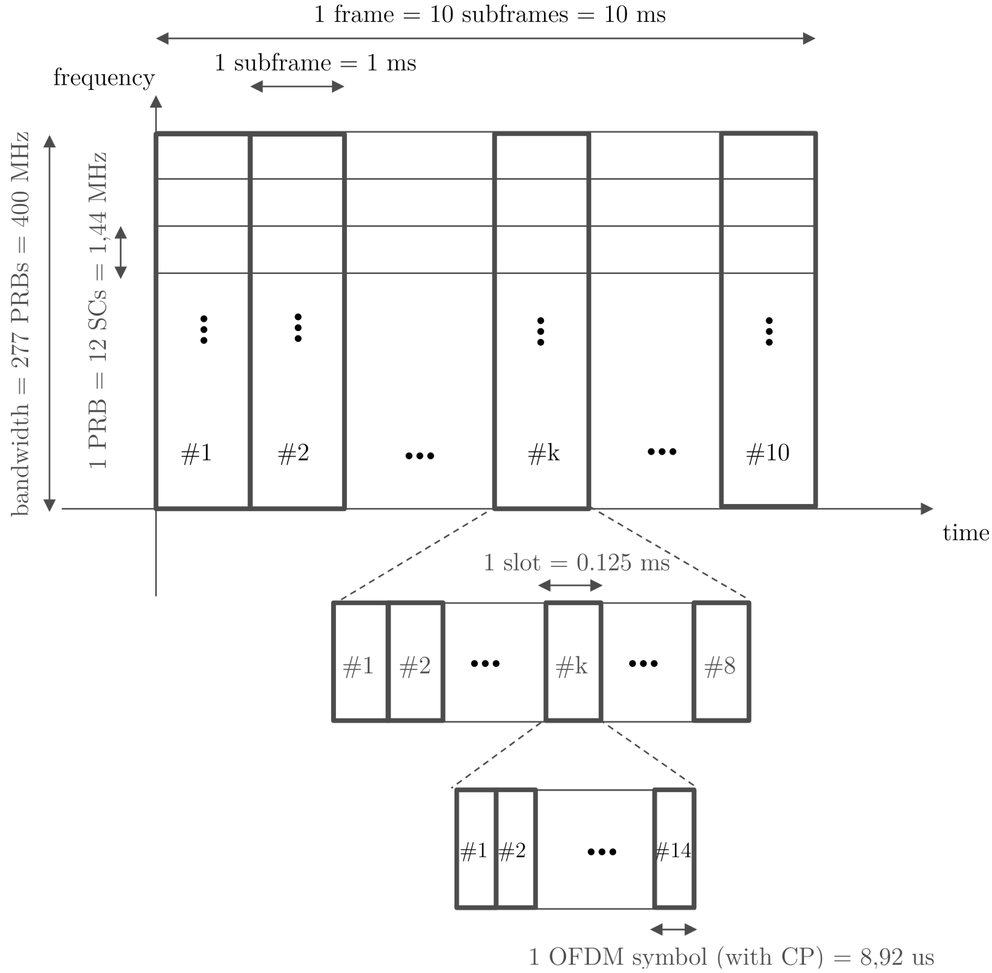

FIGURE 2.10: Time and frequency domain of a nr frame structure with $\mu = 3$ and a channel bandwidth of 400MHz [2].

$$SCS = 15 \cdot 2^{\mu} kHz, \quad (2.6)$$

$$T_{Slot} = \frac{1}{2^{\mu}} ms, \quad (2.7)$$

$$T_{OFDM} = \frac{T_{Slot}}{N_{Symbol\ per\ Slot}}, \quad (2.8)$$

where 3GPP defines a total of five different numerologies numbered from 0 to 4. The different parameters are summarized in Table 2.2. Higher numerologies have a larger SCS and shorter OFDM symbol length, according to 2.7 and 2.8. The short OFDM symbol length can be beneficial for latency-critical applications as the number of slots per subframe increases. However, this also negatively impacts spectral efficiency and data rate due to the requirement of CPs for each OFDM symbol. For

	$\mu = 0$	$\mu = 1$	$\mu = 2$	$\mu = 3$	$\mu = 4$	$\mu = 5$
SCS [kHz]	15	30	60	120	240	480
OFDM symbol length [μs]	66.67	33.33	16.67	8.33	4.17	2.08
Cyclic prefix [μs]	~ 4.8	~ 2.4	~ 1.2	~ 0.6	~ 0.3	~ 0.15
Number of subframes in frame	10	10	10	10	10	10
Number of slots in subframe	1	2	4	8	16	32
Slot length [μs]	1000	500	250	125	62.5	31.25
Number of OFDM symbols in slot	14	14	14	14	14	14
Number of subcarriers in a PRB	12	12	12	12	12	12

TABLE 2.2: Supported numerologies in the CTTC NR module [37].

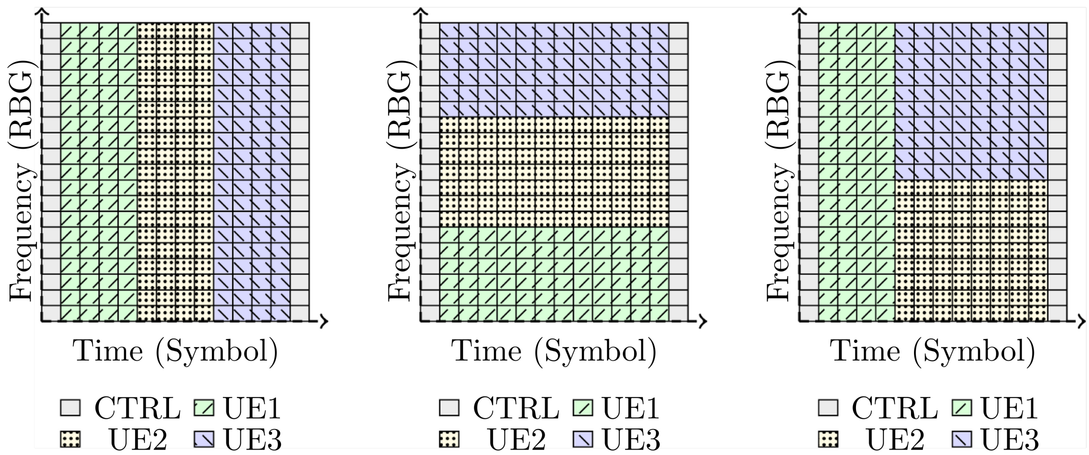

(a) (b) (c)

FIGURE 2.11: Multiple access allocation schemes for one slot in the CTTC NR module [37].

high data rate applications, smaller numerologies provide a better solution. So called resource blocks (RBs) are used for scheduling and consist of 12 subcarriers, independent of the numerology used. The bandwidth of an RB depends on the SCS and, therefore, the numerology. Larger numerologies have a higher bandwidth demand per RB, which makes the use of FR2 appropriate. Fig. 2.10 shows the NR frame structure for numerology $\mu = 3$. The CTTC NR module supports a sixth numerology, $\mu = 5$ as seen in Table 2.2, which is not currently specified by 3GPP but could be used in future releases.

2.5.3.3 MAC Layer

The MAC layer interacts with the PHY layer and the radio link control (RLC) layer through SAP application programming interfaces (APIs). Buffer status report (BSR) messages are send from the RLC to the MAC, containing information about the amount of data currently stored and waiting to be scheduled. This information enables the scheduler to make informed decisions [2]. A major modification in the MAC layer concerns the multiple access schemes. There are three different multiple access schemes that are supported and visualized in Fig. 2.11:

1. **TDMA with Transmission Time Interval (TTI):** The OFDM symbols within a slot are divided among the UEs to be served. Time resources are used to perform multiple access (*cf.* Fig. 2.11a).
2. **Pure OFDMA:** Within a slot, the frequency resources can be assigned to different UEs, allowing transmission to multiple UEs per slot (*cf.* Fig. 2.11b).
3. **OFDMA with variable TTI:** This is the most flexible way to assign time and frequency resources within a slot. With variable TTI, messages can be transmitted in a fraction of a slot in the time domain, allowing time and frequency resources to be divided among UEs in a single slot (*cf.* Fig. 2.11c).

OFDMA schemes cannot be used with analog beamforming due to the limitations of a single beam.

2.5.3.4 Schedulers

For each slot, a scheduler needs to decide how to allocate the available resource block groups (RBGs) to the different UEs. The decision is made at the gNB through a scheduling algorithm and transmitted to the UE via downlink control information (DCI). In the CTTC NR module, three different schedulers are supported:

- **Round-robin:** In OFDMA, the RBGs are distributed evenly among the UEs within the same beam. In TDMA, the symbols are evenly distributed among the UEs, with the possibility to use different beams for each time instance [2].
- **Proportional fair:** In OFDMA, the RBGs are evenly distributed according to a metric that takes the CQI and the average rate from previous slots into account. Depending on the configurations, either UEs with a low average rate or a high current rate relative to the average rate are prioritized. For TDMA, the allocated resources are symbols [2].
- **Maximum rate:** The RBGs or symbols are distributed to maximize the overall network throughput. The CQI is used to calculate the actual rate of different UEs [2].

2.5.3.5 Bandwidth Part Manager

To add an additional level of flexibility, the bandwidth can be split into smaller band width parts (BWPs). Each of these BWPs can have its own numerology, allowing multiple use cases, like URLLC and eMBB, which require different numerologies to be served within the same bandwidth. In the simulation, the BWPs are set up at the beginning. Each BWP has a separate PHY and MAC scheduler instance.

2.6 RELATED WORK

Directional communication necessitates beam alignment between the transmitter and the receiver [23]. Beam management operations enable the performance of IA, handover and beam tracking. The control signals used for these operations, such as SS bursts or CSI-RSs, result in a non-negligible overhead, which can impact the end-to-end performance of a network. This was validated by the authors of [38], [39] and [24], who confirmed through simulations that throughput and latency are heavily influenced by beam management operations. For this reason, a simulation framework implementing realistic beam management is important to analyse its end-to-end implications.

Based on a fork of the NYU millimeter-wave module [35], the CTTC NR module [2] provides a 3GPP compliant simulation framework for millimeter-waves. However, beam management is idealized in this module. The authors in [40] tried to close this gap by adding support for SSB transmission-based beam management into version 1.1 of the CTTC NR module. Building on this work, the authors in [24] implemented realistic beam management using CSI-RS and SSB DL transmissions for single UE scenarios in single or multi-cell networks. Overloaded cells in multi-user networks can also degrade throughput if the beam management strategy focuses solely on maximizing link quality. The authors in [41] added multi-user support to the realistic beam management framework and implemented a novel beam management strategy that considers both link quality and resource sharing to increase the per-user throughput in multi-user networks.

As achieving consistently high throughput, even in cellular hot spots, is one of the goals of 5G-NR, methods to increase throughput are sought after. One such method, as pointed out by [42], is the use of SU-MIMO. By utilizing a high number of antenna elements and a hybrid beamforming antenna structure, it is possible to send multiple data streams to a single UE within the same time-frequency resource, thereby multiplying the throughput. The trade-off is increased antenna complexity and the division of the available power between the multiple streams instead of one.

Conducting simulations is an effective way to better understand the general effect of SU-MIMO on a network. In the network simulator ns-3, different modules have already implemented forms of MIMO. The millimeter-wave module from NYU has received support for MU-MIMO [43], but it still lacks an implementation of SU-MIMO. There are several implementations of SU-MIMO and MU-MIMO in ns-3 WLAN modules based on the IEEE 802.11 standard, including [44] and [45]. In the ns-3 LTE module (LENA) developed by the CTTC, there is an implementation of 2x2 SU-MIMO, but many idealized assumptions regarding stream propagation and inter-stream correlation were made, rendering it less realistic. The 3GPP compliant CTTC NR module has been extended to support SU-MIMO and spatial multiplexing by the work in [46]. This implementation is based on a particular SU-MIMO case using dual polarized antennas, which limits the number of usable streams per user to two. Additionally, an unrealistic inter-stream interference rejection model is assumed. This framework was recently extended in [47] to support a more general SU-MIMO. With this extension, the CTTC NR module supports 3GPP 5G compliant SU-MIMO through hybrid beamforming and closed-loop MIMO with a more accurate inter-stream interference calculation. Currently, only two streams per user are supported, but this is planned to be extended to four streams in the near future.

SU-MIMO has not yet been implemented in a realistic beam management framework, especially in a multi-user scenario. This work will address that by combining the multi-user realistic beam management framework in [41] with the SU-MIMO implementation in [47]. Furthermore this paves the way for an MU-MIMO implementation. Through simulations, the end-to-end implication of SU-MIMO considering different beam management strategies in a multi-user environment will be analysed.

3

NS-3: FRAMEWORK IMPLEMENTATION

In this thesis, a framework with realistic beam management operations, beam management strategies in a multi-user, multi-gNB environment and a general SU-MIMO implementation supporting up to two streams per UE is developed. The implementation of the realistic beam management operations, referred to as the flexRLM framework throughout this thesis, is based on an extension of version 1.1 of the CTTC NR module as presented in [41], relying on ns-3 version 3.32. Conversely, the SU-MIMO implementation was introduced by CTTC's NR module version 3.0 [47], introducing general SU-MIMO capabilities into the framework utilizing ns-3 version 3.41.

To create a framework combining all the presented functionalities, the extensions made to the version 1.1 of the CTTC NR module to obtain the framework in [41] were recreated within version 3.0 of the CTTC NR module. Additionally, the extensions made to version 3.32 of ns-3 were recreated within version 3.41 of ns-3. During this process, some extensions needed modifications to ensure full compatibility with the SU-MIMO implementation.

This chapter presents the changes necessary to implement general SU-MIMO and outlines the modifications required for the flexRLM framework to be compatible. The extensions discussed include updates to the antenna and spectrum modules in ns-3, the PHY layer implementations of the CTTC NR module and the computational process within ns-3 and the CTTC NR module. Lastly, an overview of the flexRLM framework is provided.

3.1 SU-MIMO FRAMEWORK

3.1.1 ns-3 Antenna

One of the main prerequisites for performing SU-MIMO is a hybrid antenna architecture, allowing simultaneous transmissions over multiple beams. This requires an antenna to have separate subarrays, each with its own RF chain for receiving and transmitting signals. This capability is introduced in the *UniformPlanarArray* class, which implements an uniform planar array (UPA) antenna model. There are two methods to generate an antenna with multiple subarrays.

The first method uses the polarization slant angle of an antenna element to divide them in two groups. The polarization slant angles of the two groups are separated by 90 degrees and stored in the variables *m_cosPolSlant* and *m_sinPolSlant*. If dual polarization is used, the number of antenna elements doubles and the two polarizations overlap as shown in Fig. 3.1. Each polarization has its own RF chain and can transmit a signal in a specific beam direction. The two streams experience no interference between each other due to the 90-degrees polarization slant angle separation.

The second method utilizes multiple ports in the antenna to create separate subarrays. The variables *m_numVPorts* and *m_numHPorts* store the number of vertical and

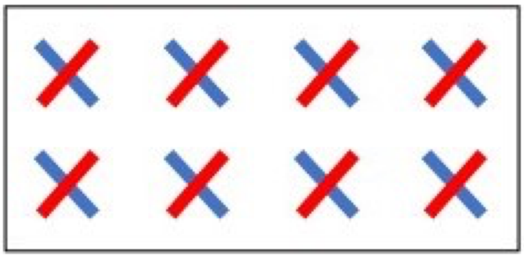

FIGURE 3.1: Dual Polarized Antenna with 4 Rows and 2 Columns [46].

horizontal ports in the antenna, respectively. Each port has its own RF chain and can transmit a signal in a specific beam direction. This enables the transmission of multiple beams simultaneously. Unlike the polarization method, the antenna elements of the different ports are spatially separated.

Since the *UniformPlanarArray* class is not included in the version 3.32 of ns-3, the flexRLM framework originally uses the *ThreeGppAntennaArrayModel* class for antenna modeling. To make this framework compatible with the SU-MIMO implementation, the *UniformPlanarArray* class abd its functions was introduced for antenna modeling.

3.1.2 ns-3 Spectrum

Major changes had to be made in the spectrum module to support SU-MIMO. One of these changes is to support the multiple array subpartitions in the antennas. The *ThreeGppChannelModel* class is responsible for generating the channel matrix. Due to the multiple subpartitions, multiple channel matrices need to be considered during a transmission, one per transmit and receive subarray pair. However, the channel matrices between the same pair of nodes share common channel parameters. It is important to differentiate the common channel parameters from those specific to the transit/receive antenna subpartition array pair so that they do not get regenerated for each pair. For this reason, the *GetNewChannel* function, which generates the channel parameters, was split into two functions: *GetNewChannelParams* and *GetNewChannelMatrix*. These new functions save the generated channel parameters into separate structures, *ChannelParams* and *ChannelMatrix*. *ChannelParameters* stores the parameters common to a node pair (e.g., channel condition, cluster powers, cluster delays, angle of departure (AoD), angle of arrival (AoA), delay spread), while *ChannelMatrix* stores those specific to each phased antenna array pair, most importantly the channel matrix. This new channel parameter storage structure can be seen in Fig. 3.2

The flexRLM framework introduces a raytracing channel model using raytracing data to calculate the channel parameters. To use this model with SU-MIMO, the corresponding *GetNewChannel* function needed to be separated in the same way as explained above. The *GetNewChannel* function is also extended to support multiple ports or dual polarization in the calculation of the *ChannelMatrix*. This extension needed to be mirrored in the *GetNewChannel* function for the raytracing channel model in order to ensure compatibility.

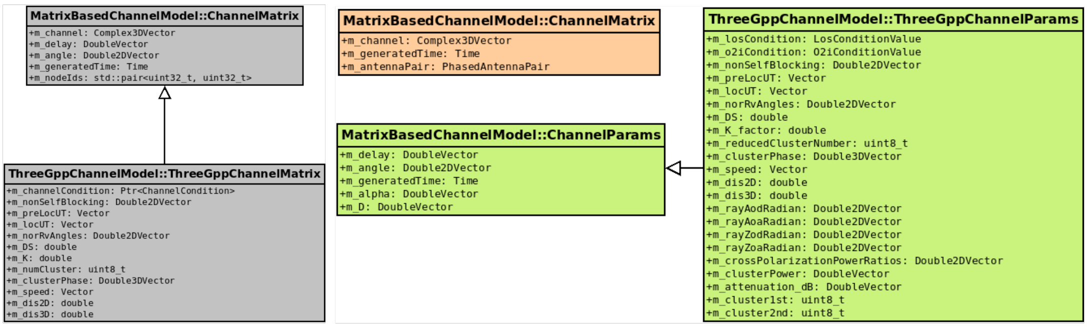

FIGURE 3.2: Splitting the Channel Parameter Storage Structure [46].

Other changes in the spectrum module concerned the calculation of the received power spectral density (PSD). The *DoCalcRxPowerSpectralDensity* function is responsible for calculating the PSD and its underlying functions need the antenna array objects for their calculations. To enable the transmission and reception of antenna array objects to be passed to the spectrum propagation loss model in the form of *PhasedArrayModel* objects a new spectrum propagation loss model interface, *PhasedArraySpectrumPropagationLossModel* is used. This change removes a hard limitation of the *ThreeGppSpectrumPropagationLossModel* to support maximally one antenna array instance per UE or gNB. With these changes, multiple antenna arrays per device on the same *SpectrumChannel* are allowed.

With the introduction of multiple ports, it is no longer sufficient to represent a received signal with only a PSD. The frequency domain channel matrix, with dimensions of `receive antenna ports × transmit antenna ports × RBs`, and the precoding matrix, with dimensions `transmit antenna ports × transmit streams × RBs`, are needed to correctly depict the received signal plus interference. Therefore, the *CalcRxPowerSpectralDensity* function is extended to return a pointer towards *SpectrumSignalParameters* which includes the PSD, the frequency domain spectrum channel matrix and the precoding matrix.

3.1.3 *Finding Optimal Precoding Matrices*

In a real network, the gNB needs to decide whether to use MIMO based on feedback from the UE. This feedback includes the precoding matrix indicator (PMI), rank indicator (RI) and corresponding CQI. The rank indicator specifies the number of MIMO streams that would maximize the transport block size when using the corresponding precoding matrix. The PMI is an index of a set of predefined precoding matrices from a codebook; in our case, the 3GPP Type-I single panel codebook, implemented in the new *NrCbTypeOne* class. To find these optimal values on the UE side, a new class called *NrPmSearchFull* is implemented. It uses an exhaustive search method where the resulting SINR of all possible precoding matrices is computed and the highest is selected. After the exhaustive search, the optimal rank, the corresponding optimal PMI, and the CQI are packaged into a feedback message to be sent to the gNB. In single input single output (SISO) communication, CQI reporting includes only a single wideband CQI value. For SU-MIMO, this needs to be extended so that each MIMO stream receives a report, which includes the PMI and RI. For this purpose, the original

DlCqiInfo structure is extended to include the optimal PMI and optimal rank through the variables *m_sbPmis* and *m_ri*, respectively.

3.1.4 OFDMA Downlink Transmission

Originally, the CTTC NR module's main multiple access scheme within a single time slot was TDMA. Packets intended for a specific UE were grouped into a single packet burst, creating an independent representation for each signal to accurately model the transmission. This ensured that the packets sent to each UE, the DL allocation, and the transmitted physical signal were interconnected. With the introduction of OFDMA into the module, packets for separate UEs that could be served with the same beam were combined, which removes this connection between packet burst and UE. The transmitted physical symbol now consists of a combination of all the signals transmitted to different UEs. In the case of MIMO, transmissions to different UEs can have distinct ranks. This poses a problem as merging the representation of MIMO signals of different ranks into one physical signal is challenging.

To address this issue, the method to enable OFDMA in the DL had to be revised. By introducing a radio network temporary identifier (RNTI), the connection between a packet burst and the receiving UE was reestablished. After this remodeling, all DL allocations are transmitted with independent signal representations, eliminating the need to merge different MIMO signals.

3.1.5 MIMO SINR Computation

The NR model for interference calculation has been expanded to include support for MIMO SINR calculations. Specifically, the *NrInterference* class has been extended to support the calculation of the interference-and-noise covariance matrix needed to compute the SINR. The new functions are *CalcOutOfCellInterfCov*, which calculates the interference caused by entities outside of the current cell, *AddInterference* which adds the covariance of the provided signal to an existing covariance matrix and *ComputeSinr*, which computes the SINR.

To understand how the SINR of a MIMO signal is calculated, it is important to understand how a MIMO signal is received. At the UE, a receive filter is used to minimize the inter-stream interference and maximize the SINR. In this framework, the minimum mean-squared error interference rejection combining (MMSE-IRC) receiver is used. This receiver minimizes the mean square error (MSE) of the transmitted symbols with the received symbols expressed through:

$$\hat{b} = R^H(H \cdot P \cdot b + w), \tag{3.1}$$

where R is the receive filter of dimensions equal to the number of UE `antenna ports × transmitted data streams by the gNB`, H the channel matrix with dimensions `UE antenna ports × gNB antenna ports`, P the transmit precoding matrix with dimensions `gNB antenna ports × transmitted streams`, w the received noise-plus-interference and $\hat{b}$ and b the received and transmitted symbols, respectively. The MSE can be represented through the MSE-matrix given by:

$$E = \mathbb{E}\{(\hat{b} - b)(\hat{b} - b)^H\}, \tag{3.2}$$

where E is the MSE-matrix with dimensions `transmitted data streams` $\times$ `transmitted data streams`. An MMSE-IRC receiver is given by:

$$R^{mmse} = (HPP^H H^H + W)^{-1} HP, \tag{3.3}$$

where W is the covariance of the noise-plus-interference received and R^{mmse} is the MMSE-IRC receiver. When this receiver is used, the MSE-matrix can be expressed as:

$$E = (I + P^H (H^{intfNorm})^H H^{intfNorm} P)^{-1}, \tag{3.4}$$

where $H^{intfNorm}$ is the interference-normalized channel. Using the Cholesky "LLT" decomposition of W,

$$W = LL^H, \tag{3.5}$$

$H^{intfNorm}$ can be written as:

$$H^{intfNorm} = L^{-1} H. \tag{3.6}$$

Finally, the SINR calculations simplify to a simple equation using the diagonal elements of the MSE-matrix:

$$SINR_l = \frac{1}{E(l, l)} - 1 \tag{3.7}$$

where $SINR_l$ denotes the SINR of the l-th stream. By this, only the precoding matrix P and the interference normalized channel $H^{intfNorm}$ are needed to compute the SINRs of the different streams in a signal.

The SU-MIMO framework introduces a few new classes to facilitate the presented SINR calculations. The *NrCovMat* class saves the interference-plus-noise covariance matrix W needed for the Cholesky "LLT" decomposition in (3.5). Furthermore, the *CalcIntfNormChannel* function efficiently computes the interference normalized channel $H^{intfNorm}$ through (3.6). The $H^{intfNorm}$ matrix is then stored in the *NrIntfNormChanMat* class, which also contains the function *ComputeSinrForPrecoding* to compute the SINR through (3.7) based on the MSE-matrix. Lastly, the *NrSinrMatrix* class saves the MIMO SINR matrix with dimensions `transmitted streams` $\times$ `RBs`. Since multiple streams are encoded in the same transport block (TB), which is the payload passed between the MAC and PHY layers, no major changes to the MAC layer are needed.

3.1.6 Enabling MIMO

To use SU-MIMO in a simulation, the attribute *EnableMimoFeedback* in the *NrHelper* class has to be set to true. When this attribute is enabled, the *NrHelper* class connects an *NrPmSearch* algorithm to each *NrUePhy* instance. Additionally, important callbacks like *NrSpectrumPhy::UpdateMimoSinrPerceived* and *NrUePhy::GenerateDlCqiReportMimo* are set. It is possible to configure SU-MIMO parameters such as the rank limit using the *SetupMimoPmi* function.

3.1.7 Computational Changes

Calculations that were previously done in the time domain using the time domain channel matrix are now shifted towards the frequency domain using the frequency domain channel matrix to support MIMO. These two 3D structures have a significant size difference. The third dimension of the time domain channel matrix is relative to the number of clusters, typically between 10 and 20, while the third dimension of the frequency domain channel matrix depends on the number of RBs, reaching over 275. This significantly affects the computational performance of the entire framework.

To address this, the old 3D data structures composed of a *std::vector* of a *std::vector* of a *std::vector* were replaced with a completely new data type. This data type is implemented in the *ValArray* class, introducing *std::valarray*, which is then used in the *MatrixArray* class to create 3D arrays structured like an array of matrices. This significantly improves operations involving 3D structures an thus enables SU-MIMO calculations in a timely manner. To be compatible with this new data type, the *std::vector* instances used in the flexRLM framework needed to be changed to the new *std::valarray* structure. Additionally, all access operators, function arguments and function return values needed to be adapted to the new data type.

The implemented MIMO interference and SINR calculations involve the use of matrix inverses and singular value decompositions (SVDs). This can be seen in (3.4) and (3.6). To compute these calculations on 3D structures, a new template library called Eigen3 [48] is needed. Eigen3 is a C++ template library for linear algebra, including matrices, vectors, numerical solvers and related algorithms. It must be downloaded to perform SU-MIMO simulations; without it, only SISO simulations can be performed.

3.2 FLEXRLM FRAMEWORK

The flexRLM framework is based on an extension of the CTTC NR millimeter-wave module that incorporates realistic beam management control operations [24]. Specifically, SSBs and CSI-RSs are implemented with accurate scheduling, transmission and reception. The considered millimeter-wave network is NSA-DL, with control signal transmission handled through an LTE connection. This framework is further extended in [41] to include multi-user support and muti-gNB radio link monitoring (RLM) for joint beam management and load balancing.

3.2.1 Dual Connectivity

In a 5G-NR NSA-DL network, control signals are transmitted over the LTE network. Therefore, a connection between an eNB and all UEs in the simulation is necessary. This connection is established through the *LteRrcProtocolIdeal* and *NrRrcProtocolIdeal* classes. This allows UEs connected to the network via 5G-NR to link with an LTE eNB coordinator, facilitating UL control signal transmissions through the connection. The DL sounding information gathered by the SSBs and CSI-RSs can be sent via the eNB coordinator to the corresponding gNB using the *DoSendSSBRSReport* function. Other important beam management operations are also implemented.

3.2.2 Realistic Scheduling, Transmission and Reception of SSBs

- **Scheduling:** All DL transmissions are scheduled in the *DoScheduleDl* function of the *NrMacSchedulerNs3* class, so changes need to be added to this function for SSB scheduling. Firstly, the *IsSSBRequired* function is called to check for each time slot if an SSB is required. If required, *FormSSBlock* schedules an SSB in the time-frequency resource and determines its antenna direction based on *m_sfnBeamVectorMap*, which establishes a connection between beamforming vectors and subframe and slot number. Finally, the slot allocation information is passed to the *NrGnbPhy* instance.

- **Transmission:** To perform a beam sweep, it is crucial that the UEs and gNBs know where to orient their beams. The beamforming vector (BFV) map contains this information. At the beginning of the simulation, each *NrGnbPhy* and *NrUePhy* instance generates a BFV map through the *DoGenerateBeamVectorMap* function.

  The transmission of all control messages through the PHY layer is handled by the *DlCtrl* function. It accesses the *IsSSBRequired* function of the *NrGnbMac* class to determine whether or not to queue an SSB. If an SSB is queued, the beam manager sets the specified direction and the message is passed to the *NrSpectrumPhy* instance.

- **Reception:** The SSBs are received by the *NrSpectrumPhy* class, which retrieves the reference signal receive power (RSRP) and the SNR, saving it inside a map called *m_cellIDSSBMap*. This variable contains the SNR values of all the SSBs sent in different directions and by different gNBs and passes them to the *NrUePhy* instance. There, the *ProcessSSBs* function is called, which ensures with the *CheckIfSweepIsCompleted* function that all SSBs from different directions and gNBs are collected. If so, the best providing gNB and beam direction are determined by finding the maximum SNR value in the *m_cellIDSSBMap* map through the *DetermineOptimalLink* function. Finally, the RA procedure is initiated, provided the maximum SNR value exceeds the coverage threshold. If a RLF triggered the beam sweep procedure, a connection to the chosen gNB needs to be established through *ReEstablishConnectionWithCell*; otherwise, only the new BFV needs to be set.

3.2.3 Realistic Scheduling, Transmission and Reception of CSI-RSs

- **Scheduling:** Similar to the SSB, the function *IsCSIRSRequired* checks in each time slot whether a CSI-RS should be scheduled. Upon scheduling, the UE needs to be informed about the upcoming transmission through DCI. For that, a *DciInfoElementTdma* element gets passed down to the *NrGnbPhy* instances to be transmitted to an UE.

- **Transmission:** The *DoSetCSIRSRLMResources* function sets different CSI-RS parameters for each receiving UE, such as the offset, number of CSI-RS per SS burst, periodicity and international mobile subscriber identity (IMSI). The gNB has a resource map (*mapOfCSIRSResources*) detailing the time of each scheduled CSI-RS. An RLM vector inside the PHY layer stores the important parameters of the beams monitored by the CSI-RS, with a maximum of eight BPLs being monitored simultaneously. Upon transmission, the antenna array of the gNB needs to be directed by the beam manager towards the monitored BPL as the currently serving and monitored BPLs differ by definition. Finally, the CSI-RS message is passed to the *NrSpectrumPhy* instance were the transmission is conducted. To resume the DL data transmissions, the *ChangeBeamformingVector* function steers the antena back to the serving BPL.

- **Reception:** The CSI-RS control messages are collected by the *StartRx* function of the *NrSpectrumPhy* class. The gathered information is then passed to the *NrUePhy* class, which uses its *ProcessCSIRSs* function to extract the measured SNR and identifications on the beam used for the transmission, saving it in *m_recvCSIMap*. This map is then sorted by the SNR and the top four BPLs are chosen to be reported in the *NrCSIRReportMessage* sent to the serving gNB. This information is used by the gNB to decide whether or not to switch BPLs depending on the quality of the current link and the reported SNR of the monitored links. If a monitored BPL from the serving gNB provides a better connection, the function *ChangeBeamformingVector* is scheduled to change to the better BPL. gNBs regularly send updates about their CSI-RS to the eNB to facilitate handover coordination.

3.2.4 NR-Connected UEs RLF Handeling

A mechanism was implemented for NR-connected UEs to detect serving link outages and initiate a beam sweep to recover from a RLF event. A RLF event is detected in the *NrUePhy* class by receiving a fixed number of succeeding DL measurements with an SNR below a set threshold. When this occurs, the *DoNotifyOutOfSyncNr* function is called and the *RadioLinkFailureDetected* function is scheduled. If no improvements happen by the time the function executes, the UE informs the eNB that it is no longer served by the previous gNB and they disconnect. The UE then initiates a beam sweep to find a new gNB that can provide better link quality.

3.2.5 flexRLM

RLM describes the beam management procedure for connected UEs to maintain a stable link, including operations like beam tracking, beam switching and mobility management. The default 5G-NR RLM actively monitors promising BPLs via SSBs, only considering the currently serving cell. If one of the monitored BPLs of the current cell exhibits better beam quality (higher SINR), a beam switch can be performed. This RLM strategy does not consider inter-cell mobility, meaning that if none of the beams from the currently serving cell can provide a sufficient SINR, a handover to another gNB must be initiated. For that, a beam sweep is necessary to discover the best BPL of the new gNB. Additionally, multi-user resource sharing is not considered in the beam management decisions, which could lead to throughput degradation caused by overloaded cells.

To address this shortcoming, the authors of [41] propose a coordinator-based flexible RLM framework that enables joint beam management and low-complexity load balancing in multi-user DL millimeter-wave networks. In flexRLM, the monitored BPLs consider beams not only from the currently serving gNB but also from other gNBs. The ratio of monitored beams between the serving and other candidate gNBs can be configured flexibly. Monitoring beams from other cells has the advantage that, if the currently serving cell cannot provide a stable BPL, a fast handover to another gNB without the need of a beam sweep is possible. Periodic transmissions of SSBs by the serving and other cells monitor the long-term channel dynamics, ensuring that the monitored BPLs are updated. Furthermore, a joint decision process addressing the resource sharing problem in a multi-user scenario is implemented. The LTE coordinator has the flexibility to use the monitored BPLs for network-wide load balancing operations. The coordinator periodically checks if each gNB is congested. If congestion is detected, fast load-balancing handover procedures are initiated to relieve the congested gNB. This process is facilitated by monitoring beams from other gNBs in addition to the serving one. Before a handover, it is checked whether the target gNB is congested; if it is, another gNB is sought.

The implementation of flexRLM relies solely on existing LTE-NR radio resource control (RRC) messaging and no additional messages are introduced. The additional changes in the implementation are presented in detail in [24].

4

SYSTEM MODEL AND SIMULATION SETUP

This chapter details the system model and simulation setup used in this thesis. Section 4.1 describes the simulation setup, covering the channel model, network deployment, UE mobility, SU-MIMO configurations and other general parameters. Section 4.2 introduces the two beam management strategies employed in the simulations. Section 4.3 outlines the different simulation scenarios, while Section 4.4 specifies the metrics used for performance evaluation.

4.1 SIMULATION SETUP

4.1.1 Channel Model

The purpose of a channel model in a network simulator is to accurately replicate the behavior and characteristics of the communication channel between transmitters and receivers. This includes calculating the received power of a signal based on the following equation:

$$P_{rx} = P_{tx} + G_{bf} - PL, \tag{4.1}$$

where P_{rx} is the receive power and P_{tx} is the transmit power, G_{bf} is the beamforming gain and PL is the pathloss in dB. The CTTC NR module includes a statistical 3GPP compliant channel model that will be presented in this section and used throughout the thesis. A statistical channel model uses statistical methods to describe the effects of signal propagation. The 3GPP model relies on real-life measurement data from measurement campaigns by 3GPP partners. In the 3GPP channel model described in [49], the calculation of the received signal power can be divided into several steps.

4.1.1.1 Prerequisites

Before the simulation starts, certain prerequisites need to be set, such as the scenario, network layout and antenna array parameters.

- **Scenario:** Various simulation environments can be chosen. Depending on the selected scenario, measurement campaigns conducted in that specific environment provide the statistical data used in the model. Possible simulation environments include urban macrocell (UMa), urban microcell (UMi), backhaul, vehicle-to-vehicle (V2V), indoor industrial scenarios and other specific scenarios detailed in [49]. For the simulations in this thesis, the UMi street canyon scenario is used, capturing real-life scenarios in a city or station square. The gNBs are positioned at a height of approximately 10 meters (below the rooftop level of surrounding buildings). The receiver height ranges from 1.5 to 2.5 meters, simulating pedestrians walking on the sidewalk.

- **Antenna modelling:** Uniform rectangular panel array antennas are used. In this thesis, only single panel antennas are used, which may or may not be polarized. The antenna elements within the panel are spaced evenly.

- **Network layout:** The network layout will be presented in the following section.

4.1.1.2 Large Scale Parameter Calculation

The second step of calculating the received signal power involves computing large scale parameters such as pathloss, delay spread, angular spread and shadow fading.

- **LOS probability:** The 3GPP channel model uses a LOS probability calculated based on the simulation scenario and the distance between the UE and gNB, as per the equations in [49]. The Pathloss is separated into LOS and non line of sight (NLOS), calculated using the equations in [49]. Factors considered include the propagation distance, operational frequency, and the heights of the UE and gNB.

- **Other parameters:** Delay spread and angular spreads are generated randomly while still considering the simulation scenario.

4.1.1.3 Small Scale Parameter Calculation

In a next step, small scale parameters such as cluster delay, cluster power, and arrival and departure angles need to be calculated.

- **Cluster delays:** General cluster delays are assigned randomly using a delay distribution from Table 7.5-6 [49]. By definition, the LOS link is the cluster with the lowest delay.

- **Cluster powers:** Cluster powers are calculated based on the cluster delay using an exponential delay distribution.

- **Arrival and departure angles:** Arrival and departure angles for azimuth and elevation, as well as the initial phases, are determined randomly.

4.1.1.4 Channel Coefficient Calculation

Using all the parameters, the channel coefficients for each of the N clusters, where a cluster represents a group of multipath components with similar delay and angle characteristics, and each receiver/transmitter element pair can be calculated. The channel matrices are divided into LOS and NLOS channel matrices.

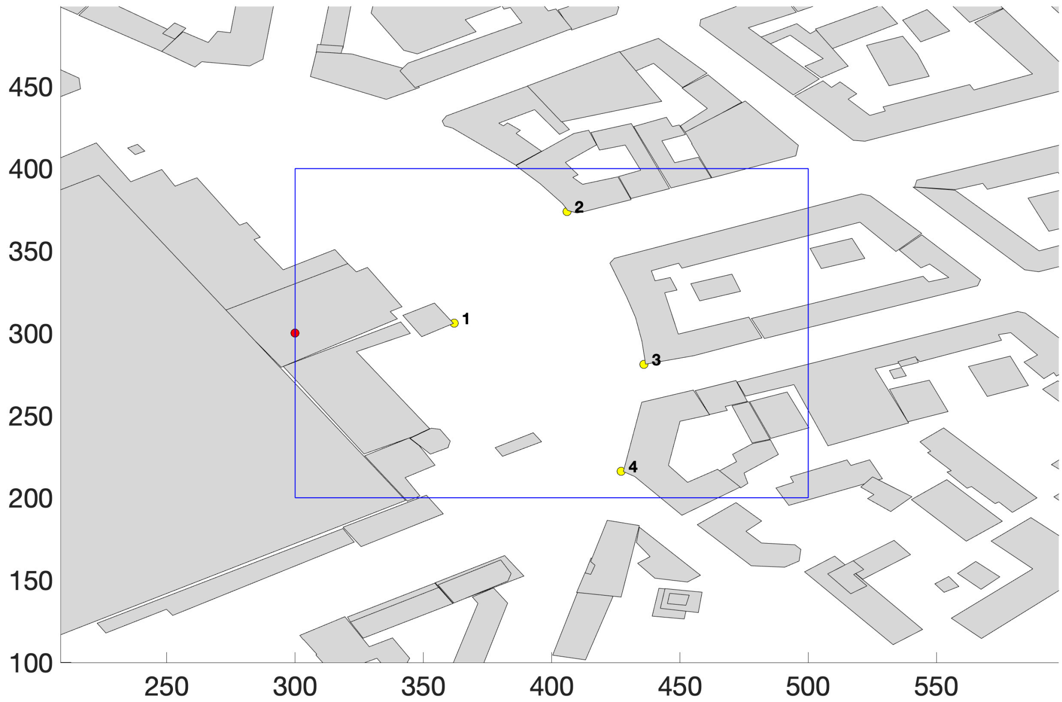

FIGURE 4.1: Network deployment of the simulation scenario near Frankfurt am Main main station.

4.1.1.5 Spatially-Consistent UE/gNB Mobility Modeling

The 3GPP channel model also includes spatially-consistent UE/gNB mobility modeling. In this model, the random parameters simulating small-scale fading are varied within a predefined range, ensuring consistency with the previously calculated channel state. This approach shortens channel calculations as not all parameters need to be recalculated at each time instance, maintaining the stability of the channel model and avoiding abrupt changes due to complete recalculations. The channel model is accessed through the *NrSpectrumPhy* instances.

4.1.2 Simulation Environment and network deployment

The simulation environment is a `200 m × 200 m` area located east of the main train station in Frankfurt am Main, Germany, and is outlined by a blue square in Fig. 4.1. This environment, characterized by a high density of pedestrians requesting significant mobile data, is ideal for a 5G-NR study with SU-MIMO and corresponds to the UMi scenario chosen in the 3GPP channel model. The gNBs are positioned at the corners of buildings at a height of 10 m, depicted as blue dots in Fig. 4.1. The red dot symbolises the LTE coordinator, which is responsible for managing handovers and control signals.

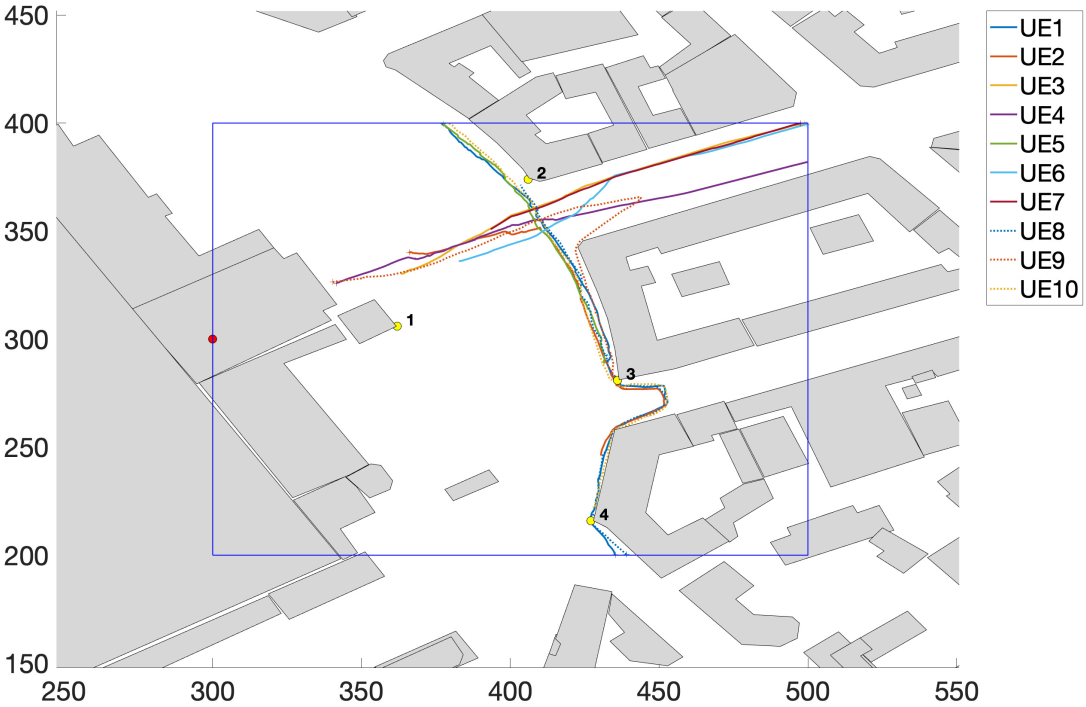

FIGURE 4.2: Walk paths for 10 UEs in the simulation environment with a duration of 100 s.

4.1.3 UE Mobility Setup

The realistic pedestrian simulation software *Viswalk* was used to generate the UE walking paths for the simulation. *Viswalk* utilizes a realistic 3D map of the environment, including details such as the locations of crosswalks and traffic lights, to create accurate pedestrian walking data. The time resolution of the walking path data is 250 ms, with an average movement speed of 1 m/s. A set of 10 UEs was chosen to limit the simulation time to a reasonable duration as activating SU-MIMO with a larger number of UEs significantly increases the simulation time. An area of `200 m` × `200 m` was chosen to obtain a high user density. The simulation time was set to 100 s to ensure that each UE experiences varying channel conditions along its walkpath and potentially trigger beam management events. The final walkpaths are shown in Fig. 4.2. The height of the UEs transmit and receive antennas is set to 1.5 m.

4.1.4 Simulation Parameters

The main parameters used in the simulation are displayed in Table 4.1 and are based on the simulations presented in [41]. The carrier frequency is set to 28 GHz, corresponding to the lower available spectrum of FR2. The total bandwidth is set to 400 MHz with a single BWP, simulating high data rate communication of 1 Gbps to 2 Gbps. Both the gNB and UE transmit powers are set to 45 dBm. The chosen 5G-NR numerology is $\mu = 3$. The SCS is calculated to be 120 kHz using 2.7.

The beam step value in the horizontal plane is set to 18° for UEs and 9° for gNBs. In the elevation plane, it is set to 30° for both UEs and gNBs. The horizontal range that needs to be covered by UEs and gNBs ranges from 0° to 180°, resulting in a total of 11 and 21 horizontal sectors, respectively. The elevation range for UEs spans from 30° to 90°, and for gNBs, from 90° to 150°, resulting in 3 elevation sectors for both. The total sectors that need to be covered are 33 for UEs and 63 for gNBs.

A single SS burst can transmit a maximum of 64 SSBs, enough to cover all 63 gNB sectors. To complete a beam sweep, 33 SS bursts need to be sent, one for each UE sector. With an SS burst duration of 20 ms, the beam sweep duration is calculated to be 660 ms using 2.5.

For all simulations, user datagram protocol (UDP) traffic with a constant bit rate (CBR) of either 1000 Mbps or 2000 Mbps is used. The packet size is set to 1400 bytes. The scheduler policy used is TDMA round-robin. At the start of the simulation, a UDP source is set up on a remote host linked to the evolved packet core (EPC). This connection experiences a latency of 5 ms, reflecting typical routing and computational delays.

	Parameter	**Value**
PHY & Link Layer	Carrier frequency	28 GHz
	Bandwidth	400 MHz
	TX power	45 dBm
	Numerology	3
	SCS	120 kHz
	UE horizontal granularity	18°
	gNB horizontal granularity	9°
	UE vertical granularity	30°
	gNB vertical granularity	30°
	UE sectors	33
	gNB sectors	63
	Number of SSBs per SS burst	64
	SS burst duration	20 ms
	Beam search duration	660 ms
	UE antenna	4×4
	gNB antenna	8×8
	UE polarization slant angle	90°
	gNB polarization slant angle	0°
MAC & Upper Layers	Transport layer protocol	UDP
	CBR	1 Gbps / 2 Gbps
	Scheduler policy	TDMA round-robin

TABLE 4.1: Simulation Parameters.

4.1.5 SU-MIMO Configurations

Two distinct antenna configurations are used to perform SU-MIMO in the simulation. In both configurations, a single-panel 2-port codebook is employed for precoding, utilizing an exhaustive search to determine the optimal PMI and RI. The antenna dimensions are 8×8 for the gNB and 4×4 for UEs in both cases.

1. **Polarization:** Each antenna element is superposed with another antenna element of different polarization, effectively doubling the total number of antenna elements from 16/64 to 32/128 for UEs/gNBs. The two groups of antenna elements, distinguished by their polarization, are connected to separate RF chains. The polarization slant angles for the gNB and UE are set to 0° and 90°, respectively.

2. **Port:** The number of horizontal ports is set to two, and the number of vertical ports is set to one. This configuration divides the antenna elements on the single panel horizontally into two groups, each with its own RF chain, while keeping the total number of antenna elements constant.

For reference, a configuration with no polarization and both horizontal and vertical ports set to one was used. This configuration has no SU-MIMO capabilities and only a single RF chain.

4.2 BEAM MANAGEMENT STRATEGIES

4.2.1 *Threshold-Based Beam Management*

The beam management operations are based on two different SNR thresholds as presented in [41]:

- γ_{RLF} = -5 dB,
- γ_{MR} = 22.7 dB,

The RLF threshold is represented byγ_{RLF}. If a UE experiences an SNR below γ_{RLF}, the link quality is considered insufficient for communication, and it is treated as a RLF. This information is shared by the coordinator with the gNB, and the UE gets deregistered. To recover the communication link, an initial access procedure is initialized.

The maximum achievable data rate using the highest supported modulation and coding scheme (MCS) is represented by γ_{MR}. If a UE's SNR is between γ_{RLF} and γ_{MR}, several beam management events can occur. Firstly, it is checked if there is a better BPL among those monitored by CSI-RSs. If so, either a beam switch (better BPL on the serving gNB) or a fast handover (better BPL on another candidate gNB) is performed. If no better BPL is found, a beam sweep is conducted, which could lead to a handover. Additionally, a variable time-to-trigger handover procedure is implemented. The coordinator schedules a handover for a certain time in the future, with the wait time decreasing as the SNR difference between the target gNB and the current gNB increases. However, if the current link stabilizes during the wait time, the handover is not executed.

UEs with an SNR above the γ_{MR} threshold experience no beam management events. However, if the serving gNB is congested and a non-congested candidate gNB is available, the LTE coordinator can initiate a fast load-balancing handover.

4.2.2 Strategies

Several parameters essential for the described beam management procedures are configurable. The number of monitored BPLs is fixed at 4, but the number of BPLs monitored from gNBs other than the serving one can be set from 0 to 4. Load balancing can be enabled or disabled. The refreshing of the BPLs monitored by CSI-RSs via periodic SSB transmissions can also be enabled or disabled. The strategies used for the simulations are presented below:

- **Strategy 1: default 5G-NR RLM** This corresponds to the default 5G-NR beam management strategy presented in Section 3.2.5. No BPLs from cells other than the serving one are monitored, making load balancing operations impossible, as they require information on the link quality of candidate gNBs. Additionally, periodic SSB transmissions to update CSI-RSs are disabled.
- **Strategy 2: flexRLM** This corresponds to flexRLM as presented in Section 3.2.5 of this thesis. Two BPLs from other candidate gNBs are monitored, and the monitored BPLs are refreshed through periodic SSB transmissions. The load balancing functionalities are disabled.

4.3 SIMULATION SCENARIOS

This section presents the two scenarios evaluated for this thesis. All scenarios share the parameters listed in Table 4.1 and the simulated environment depicted in Fig. 4.1. The number of UEs and the CBR vary across these scenarios.

4.3.1 Scenario 1

The first scenario simulates the effects of SU-MIMO on a single UE. The walk path is shown in Fig. 4.3. The simulation was conducted with the two SU-MIMO configuration presented in Section 4.1.5. As a reference, a simulation with no SU-MIMO was also conducted. Additionally, for each SU-MIMO configuration, the simulation was performed with default 5G-NR RLM and flexRLM. The simulations duration is 100 s, allowing the UE to travel a significant distance and experience multiple beam management events, enabling the analysis of the performance of the different beam management strategies. This scenario was simulated with a CBR of 1000 Mbps and then with a CBR of 2000 Mbps to simulate users with varying high data rate requirements and to showcase the high throughput capabilities of SU-MIMO. This scenario aims to demonstrate the functionality of SU-MIMO and the resulting throughput advantages. Additionally, it compares the two beam management strategies and analyses their interaction with the SU-MIMO configurations.

4.3.2 Scenario 2

The second scenario simulates the effects of SU-MIMO in a multi-user environment. The walk paths of the 10 UEs are shown in Fig. 4.2. The same SU-MIMO configurations and beam management strategies used in *Scenario 1* are applied here. The simulation time is also set to 100 s. The CBR requested by the UEs is set to 1000 Mbps.

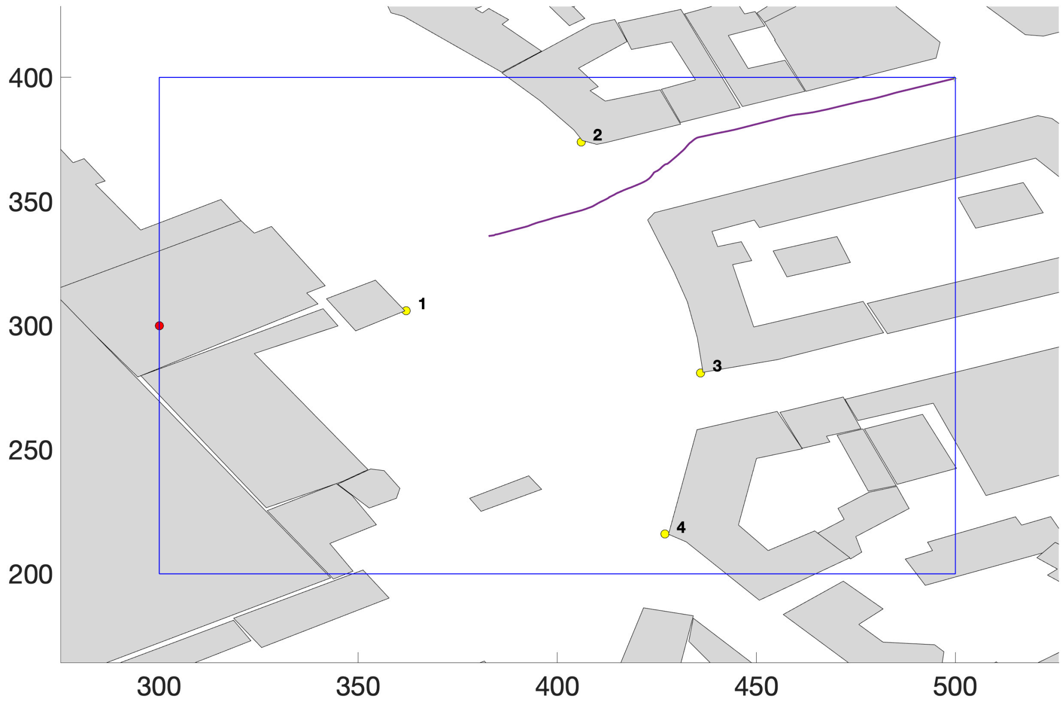

FIGURE 4.3: Walk path for the single UE simulation with a duration of 100 seconds.

Each gNB in the network can provide a maximum throughput of 1.2 Gbps, which is only enough to provide a single UE with the requested data rate. The limitation arises because there are 14 OFDM symbols in a slot, and each symbol can approximately provide 100 MHz of bandwidth, but two symbols need to be reserved for control messages. This scenario is particularly interesting as it examines the performance and behavior of SU-MIMO in a highly loaded network where multiple users compete for limited resources. It aims to demonstrate how different beam management strategies cope with such high demand and how effectively SU-MIMO can enhance throughput in a congested environment. By analyzing this scenario, we can understand the strengths and weaknesses of the beam management strategies and SU-MIMO configurations under heavy network load, providing insights into their practical applicability in real-world multi-user settings.

4.4 PERFORMANCE EVALUATION METRICS

The end-to-end performance of the scenarios described in Section 4.3 is evaluated according to the following metrics:

1. **Throughput:** The throughput in a network is the amount of data successfully transferred from one point to another in a given amount of time, measured in Mbps. Throughput can be measured at different layers of the protocol stack; in this thesis, throughput at the UDP, IP, and MAC layers is considered. For the UDP and IP layers, the sum of the bytes passing is periodically record and divided by the time interval. MAC throughput is only logged when an actual

transmission takes place. Throughput can be influenced by several factors, including channel quality, requested data rate, and the use of SU-MIMO.

2. **Link Quality:** The link quality is represented by the SINR, which is crucial for the threshold based operations. Beam management events are triggered based on the estimated SINR, making it an important metric for assessing link quality.

3. **Beam Management Events:** The beam management events are analyzed based on their quantity, frequency, and type. Additionally, the causes of specific beam management events are examined to understand their triggers and implications.

5

Results

This chapter presents and analyzes the results of the two simulation scenarios described in Section 4.3. Section 5.1 explores the impact of two SU-MIMO configurations on network throughput and SINR experienced by a single UE, and compares the beam management strategies discussed in Section 4.2. Section 5.2 examines the effects of SU-MIMO configurations in a multi-user environment, focusing on network throughput and SINR at the UE, with a further comparison of the beam management strategies from Section 4.2.

5.1 Scenario 1: Single-User Simulation

The first scenario features a single UE simulated for a duration of 100 s. Separate simulations were conducted for the UE requesting a data rate of both 1 Gbps and 2 Gbps. Additionally, separate simulations were performed for each configuration: port, polarization, and no SU-MIMO (*cf.* Section 4.1.5). Each beam management strategy from Section 4.2 was also tested independently, bringing the total number of simulations to 12.

Section 5.1.1 compares the different SU-MIMO configurations using flexRLM with the UE requesting 1 Gbps data rate. Section 5.1.2 repeats this comparison with the UE requesting 2 Gbps data rate. Finally, Section 5.1.3 contrasts flexRLM and default 5G-NR RLM with 2 Gbps data rate requested, specifically for the port and no SU-MIMO configurations. Each section evaluates the network throughput and the SINR experienced by the UE.

5.1.1 SU-MIMO Configurations with 1 Gbps requested

5.1.1.1 Link Quality

Fig. 5.1 presents the instantaneous SINR, cell ID, and triggered beam management events for the polarization, port, and no SU-MIMO cases for the simulated UE. The red and green dots represent beam sweeping events, with red dots indicating events initiated by the UE and green dots indicating those triggered by the LTE coordinator. The blue dots depict beam switches performed using the monitored BPLs. Upon close inspection of the instantaneous SINR graphs, it is evident that an exhaustive beam search initiated by the UE is performed at the beginning of each simulation, corresponding to the IA procedure. After approximately 680 ms, the UE connects to its first cell, and data transmission begins.

Fig. 5.2 shows the estimated SINR for the simulated UE over time at the cells 1, 2, 3, and 4 with blue, red, green, and yellow lines respectively. This estimated SINR is used in combination with the beam management thresholds (*cf.* Section 4.2.1) to initiate beam management operations. Together, these graphs illustrate the experienced SINR

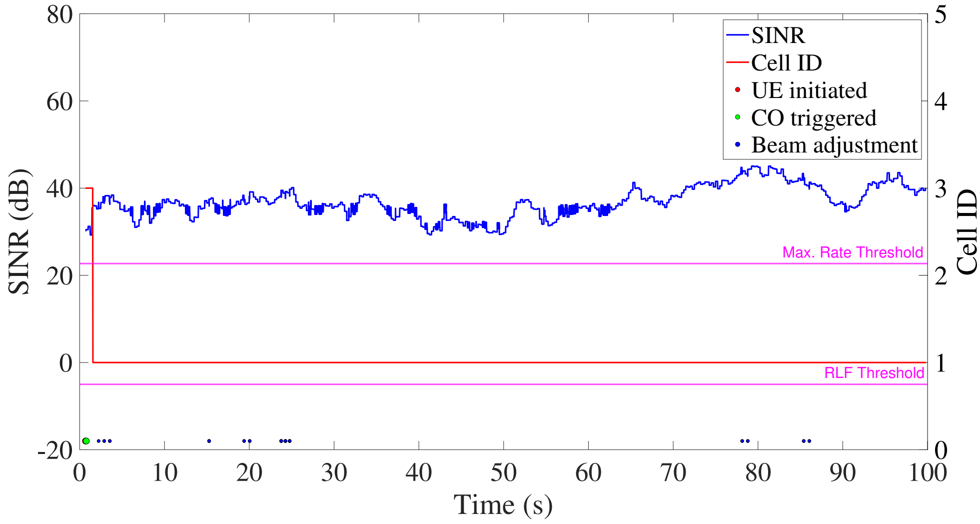

(a) No SU-MIMO

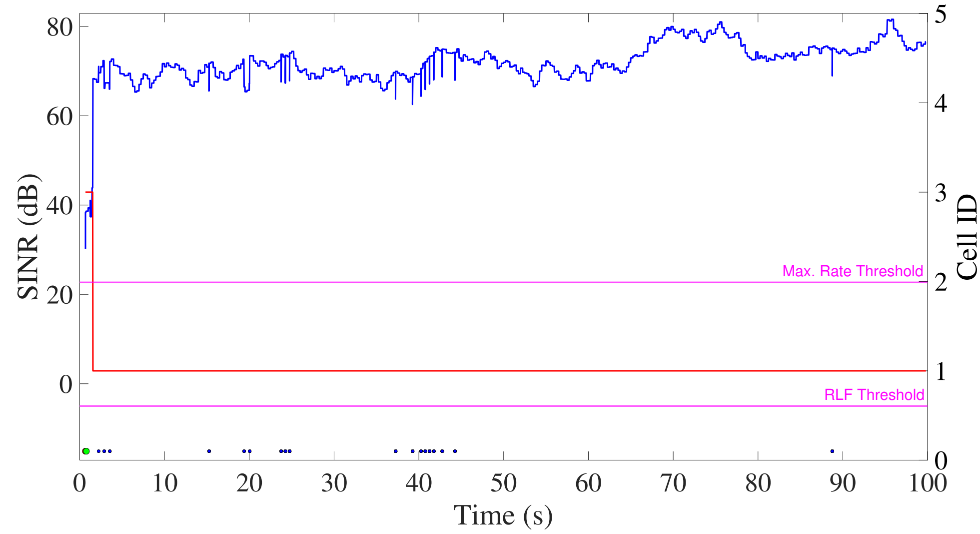

(b) Polarization

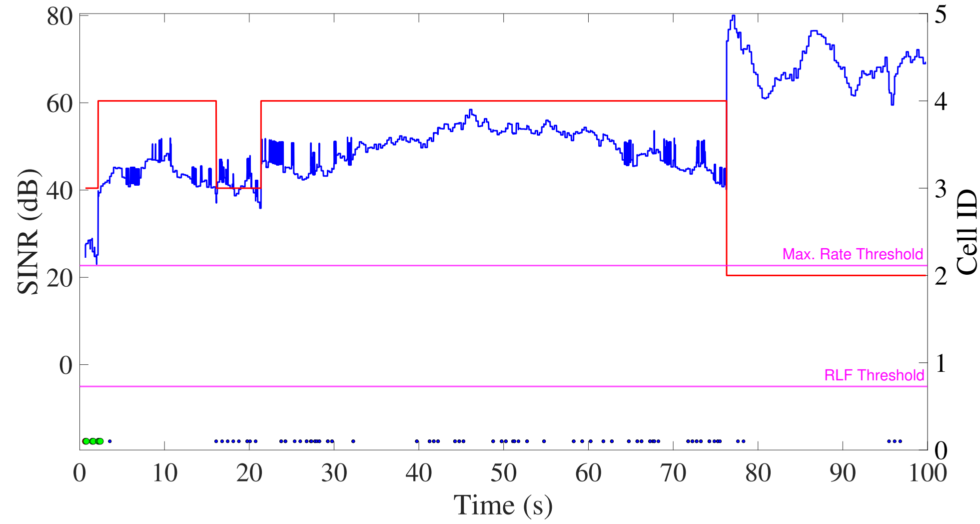

(c) Port

FIGURE 5.1: Instantaneous SINR graphs of the simulated UE for (a) no SU-MIMO, (b) polarization, and (c) port configuration with 1 Gbps requested and flexRLM.

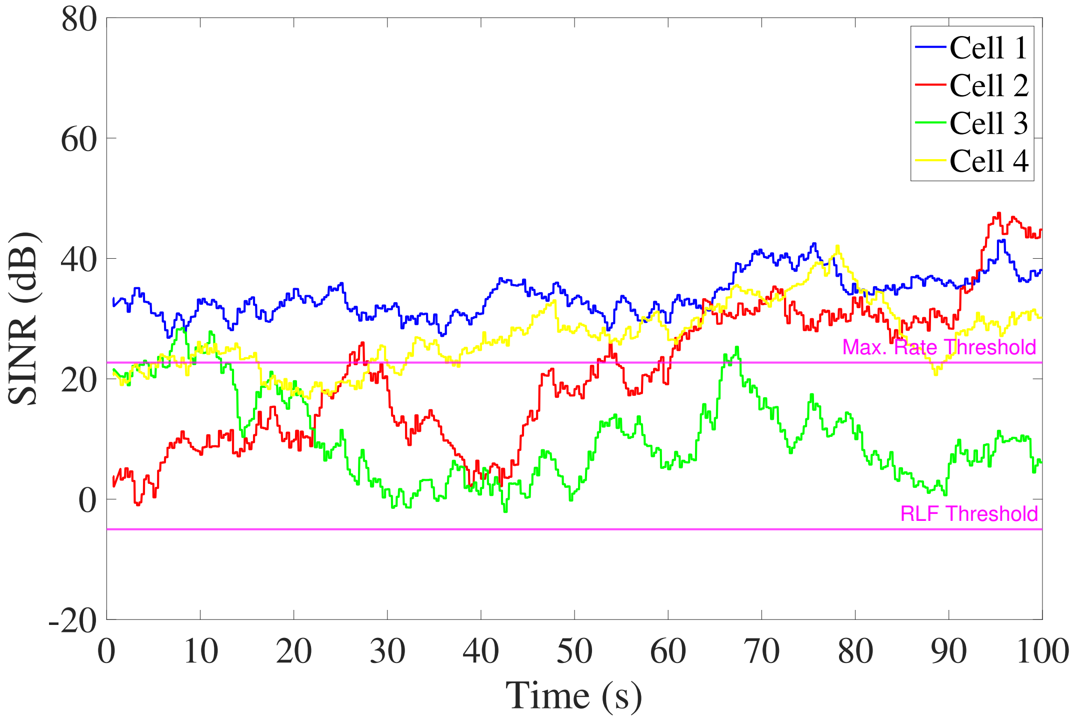

FIGURE 5.2: Estimated SINR graph of the simulated UE for all 4 cells in the polarisation configuration with 1 Gbps requested and flexRLM.

at the UE throughout the simulation and provide an explanation for the initiated beam management events.

First, we compare the no SU-MIMO case (Fig. 5.1a) with the polarization case (Fig.5.1b). In both simulations, the UE connects to the same cells throughout the simulation. Initially, the UE connects to cell 3, but due to an estimated SINR below the maximum rate threshold, depicted by the green line in Fig. 5.2, the LTE coordinator initiates a beam sweep at 0.78 s. After a time of 780 ms, which corresponds to the beam sweep and handover duration, the UE connects to cell 1. At cell 1 the estimated SINR, depicted by the blue line in Fig. 5.2, constantly remains above the maximum rate threshold, preventing further beam sweeps and handovers.

Despite identical connected cells, the instantaneous SINR levels differ significantly. The general curvature is roughly the same, however the polarization configuration achieves higher SINR values, with a mean SINR at 72 dB compared to 37 dB for no SU-MIMO. This substantial difference results from the doubled antenna elements increasing the antenna gain in the polarization case. In both cases the SINR is stable with limited variance around 40/70 dB. The number of beam switch events is relatively low in both cases, with 13 for no SU-MIMO and 18 for polarization, corresponding to 7.8 and 10.8 switches per minute, respectively. This is due to the UE's walk path towards base station 1 (Fig. 4.3), which minimizes the need for frequent beam changes.

Next, we compare the link quality and beam management decisions of the no SU-MIMO configuration with the port configuration. This comparison is more com-

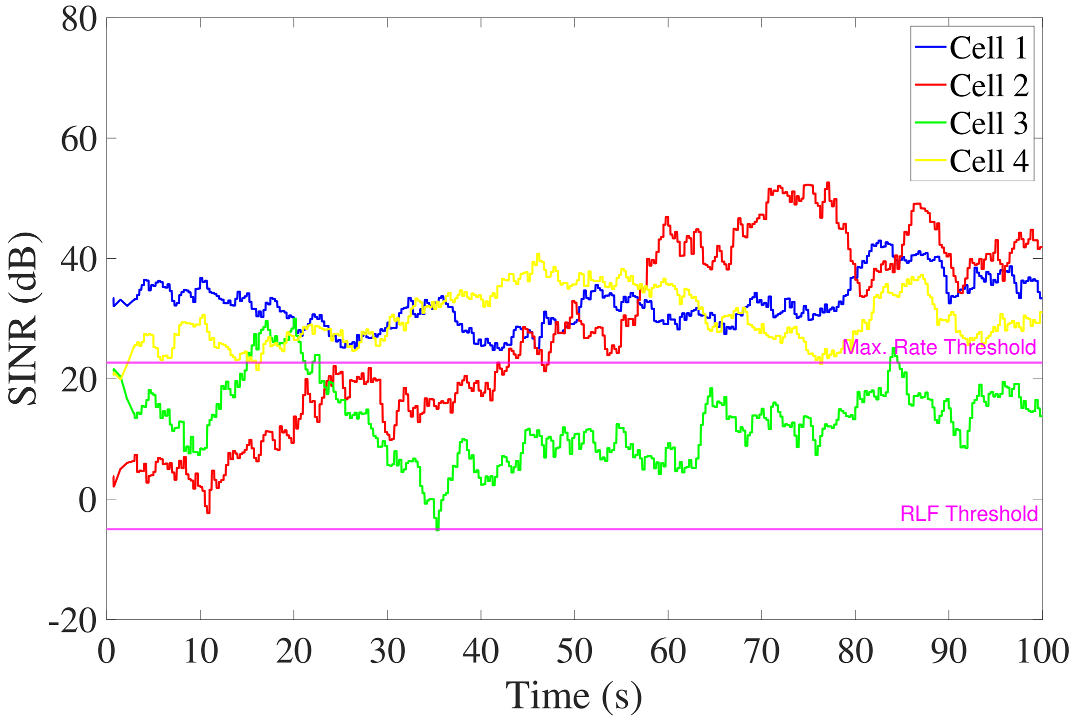

FIGURE 5.3: Estimated SINR graph of the simulated UE for all 4 cells in the port configuration with 1 Gbps requested and flexRLM.

plex due to different serving cells throughout the simulation. Both simulations initially connect to cell 3. However, in the port case, the UE connects to cell 4 following a beam sweep at 2.4 s, while in the no SU-MIMO case, it connects to cell 1. This difference stems from the channel model's inherent randomness, leading to variations in large scale parameters between simulations. Due to this initial difference in serving cells, the beam management events differ significantly between the two simulations. In the no SU-MIMO case, the estimated SINR of serving cell 1 consistently remains above the maximum rate threshold, so the coordinator or UE does not initiate any beam sweeps, and the connection to cell 1 is maintained. In contrast, in the port case, around 16 s, the estimated SINR drops below the maximum rate threshold, as seen in Fig. 5.3 with the yellow line, but no beam sweep is initiated. This is because one of the monitored BPLs of a candidate cell provides sufficient link quality, leading to a fast handover to cell 3 without the need for a beam sweep. Similar handovers occur from cell 3 to cell 4 at 21.4 s and from cell 4 to cell 2 at 76.3 s. This final cell provides a significantly higher SINR of up to 80 dB compared to cell 1 in the no SU-MIMO case, due to its close proximity to the UE's walk path (Fig. 4.3).

The mean SINR in the port case is with 53 dB, higher than the 37 dB in the no SU-MIMO case. However, this does not conclusively indicate a general SINR improvement with the port configuration due to the differing serving cells. The port case also experiences more beam switches (61 total) compared to the no SU-MIMO case (13 total), attributable to alignment issues with cells 2, 3, and 4 being perpendicular to the UE's walk path.

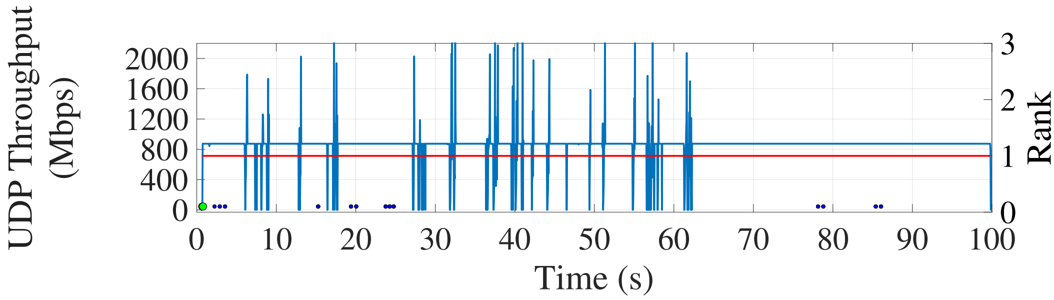

(a) UDP

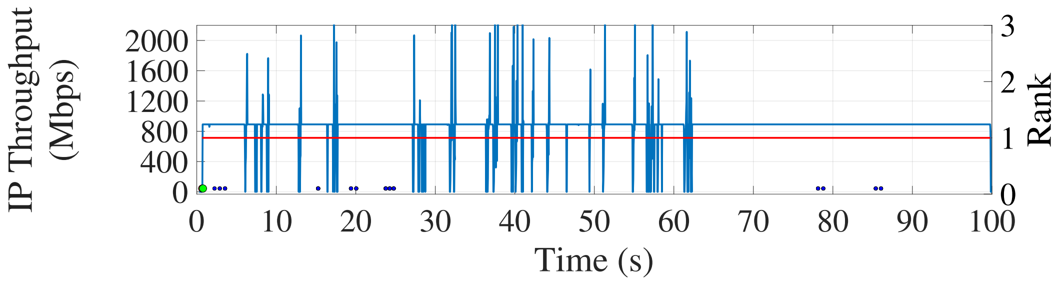

(b) IP

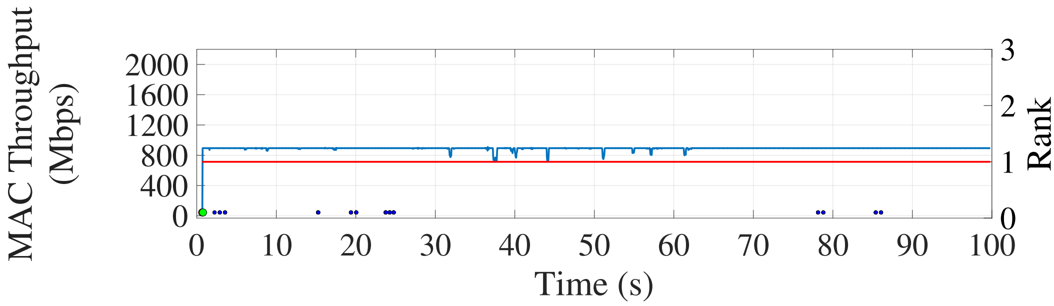

(c) MAC

FIGURE 5.4: Throughput graphs of the simulated UE for no SU-MIMO at the (a) UDP, (b) IP, and (c) MAC layer with 1 Gbps requested and flexRLM.

5.1.1.2 Throughput

Throughput can be logged at different layers of the protocol stack. Fig. 5.4 compares the throughput data from the MAC (Fig. 5.4c), IP (Fig. 5.4b), and UDP (Fig. 5.4a) layers for the no SU-MIMO configuration. The blue lines represent the throughput in Mbps over time, while the red lines indicate the rank over time, synonymous with the amount of streams used at any given time. Similar to the instantaneous SINR graphs, the blue, red, and green dots represent beam switches, beam sweeps initiated by the UE, and beam sweeps initiated by the coordinator, respectively. Up until 680 ms, the throughput is 0 Mbps because the UE is not connected to any cell yet. After IA, all three layers show a constant throughput of around 894.1 Mbps (MAC), 891.4 Mbps (IP), and 873.9 Mbps (UDP), respectively. There is a gradual decrease in throughput for higher layers in the protocol stack, due to the increased likelihood of packet integrity degradation and error detection at higher layers. Although the general shape of all three graphs matches, spikes are observed in the IP and UDP throughput graphs. Downward spikes result from failed packet transmissions, while upward spikes result from successful HARQ re-transmissions occurring right after the failed transmissions. The MAC layer does not show throughput dropping to zero during failed transmissions because it only logs throughput upon successful transmissions. By examining the location of the spikes and comparing them with the instantaneous SINR graph in Fig. 5.1a, it becomes evident that the spikes occur when the channel experiences rapid variation. This variation is represented by a thicker blue line indicating fluctuations in instantaneous SINR. The first rapid variation occurs at 6 s, with a corresponding downward spike in the throughput graph at 6.1 s. Further variations and corresponding spikes are observed at 7.3 s, 8 s, and 8.8 s. These variations are likely caused by the channel model, resulting in errors during packet transmission. To maximize the information obtained from the throughput graphs, IP throughput is used throughout the remainder of this thesis, as it is one of the graphs that clearly depicts the spikes.

The purpose of SU-MIMO is to increase the achieved throughput by sending multiple streams simultaneously. To compare the effects of different configurations, it is essential to examine the throughput graphs. Fig. 5.5, shows the IP throughput graphs for the no SU-MIMO (Fig. 5.5a), polarization (Fig. 5.5b), and port (Fig. 5.5c) configuration, with the blue line representing throughput in Mbps over time and the red line indicating the current rank used.

All three configurations show a constant throughput of 866 Mbps (no SU-MIMO), 885 Mbps (polarization), and 870.3 Mbps (port). The slight differences in throughput can be explained by the frequency of spikes in each configuration. A lower number of spikes correlates with fewer packet transmission errors, thereby increasing throughput. In all three cases, SINR remains above the maximum rate threshold throughout the simulation, allowing the highest MCS to be used consistently, resulting in similar throughput levels. SU-MIMO does not seem to impact throughput through the simultaneous transmission of two streams. Rank two is used throughout the entire polarization simulation and the majority of the port simulation. During the first two seconds of the port simulation, the UE is connected to cell 3, where SINR fluctuates between 23 dB and 29 dB, which is insufficient to consistently support rank two transmissions. The use of rank two does not double the throughput because a single stream is sufficient to serve the requested 1000 Mbps. The polarization configuration shows no spikes in the throughput graph, which can be explained by the absence of increased SINR variation (thicker blue line) as seen in Fig. 5.1b. Since these variations cause spikes, their absence in the SINR graph results in a smooth throughput graph for the polarization case.

In summary, the polarization configuration significantly increases SINR due to the doubling of antenna elements, resulting in higher antenna gain. The port configuration also shows a slightly higher SINR than the no SU-MIMO configuration, but direct comparison is complicated by variations in serving cells. The throughput is slightly increased in the two SU-MIMO configurations due to SINR stability, rather than the use of two streams, since a single stream is sufficient to serve the requested 1000 Mbps. To fully understand the potential of SU-MIMO, it is crucial to evaluate scenarios with higher requested data rates that cannot be served by a single stream. Therefore, the

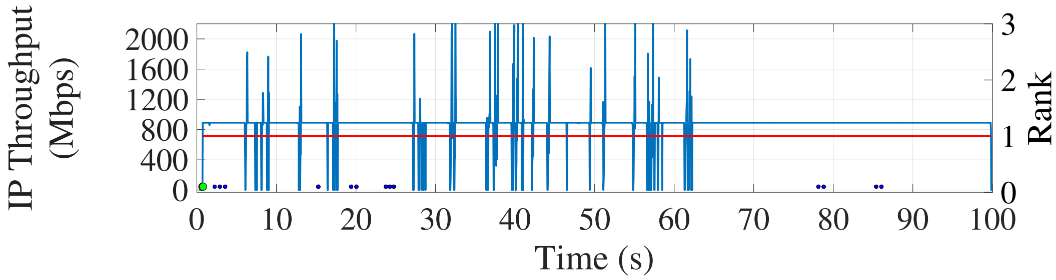

(a) No SU-MIMO

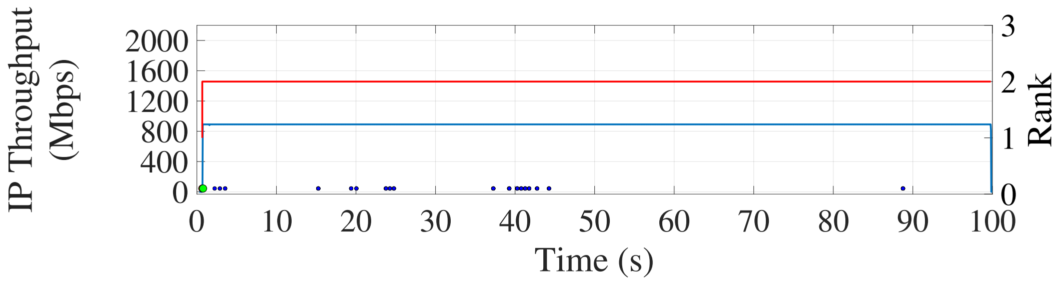

(b) Polarization

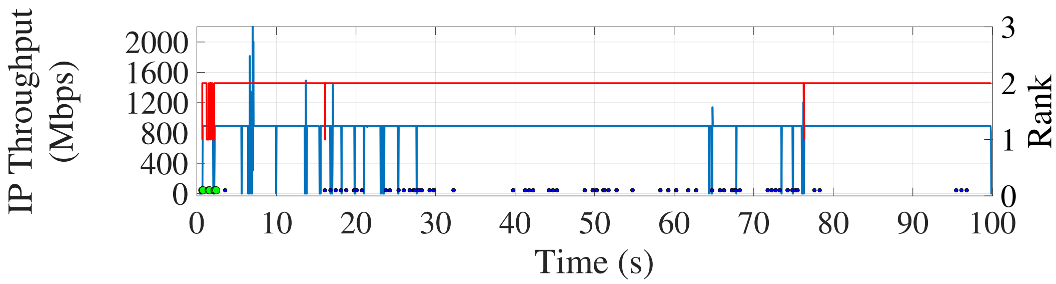

(c) Port

FIGURE 5.5: Throughput graphs of the simulated UE for (a) no SU-MIMO, (b) polarization, and (c) port configuration with 1 Gbps requested and flexRLM.

simulation is repeated with a requested data rate of 2000 Mbps, which surpasses the 1200 Mbps that each cell can serve.

5.1.2 SU-MIMO Configurations with 2 Gbps requested

5.1.2.1 Link Quality

The instantaneous SINR experienced by the UE in the polarization, port, and no SU-MIMO configurations when requesting 2000 Mbps is very similar to the simulations conducted with a 1000 Mbps request. The curvature and beam management events of the no SU-MIMO , polarization, and port configurations are identical to those observed in the 1000 Mbps polarization configuration case shown in Fig. 5.1.

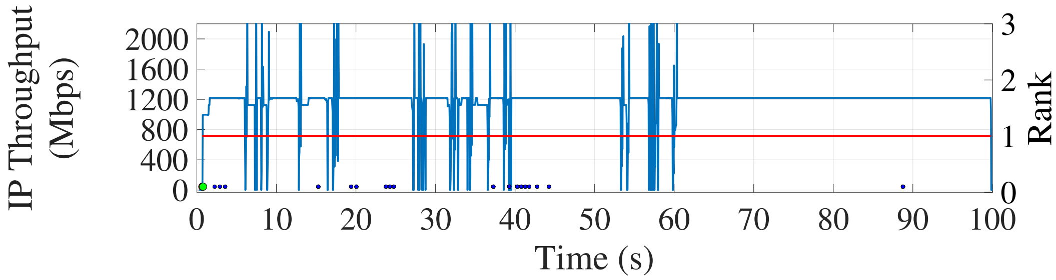

(a) No SU-MIMO

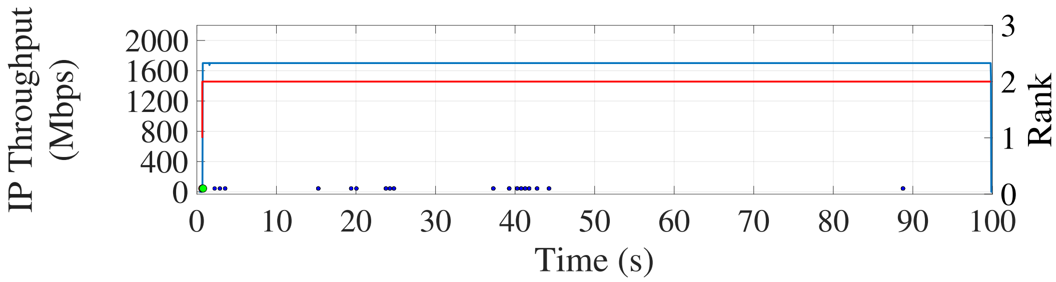

(b) Polarization

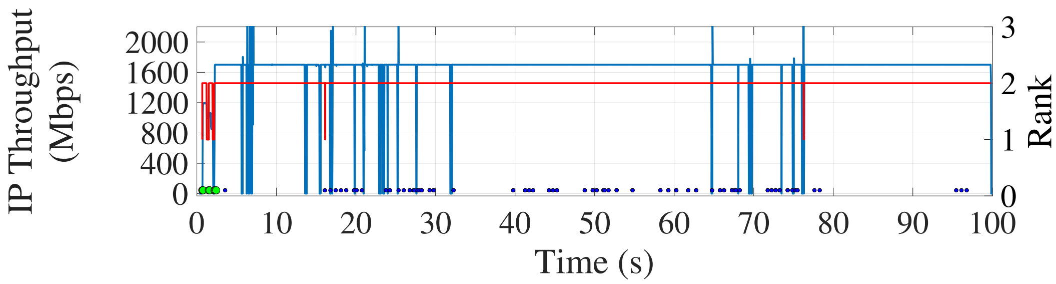

(c) Port

FIGURE 5.6: Throughput graphs of the simulated UE for (a) no SU-MIMO, (b) polarization, and (c) port configuration with 2 Gbps requested and flexRLM.

5.1.2.2 Throughput

Fig. 5.6 presents the throughput of no SU-MIMO, polarization, and port configuration. In each graph, the blue line depicts the IP throughput in Mbps over time, while the red line shows the rank used over time. Comparing these graphs highlights the impact of each configuration on IP throughput. The blue, red, and green dots represent the same beam management events as seen in the SINR graph. Overall, the throughput is stable around 1220 Mbps for the no SU-MIMO configuration and around 1700 Mbps for both the polarization and port configurations. Only the port and no SU-MIMO configurations exhibit the throughput spikes analyzed in Fig. 5.4. The instantaneous SINR in the polarization configuration remains stable around 70 dB, high enough to ensure stable throughput without spikes. As expected, the rank in the no SU-MIMO configuration can only be one. In the polarization and port configurations, rank two is maintained for most of the simulation period due to the high experienced SINR.

During the first two seconds in the port case, the instantaneous SINR is below 30 dB, causing the rank to fluctuate between one and two. This fluctuation impacts the experienced throughput, which remains below 1200 Mbps during this period, significantly lower than the mean of 1644 Mbps. Both SU-MIMO configurations show substantial throughput improvements, with the polarization configuration increasing the mean throughput by 505 Mbps (43%) and the port configuration by 458 Mbps (39%). This improvement is attributed to the use of two streams to transmit information simultaneously, nearly doubling the throughput. The no SU-MIMO case, with a mean throughput of 1186 Mbps, indicates that the single stream throughput saturates around 1200 Mbps. SU-MIMO with rank two raises this cap to approximately 1700 Mbps. The slightly lower mean throughput in the port configuration compared to the polarization configuration is explained by the lower experienced SINR, leading to more transmission errors.

In summary, both SU-MIMO configurations improve mean throughput due to SINR improvements and the use of two streams, with the polarization configuration performing slightly better than the port configuration. This demonstrates the potential of SU-MIMO to significantly enhance network performance, particularly at higher requested data rates.

5.1.3 Beam Management Strategies

This section presents default 5G-NR RLM and compares it to flexRLM, focusing on the no SU-MIMO and port configurations with the UE requesting 2 Gbps. The analysis starts with an evaluation of the link quality and beam management events for both strategies. It concludes with a comparison of throughput between the two approaches.

5.1.3.1 Link Quality

Fig. 5.7 shows the instantaneous SINR, cell ID, and triggered beam management events for the port and no SU-MIMO configurations using the default 5G-NR RLM, in contrast to flexRLM in Fig. 5.1.

Comparing Fig. 5.1a and Fig. 5.7a, it is evident that the flexRLM case exhibits less variation in instantaneous SINR and fewer handovers. In the default 5G-NR RLM simulation, UE 6 experiences handovers from cell 3 to cell 4 at 2.18 s, from cell 4 to cell 2 at 5 s, and from cell 2 to cell 4 at 9.58 s. In contrast, the flexRLM simulation has only one handover from cell 3 to cell 1 at 1.56 s. Due to the difference in serving cells, the instantaneous SINR level and curvature also differ slightly, with the default 5G-NR RLM showing a mean SINR of 43 dB compared to 38 dB in the flexRLM case. The most significant differences lie in the initiated beam management events. Default 5G-NR RLM conducts a total of 178 beam adjustments significantly more than the 13 from flexRLM. This can be attributed to the positions of cells 2, 3, and 4 relative to the walk path, requiring more beam adjustments, and the higher number of BPLs monitored in default 5G-NR, making beam switches to better links more likely. In flexRLM, a single beam sweep triggered by the coordinator results in a handover from cell 3 to cell 1 at 1.56 s, whereas default 5G-NR RLM triggers 73 beam sweeps within the first 10 s, with only a few resulting in handovers. Fig. 5.8 shows the estimated SINR at the UE over time for cells 1, 2, 3, and 4, represented by blue, red, green, and yellow

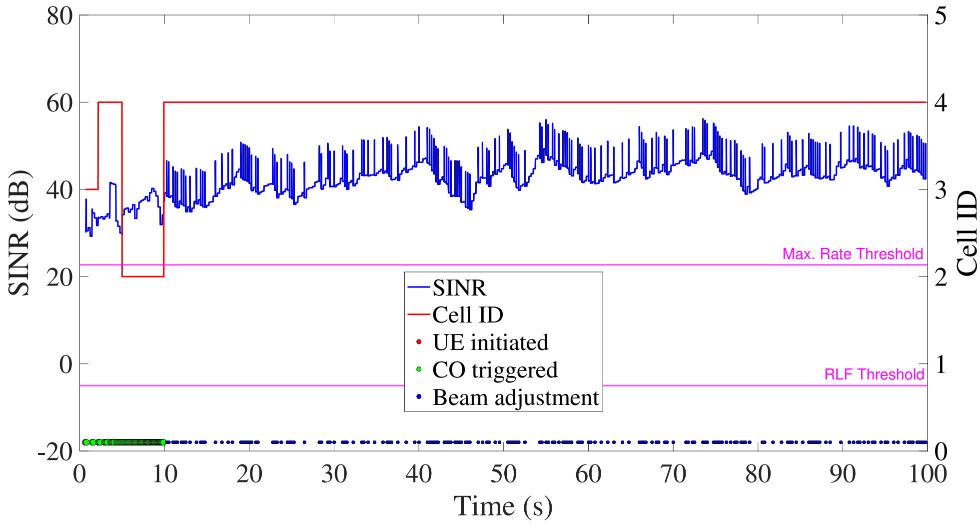

(a) No SU-MIMO

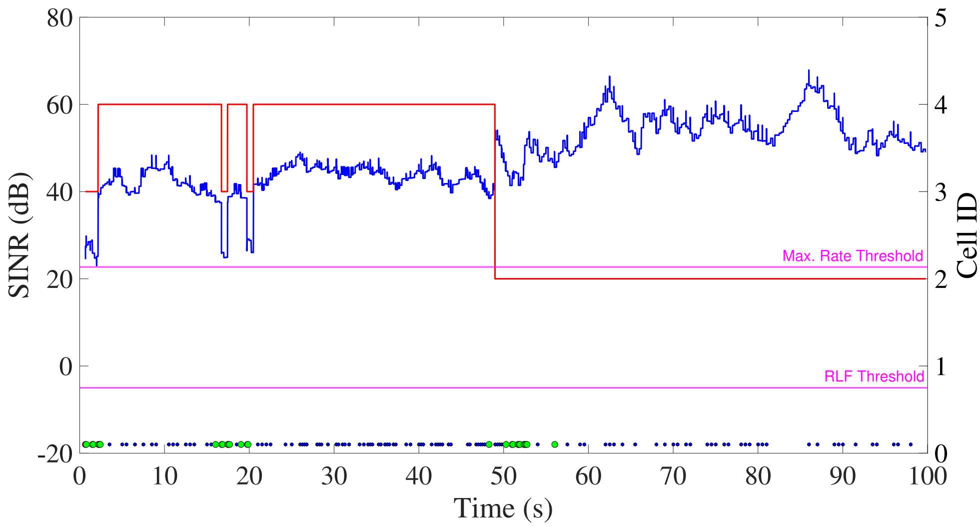

(b) Port

FIGURE 5.7: Instantaneous SINR graphs of the simulated UE for (a) no SU-MIMO and (b) port configuration with 2 Gbps requested and default 5G-NR RLM.

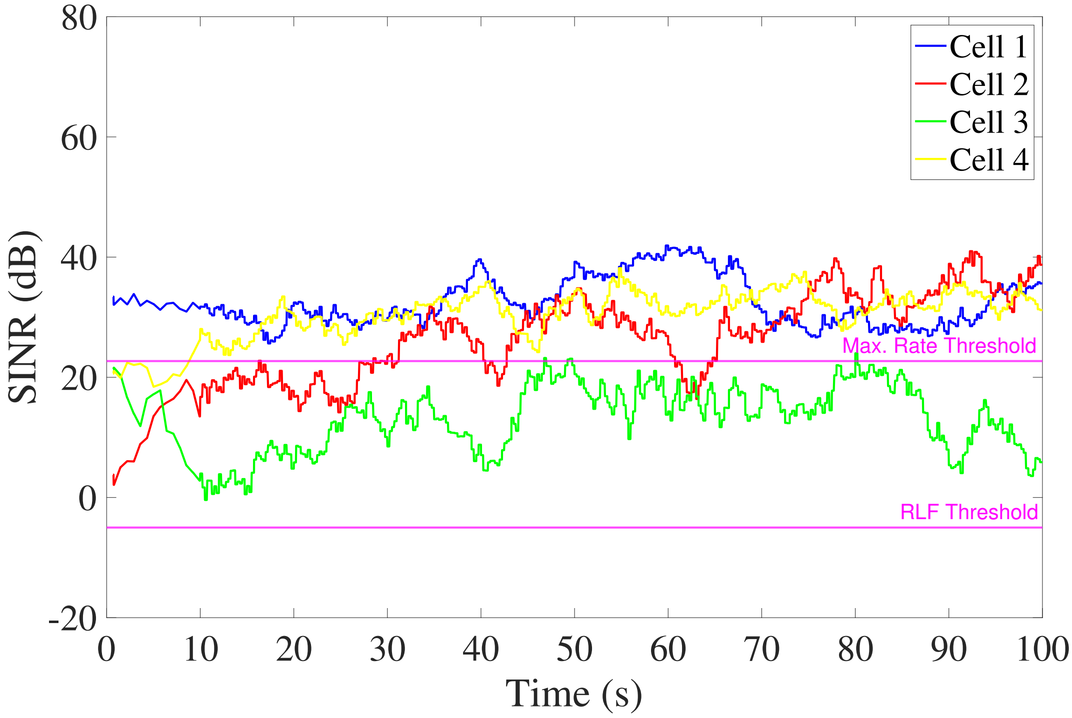

FIGURE 5.8: Estimated SINR graph of the simulated UE for all 4 cells in the no SU-MIMO configuration with 2 Gbps requested and default 5G-NR RLM.

lines, respectively. Cells 2, 3, and 4 exhibit estimated SINR levels below the maximum rate threshold from 0.78 s to 9.2 s. Cell 1, however, consistently shows an estimated SINR above the maximum rate threshold, prompting the LTE coordinator to trigger beam sweeps to initiate a handover to cell 1. This handover does not occur due to discrepancy between the estimated and experienced SINR. While the experienced SINR remains above the maximum rate threshold in the first 10 s of the default 5G-NR RLM simulation, the estimated SINR stays below it, leading to unnecessary beam sweeps. Comparing the estimated SINR of cell 1 in Fig. 5.8 with the experienced SINR in Fig. 5.1b reveals that, despite identical curvature, the SINR levels differ by approximately 4 dB. During a beam sweep, decisions on whether to initiate a handover are based on the instantaneous SINR. However, the discrepancy between the estimated and experienced SINR levels leads the coordinator to schedule unnecessary beam sweeps. These sweeps do not result in a handover because the UE is already connected to the optimal BPL according to the actual SINR. This issue complicates the evaluation of different RLM strategies, as they cannot function correctly without accurate SINR estimates. Therefore, it is crucial to adjust the SINR estimation to align with the experienced SINR to ensure proper execution of RLM strategies.

Comparing beam management events between flexRLM and default 5G-NR with the port configuration highlights the advantages of monitoring BPLs from candidate gNBs. In default 5G-NR RLM, 27 beam sweeps are performed compared to 6 in flexRLM. The number of actual handovers is similar, with 6 for default 5G-NR and 4 for flexRLM. Default 5G-NR RLM initiates beam sweeps when the estimated SINR

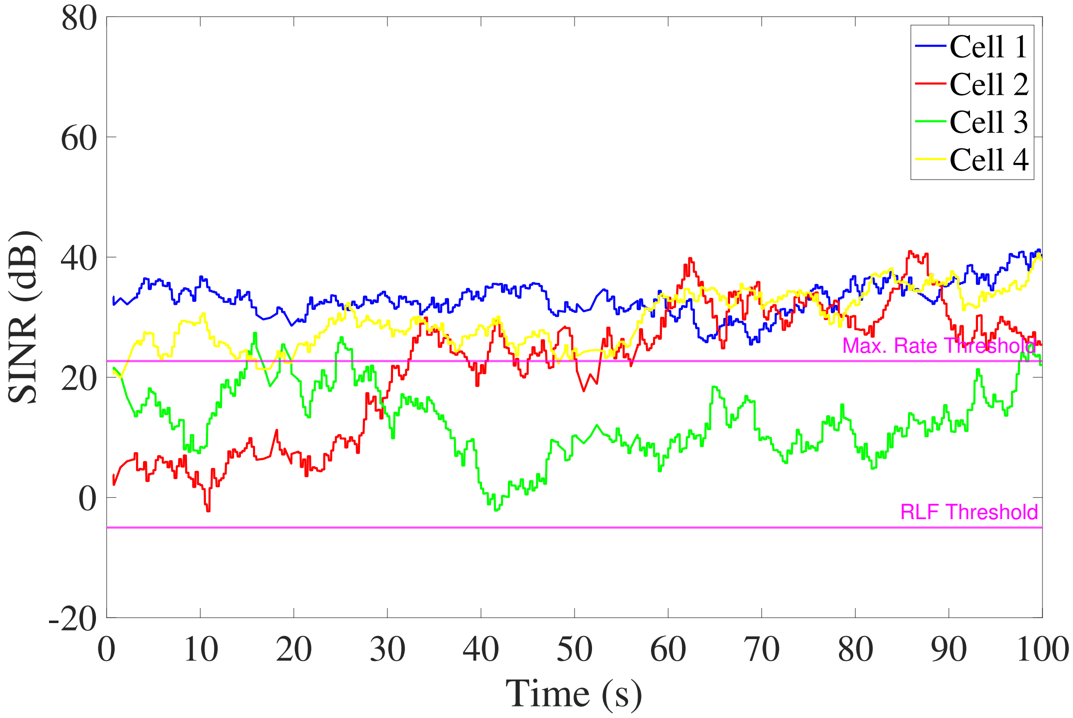

FIGURE 5.9: Estimated SINR graph of the simulated UE for all 4 cells in the port configuration with 2 Gbps requested and default 5G-NR RLM.

of the currently serving cell, depicted in Fig. 5.9, drops below the maximum threshold. For instance, at 16 s, the estimated SINR of cell 4 dips below the maximum threshold, initiating a beam sweep that results in a handover to cell 3 at 16.7 s. In contrast, in flexRLM, the estimated SINR of the currently serving cell 4 also drops below the maximum threshold at 16 s, but instead of initiating a beam sweep, a fast handover is performed to cell 3 at 16.1 s. This is possible because flexRLM monitors BPLs of candidate gNBs and checks these links when the coordinator notices a deterioration of the current link. The fast handover is 0.6 s faster than the handover involving a beam sweep and is performed at 16 s, 21.4 s, and 76 s.

5.1.3.2 Throughput

Figures 5.10 and 5.6 show the throughput for default 5G-NR RLM and flexRLM, respectively. The blue line depicts the throughput in Mbps over time, and the red line indicates the current rank. Both configurations reach the maximum data rate providable by the gNB in their specific configurations due to the overall high SINR levels. In the no SU-MIMO configuration, default 5G-NR RLM achieves a mean throughput of 1201 Mbps, while flexRLM achieves 1186 Mbps. In the port configuration, default 5G-NR RLM reaches a mean throughput of 1657 Mbps, compared to 1644 Mbps for flexRLM. The slight differences can be explained by the varying SINR levels resulting from the serving cells in each simulation.

In conclusion, the comparison between flexRLM and default 5G-NR RLM highlights several advantages of flexRLM, particularly in its ability to reduce the number

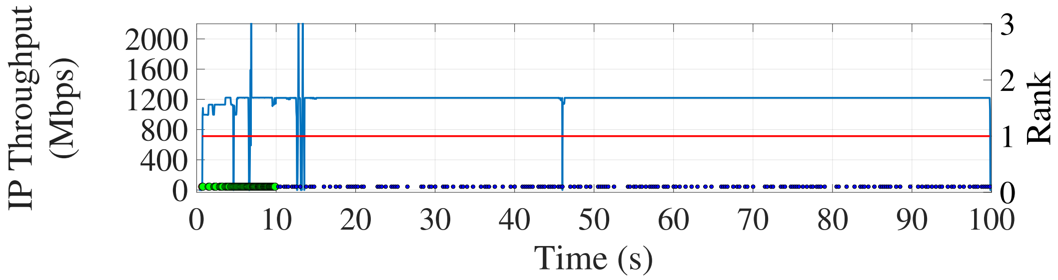

(a)

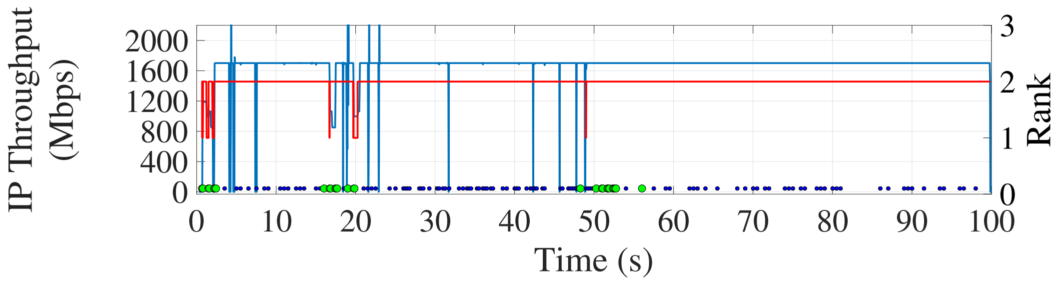

(b)

FIGURE 5.10: Throughput graphs of the simulated UE for (a) no SU-MIMO and (b) port configuration with 2 Gbps requested and default 5G-NR RLM.

of beam sweeps and faster handovers. FlexRLM's approach of monitoring BPLs from candidate gNBs allows for faster and more efficient handovers. However, a definitive comparison between the two RLM strategies is challenging due to discrepancies between the estimated and experienced SINR values. The inconsistencies in SINR estimation lead to unnecessary beam sweeps and complicate the evaluation of the RLM strategies. As such, the effectiveness of flexRLM and default 5G-NR RLM cannot be fully assessed until the SINR estimation is adjusted to align more closely with the experienced SINR. This adjustment is crucial for future comparisons to ensure accurate and reliable evaluations of different RLM strategies.

5.2 SCENARIO 2: MULTI-USER SIMULATION

The second scenario involves 10 UEs simulated over a period of 100 s. To comprehensively evaluate performance, separate simulations were conducted for each configuration: port, polarization, and no SU-MIMO, as detailed in Section 4.1.5. Additionally, each beam management strategy from Section 4.2 was independently tested, resulting in a total of 6 simulations. Each UE was set to request a data rate of 1 Gbps to simulate a highly loaded network. For reference, the exact walk paths of all UEs are depicted in Fig. 4.3.

To facilitate the analysis, several key figures are introduced. Fig. 5.12 displays box plots of SINR (dB) for different UEs, identified by their UE IDs ranging from 1 to 10. This includes all three simulated configurations: no SU-MIMO (Fig. 5.12a), polarization (Fig. 5.12b), and port (Fig. 5.12c). The blue boxes represent the interquartile range (IQR) of the SINR values, capturing the middle 50% of the data between the first quartile and the third quartile. The vertical black lines, known as whiskers, show the range of values within 1.5 times the IQR from quartile one and quartile three. Data points falling outside this range are considered outliers and are depicted as small blue dots. Inside each box, a horizontal line marks the median SINR value, indicating the midpoint of the data. Additionally, the red dot within each box represents the mean SINR value for the corresponding UE, providing an average measure of link quality.

Similarly, Fig. 5.13 presents the IP throughput in Mbps for the same set of UEs. The throughput data are shown for no SU-MIMO (Fig.5.13a), polarization (Fig.5.13b), and port (Fig. 5.13c) configurations. The statistical representation of the data points is consistent with the SINR graphs, featuring IQR boxes, whiskers, outliers, medians, and mean values.

Additionally, Fig. 5.11 illustrates the Cell ID allocation over time for the 10 simulated UEs in the network. This includes no SU-MIMO (Fig.5.11a), polarization (Fig.5.11b), and port (Fig. 5.11c) configurations. The y-axis shows the Cell ID each UE is connected to at any given time during the 100 s simulation period. Each colored line represents a specific UE, and the legend on the right side of the graph identifies the corresponding UE for each colored line.

Section 5.2.1 compares the no SU-MIMO configuration with the polarization configuration using flexRLM in a dense and highly loaded multi-UE environment . Section 5.2.2 repeats this comparison with the no SU-MIMO and port configurations. Finally, Section 5.2.3 contrasts flexRLM and default 5G-NR RLM in a multi-user environment, specifically for the port and no SU-MIMO configurations. Each section evaluates the network throughput and the SINR experienced by the UEs.

5.2.1 Polarization

This section compares the no SU-MIMO configuration with the polarization configuration, both utilizing flexRLM. The analysis begins by examining the link quality and throughput differences across all UEs in both configurations. To gain a more detailed understanding of the variations affecting specific UEs, the performance of UE 2 and UE 6 is further analyzed in terms of beam management decisions, instantaneous SINR, and throughput.

5.2.1.1 Link Quality

The link quality of the different UEs is compared between the no SU-MIMO and polarization configurations in terms of the mean instantaneous SINR, depicted as red points in Fig. 5.12a and Fig. 5.12b. Generally, the changes between the no SU-MIMO and the polarization configuration seem to be ambiguous, although more UEs show an SINR improvement when the polarization configuration is used. UE 1's mean SINR jumps from 11 dB to 40 dB, and UE 4's from 16 dB to 25 dB. In both cases, the mean SINR transitions from a value below the maximum rate threshold to one comfortably above it. UE 2, UE 7, UE 8, and UE 9 show slight SINR improvements, ranging from 1 dB for UE 9 to 8 dB for UE 8. Analysis of Fig. 5.11a and Fig. 5.11b reveals that all the UEs with improved SINR have identical serving cells in both the no SU-MIMO and polarization configuration, except for UE 8, which connects to a different cell between

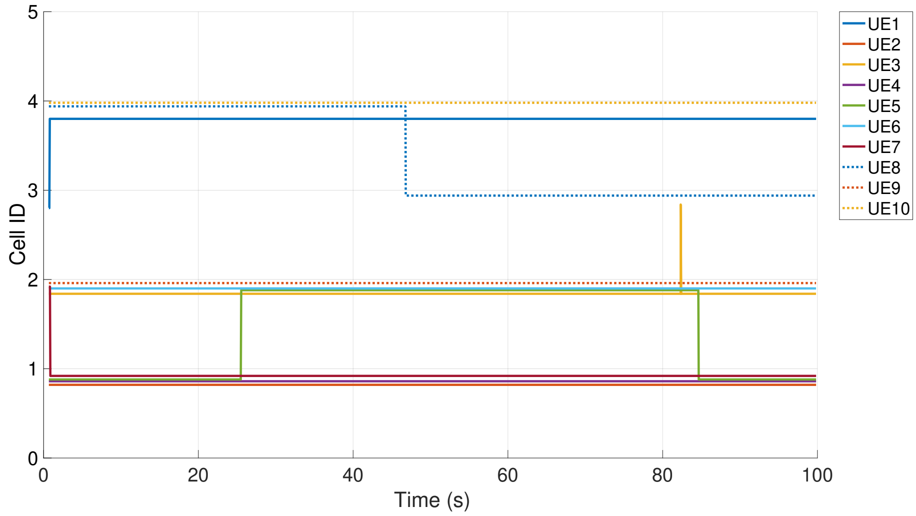

(a) No SU-MIMO

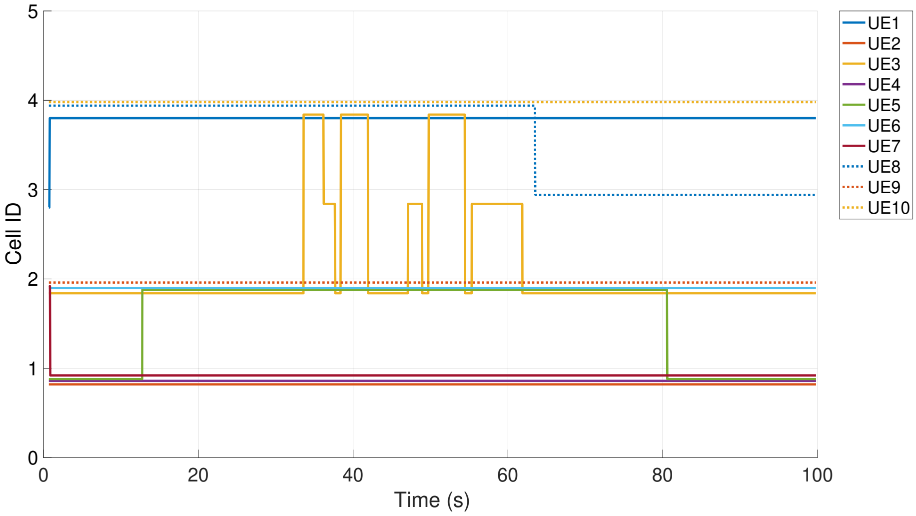

(b) Polarization

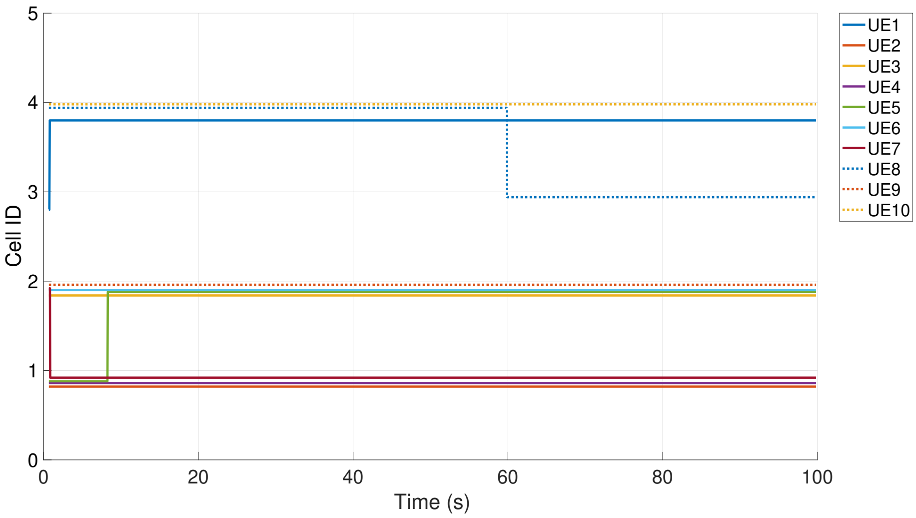

(c) Port

FIGURE 5.11: Cell ID graphs of the simulated UEs for (a) no SU-MIMO, (b) polarization, and (c) port configuration with 2 Gbps requested and flexRLM.

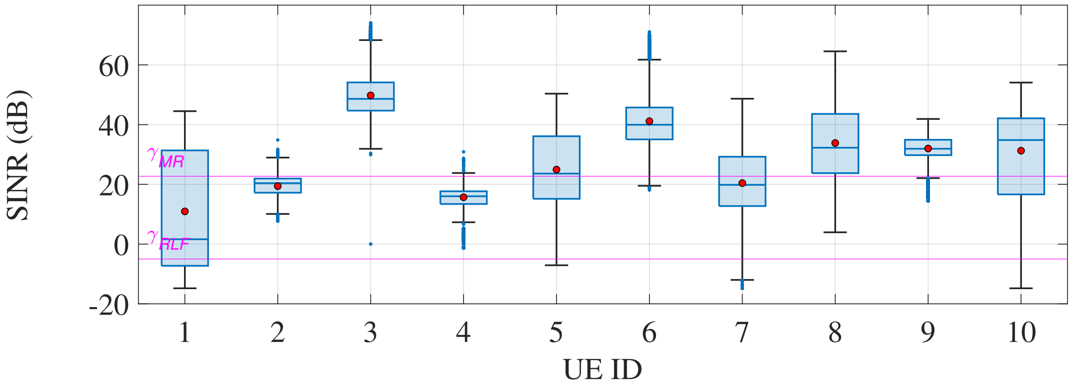

(a) No SU-MIMO

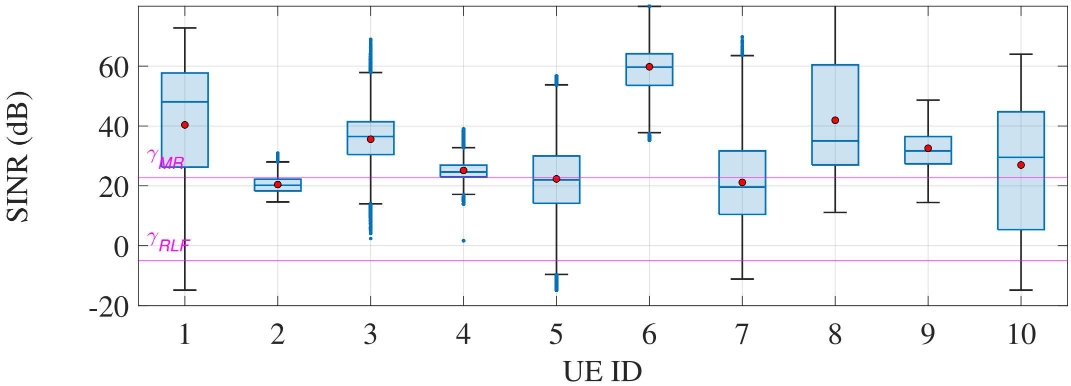

(b) Polarization

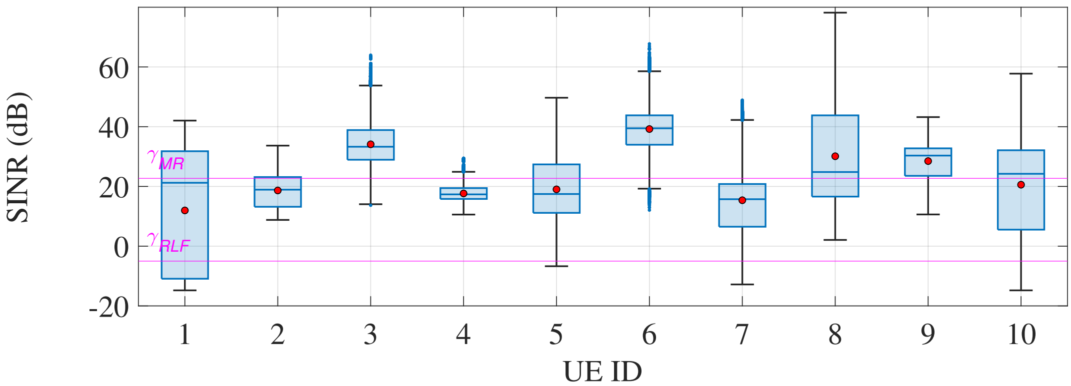

(c) Port

FIGURE 5.12: SINR boxplots of the simulated UEs for (a) no SU-MIMO, (b) polarization, and (c) port configuration with 2 Gbps requested and flexRLM.

46.8 s to 63.5 s. The SINR improvements can likely be attributed to the higher antenna array gain in the polarization configuration. Conversely, UE 3, UE 5, and UE 10 exhibit a worsening of 14 dB, 4 dB, and 4 dB respectively. Despite this, their mean SINR remains above or very close to the maximum rate threshold, suggesting minimal impact on throughput. For UE 3 and UE 5, the SINR differences can be explained by changes in serving cells between the configurations. UE 3 switches cells between 33 s and 62 s, and UE 5 does so from 12.8 s to 25.5 s and again from 80.6 s to 84.6 s. Notably, for UEs 1, 2, 4, and 7 in the no SU-MIMO configuration, and UEs 2 and 7 in the polarization configuration, the majority of the SINR values are below the maximum rate threshold. This suggests that, for most of the simulation time, the experienced SINR is inadequate. However, Fig. 5.11 indicates that these UEs do not change their serving cells. According to beam management strategies, an SINR below the maximum rate should trigger beam management events that could result in a handover. The reason for this anomaly will be explored further by analyzing UE 2 in Section 5.2.1.3.

5.2.1.2 Throughput

The throughput of the different UEs is compared between the no SU-MIMO and polarization configurations based on the mean throughput in Mbps, represented by the red dots in Fig. 5.13a and Fig. 5.13b. Overall, the throughput is increased for every UE in the polarization configuration compared to the no SU-MIMO configuration. Summing up all the mean throughput values, the polarization configuration achieves 3.869 Gbps, significantly higher than the 1.755 Gbps achieved with the no SU-MIMO configuration. However, in both cases, the throughput remains well below the maximum capacity that the four gNBs could theoretically provide. In the single user scenario, it was identified that the throughput is capped around 1200 Mbps for the no SU-MIMO configuration and 1700 Mbps for the polarization configuration. With four gNBs, a theoretical combined throughput of 4.6 Gbps and 6.8 Gbps could be possible, but this is not reached due to poor link quality experienced by some UEs, which forces them to use a lower MCS, negatively impacting the throughput. The highest mean throughput improvements are seen in UE 1, which goes from 146.5 Mbps to 545.4 Mbps, and UE 6, which goes from 203.3 Mbps to 619.6 Mbps. These UEs also exhibit the highest SINR improvements, as shown in Fig. 5.12. The blue boxes representing the IQR of the throughput are considerably larger in the polarization configuration, most notably for UE 3, UE 7, and UE 8. This is because introducing SU-MIMO allows for a higher range of possible throughput values depending on the rank and MCS. UEs rarely maintain a constant rank of two and often have to switch, resulting in a more spread-out throughput distribution. In the throughput boxplots of both configurations, there are many outliers visible as blue dots. These outliers stem from the upward and downward spikes observed in the throughput (e.g. Fig. 5.4).

In conclusion the comparison between the no SU-MIMO and polarization configurations reveals notable improvements in both SINR and throughput when using polarization. The polarization configuration generally produces higher SINR levels across most UEs, attributed to the increased antenna array gain. In terms of throughput, all UEs show an increase with the polarization configuration. This improvement is primarily due to the use of SU-MIMO, which enables the transmission of two data

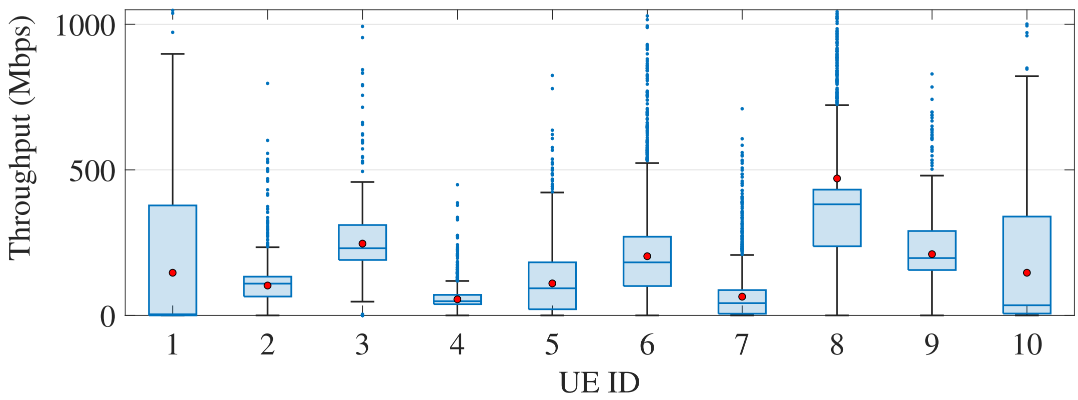

(a) No SU-MIMO

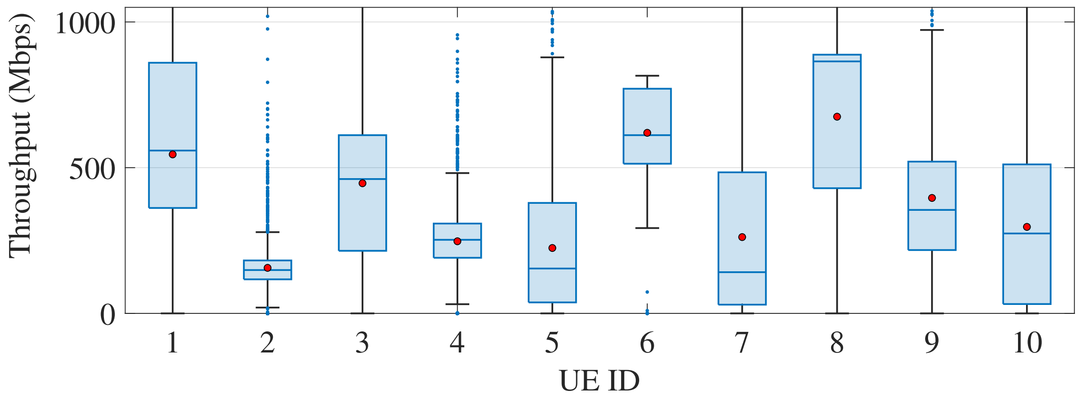

(b) Polarization

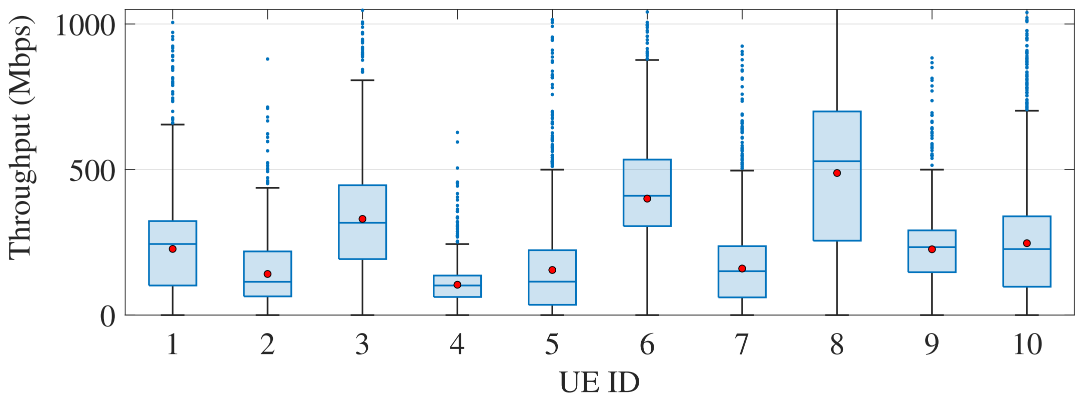

(c) Port

FIGURE 5.13: Throughput boxplots of the simulated UEs for (a) no SU-MIMO, (b) polarization, and (c) port configuration with 2 Gbps requested and flexRLM.

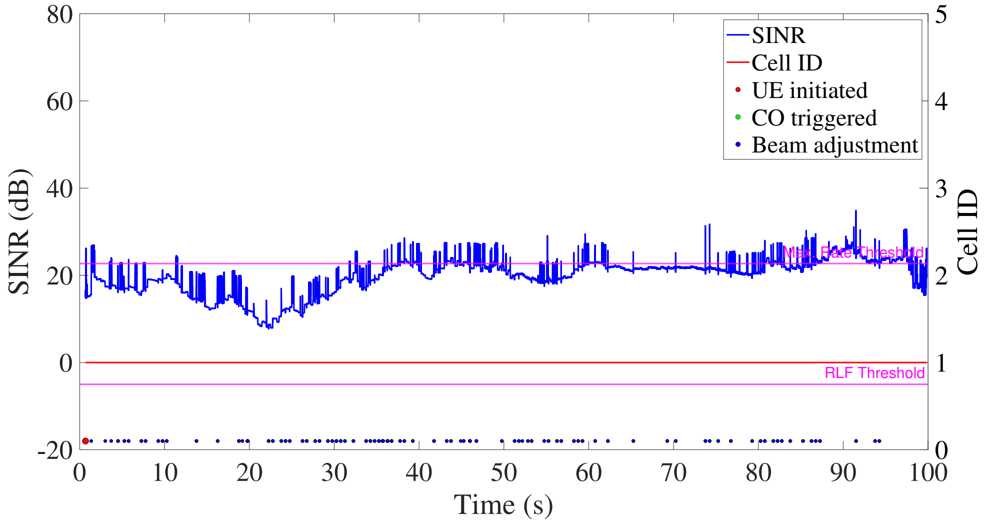

(a) No SU-MIMO

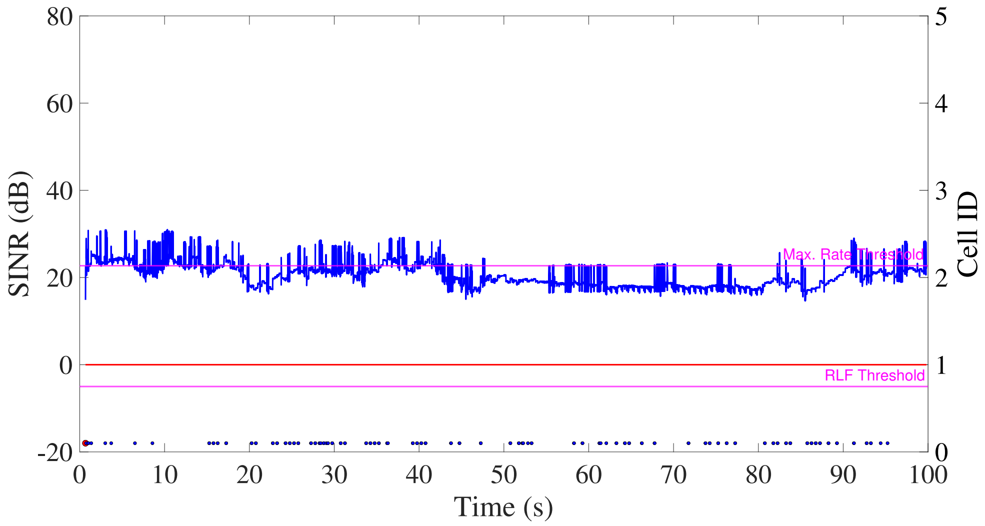

(b) Polarization

FIGURE 5.14: Instantaneous SINR graphs of UE 2 for (a) no SU-MIMO and (b) polarization configuration with 2 Gbps requested and flexRLM.

streams simultaneously, effectively doubling the potential throughput. Overall, the polarization configuration shows clear advantages over the no SU-MIMO configuration, making it a more effective choice for improving network performance in a highly loaded multi-user environment.

5.2.1.3 UE 2

To better understand the multi-user simulation, UE 2 was selected for a detailed analysis of its SINR and throughput graphs in both the no SU-MIMO and polarization configurations. UE 2 is particularly interesting because its SINR remains consistently below the maximum rate threshold, yet no handovers are conducted. Additionally, despite a modest SINR improvement of only 1 dB in the polarization configuration compared to the no SU-MIMO configuration, its throughput significantly improves by 53.5 Mbps. Fig. 5.14 shows the instantaneous SINR, cell ID, and triggered beam management events over time of the polarization and no SU-MIMO cases for UE 2. Fig. 5.16 illustrates the throughput in Mbps, rank, and triggered beam management events over time for the same cases. Finally, Fig. 5.15 displays the estimated SINR of cell 1 to 4 over time for both configurations for UE 2. Analyzing these graphs will help explain the observations mentioned above.

Looking at Fig. 5.14, the experienced SINR is consistently just below the maximum rate threshold in both configurations, and the initiated beam management events are similar. In both cases, only a single beam sweep is initiated by the UE during the IA process and several beam switches occur throughout the simulation time. The absence of coordinator-initiated beam sweeps can be explained by examining Fig. 5.15, which shows that the estimated SINR of the serving cell 1 remains above the maximum threshold throughout the entire simulation in both configurations. This discrepancy between the experienced and estimated SINR, with the curvature being identical but consistently differing by approximately 17 dB, results in faulty beam management decisions.

The throughput graphs exhibit a correlation with the experienced SINR, the used rank, and the number of UEs registered at the serving cell. In both the no SU-MIMO and polarization configuration, the curvature of the throughput closely resembles that of the experienced SINR. This is because the MCS is chosen based on the experienced SINR, with higher SINR levels resulting in fewer transmission errors. Notably, in the polarization configuration, whenever the SINR surpasses the maximum threshold, the throughput significantly increases. For example, between 35.7 s and 38.2 s, the SINR surpasses the maximum threshold, and the throughput rises from around 200 Mbps to 275 Mbps. This increase occurs because higher SINR levels allow the use of rank two, which substantially enhances the throughput. Throughout the simulation of the polarization configuration, the rank appears unstable, frequently jumping between one and two. These jumps are caused by spikes in the SINR that briefly exceed the maximum rate threshold, resulting in corresponding rank jumps. The throughput in the no SU-MIMO configuration does not exhibit this substantial increase when the maximum rate is surpassed due to the inability to use rank two. Between 25.5 s to 84.7 s the serving cell with identifier 1 in Fig. 5.11a serves only three UEs instead of the usual four, which is reflected in Fig 5.16a as increased throughput during this period. Most notably, at 84.7 s when a fourth UE connects to cell 1, the throughput drops from 123.1 Mbps to 72.8 Mbps while the SINR remains at a similar level.

In conclusion, the SINR of UE 2 remains below the maximum threshold throughout the simulation without triggering beam management events due to inaccuracies in the estimated SINR. Although the link quality conditions are not ideal for SU-MIMO, the short periods where the experienced SINR exceeds the maximum threshold are sufficient to significantly improve throughput by using rank two.

5.2.1.4 UE 6

In contrast to UE 2, UE 6 is chosen for its significant improvements in both SINR and throughput. With an SINR improvement of 18.6 dB and a throughput increase of

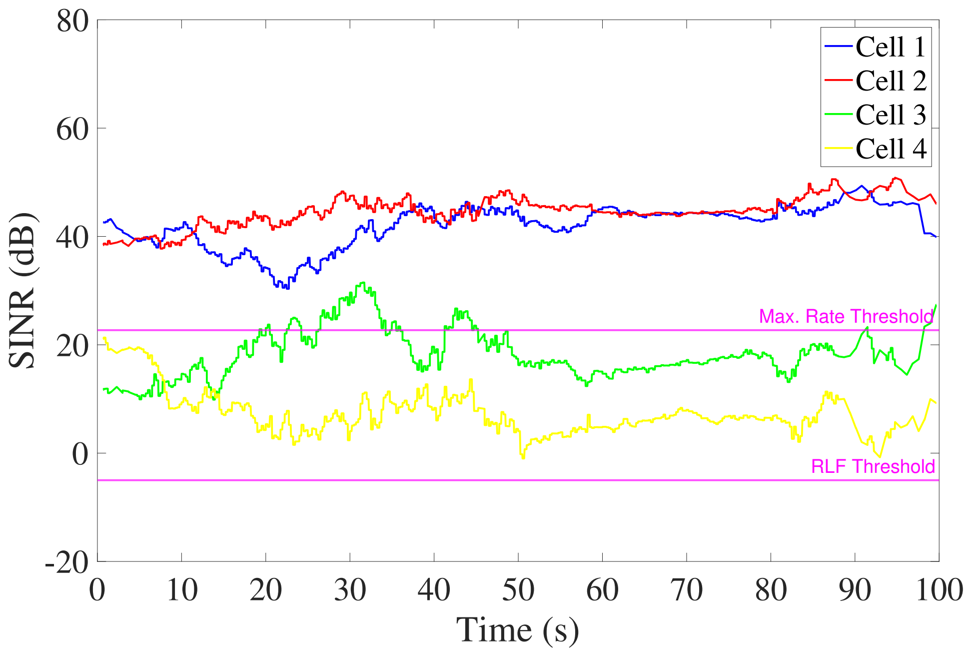

(a) No SU-MIMO

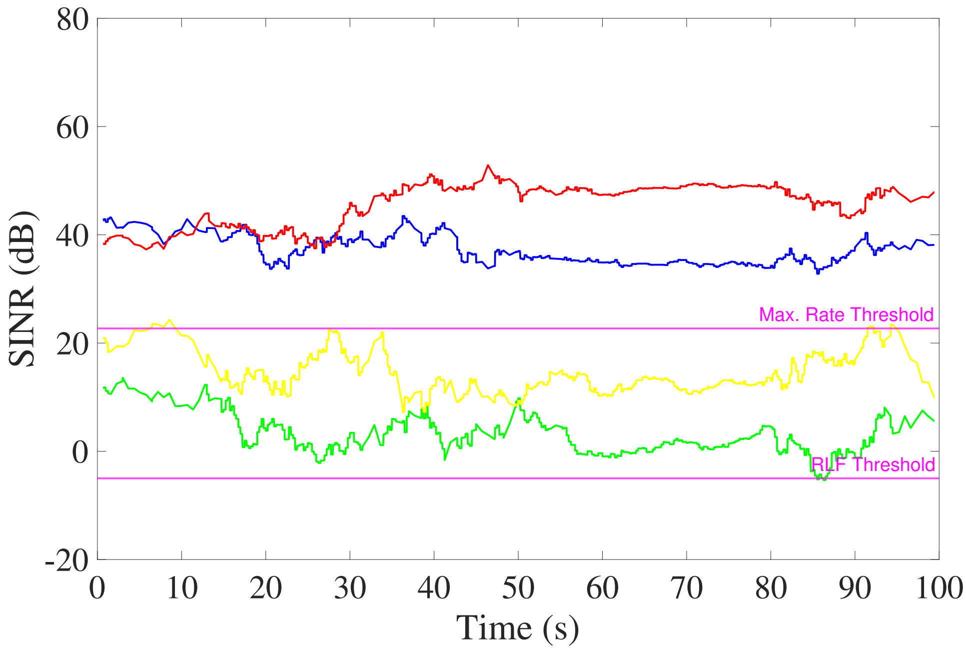

(b) Polarization

FIGURE 5.15: Estimated SINR graphs of UE 2 for (a) no SU-MIMO and (b) polarization configuration with 2 Gbps requested and flexRLM.

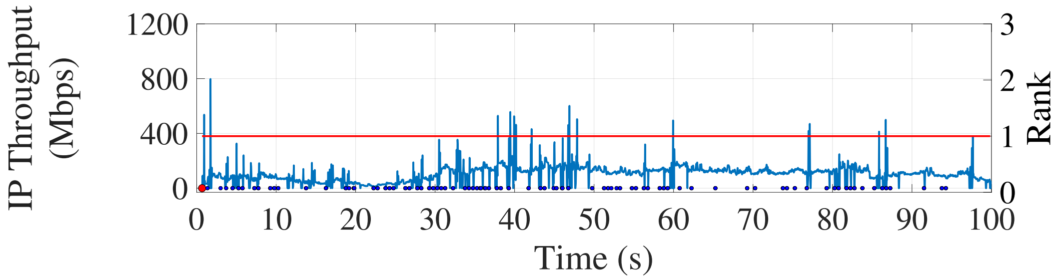

(a) No SU-MIMO

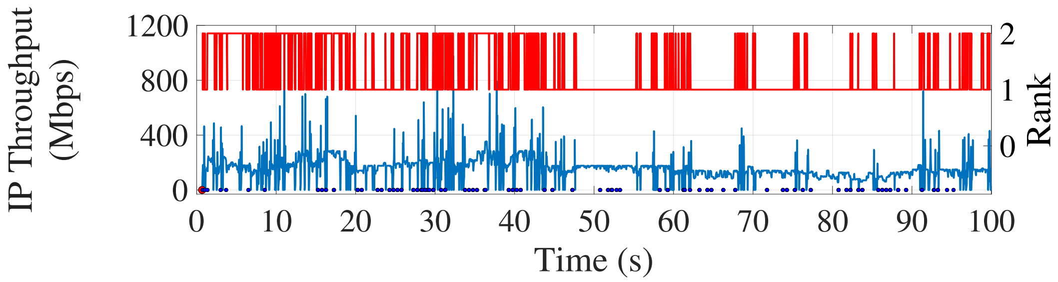

(b) Polarization

FIGURE 5.16: IP throughput graphs of UE 2 for (a) no SU-MIMO and (b) polarization configuration with 2 Gbps requested and flexRLM.

416.3 Mbps, UE 6 shows the highest gains in the simulation. Additionally, UE 6 was also analyzed in the single-user scenario, providing a basis for comparison. Fig. 5.17 displays the instantaneous SINR, cell ID, and triggered beam management events over time for the polarization and no SU-MIMO cases for UE 6. Fig. 5.19 illustrates the throughput in Mbps, rank, and triggered beam management events over time for the same cases. Finally, Fig. 5.18 presents the estimated SINR of cell 1 to 4 over time for both configurations for UE 6.

Looking at Fig. 5.17, the instantaneous SINR value remains constantly above the maximum rate threshold in the polarization configuration and almost always above this threshold, with the exception of a few downwards spikes in the no SU-MIMO case. In both cases, UE 6 is connected to cell 2 throughout the entire simulation. Only a single beam sweep is performed during the initial access process in both configurations, as the estimated SINR remains consistently above the maximum threshold (e.g. Fig. 5.18). However, the polarization configuration performs significantly more beam adjustments. Both SINR graphs exhibit strong fluctuations over a range of about 30 dB. While the general SINR trends are similar between the two configurations, the SINR levels differ significantly. The mean SINR is 41 dB in the no SU-MIMO configuration and 60 dB in the polarization configuration. This difference is attributed to the increased number of antenna elements in the polarization configuration, resulting in higher antenna gain.

When comparing the throughput graphs in Fig. 5.19, it is evident that the strong variations in the experienced SINR are reflected in significant throughput variations. This phenomenon is more pronounced in the no SU-MIMO configuration, as high

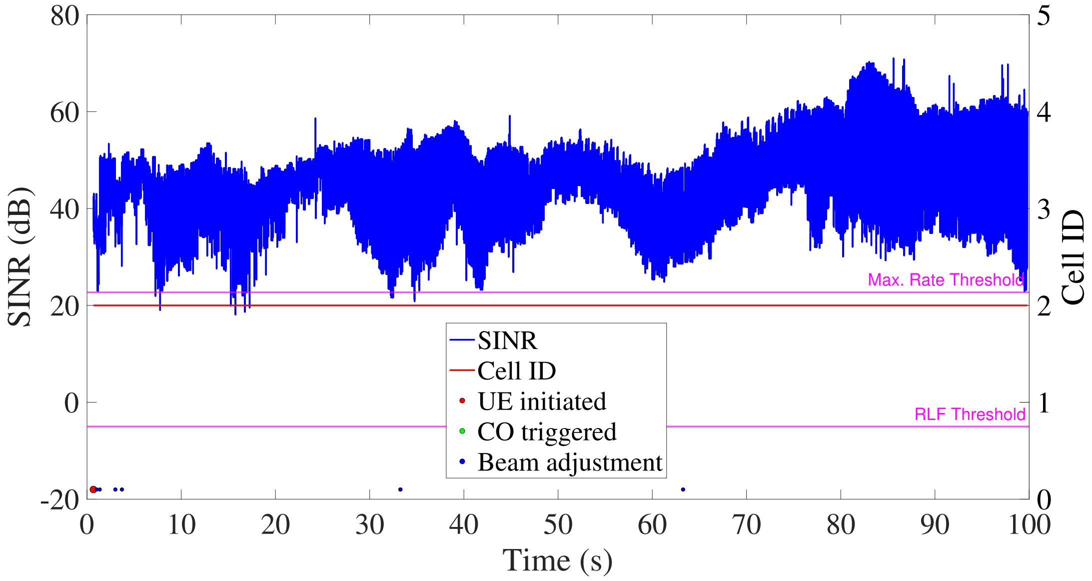

(a) No SU-MIMO

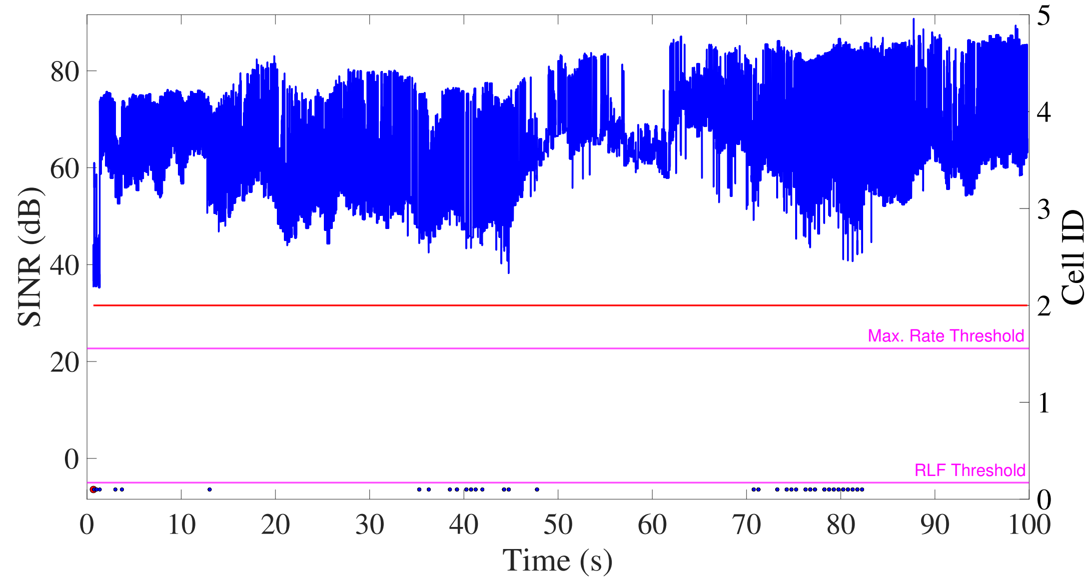

(b) Polarization

FIGURE 5.17: Instantaneous SINR graphs of UE 6 for (a) no SU-MIMO and (b) polarization configuration with 2 Gbps requested and flexRLM.

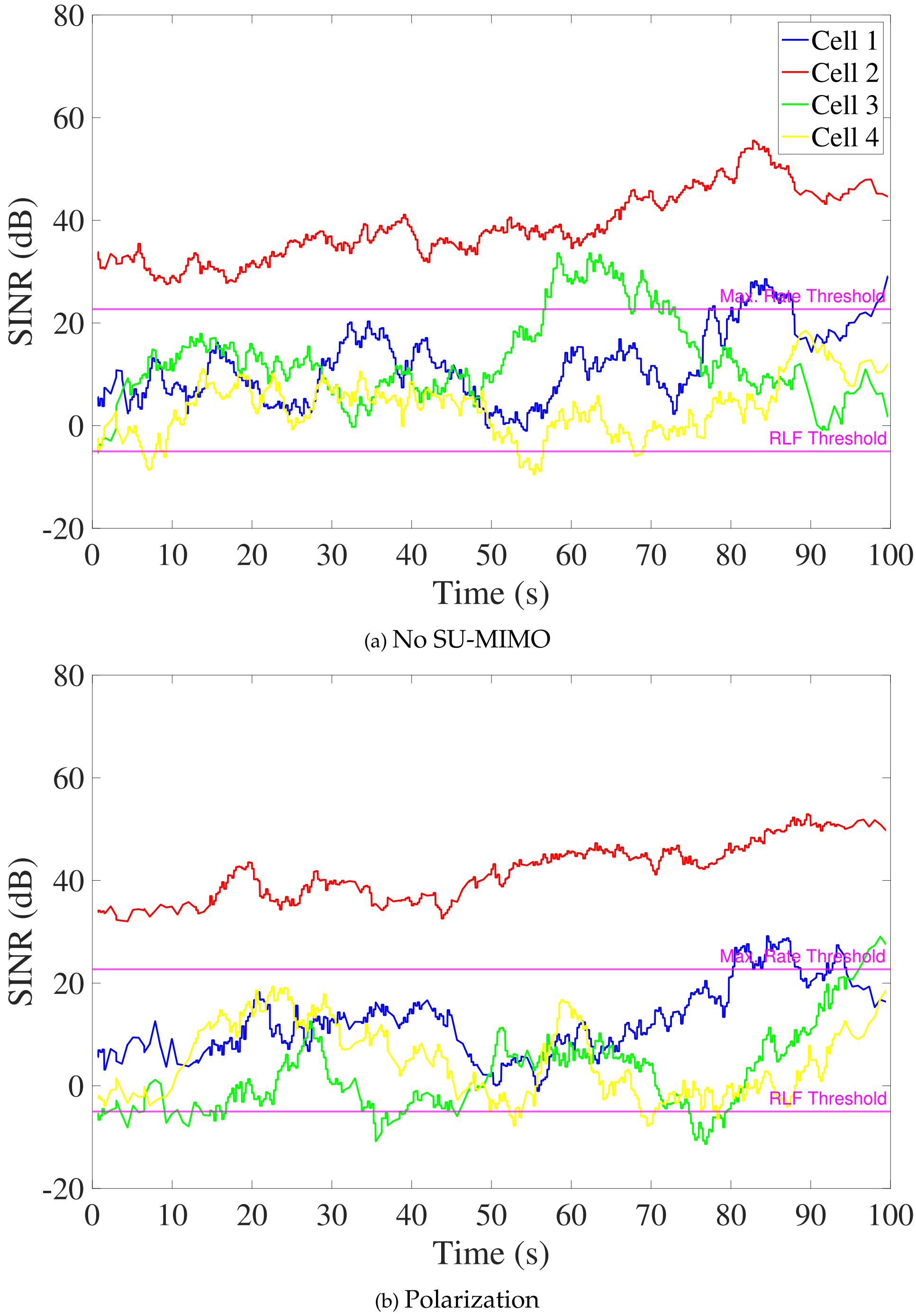

(a) No SU-MIMO

(b) Polarization

FIGURE 5.18: Estimated SINR graphs of UE 6 for (a) no SU-MIMO and (b) polarization configuration with 2 Gbps requested and flexRLM.

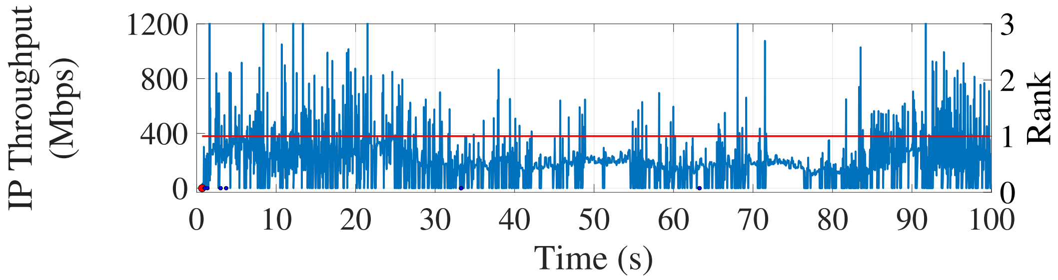

(a) No SU-MIMO

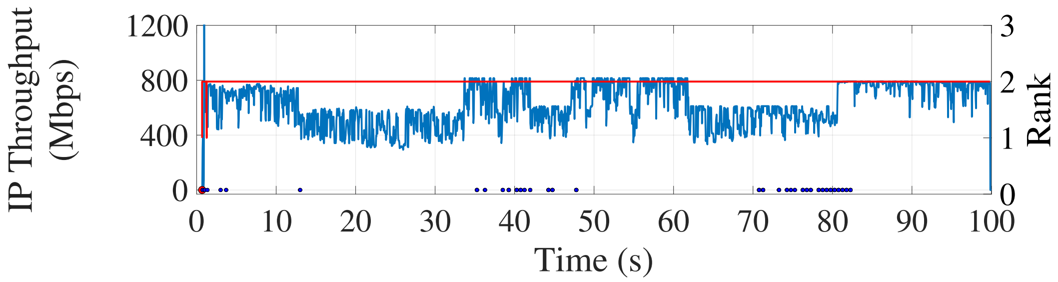

(b) Polarization

FIGURE 5.19: IP throughput graphs of UE 6 for (a) no SU-MIMO and (b) polarization configuration with 2 Gbps requested and flexRLM.

SINR variation at a lower SINR level has a greater impact on throughput than at a higher SINR level. The constant use of rank two combined with the SINR improvements resulting in fewer transmission errors and a more stable link enables the polarization configuration to achieve a much higher mean throughput rate of 619.6 Mbps, tripling the 203.3 Mbps of the no SU-MIMO configuration. In both simulations, the throughput changes drastically at several time instances, even though the SINR remains consistently over the maximum threshold. This is because the number of UEs registered to the serving cell 2 changes. Table 5.1 and Table 5.2 show the correlation between the number of UEs at the serving cell and the throughput in Mbps for the no SU-MIMO and polarization configuration, respectively. In the no SU-MIMO configuration, during the intervals when there are 3 UEs connected, the throughput is approximately 300 Mbps. However, when the number of connected UEs increases to 4, the throughput drops to around 175 Mbps. In the polarization configuration, a similar pattern is observed. The throughput is approximately 700 Mbps when 3 UEs are connected. When the number of connected UEs increases to 4, the throughput decreases to about 500 Mbps. This variation occurs because the resources at the gNB are finite and need to be distributed among all connected UEs. When the number of UEs increases, the resources available per UE decrease, resulting in a drop in throughput.

In summary, for UE 6, the polarization configuration significantly enhances both SINR and throughput compared to the no SU-MIMO configuration. The increased antenna gain in the polarization setup leads to a higher and more stable SINR. This improvement, combined with the use of rank two, triple the throughput compared to the no SU-MIMO configuration. Additionally, the analysis highlights the impact of the number of connected UEs on throughput, with fewer UEs leading to higher available resources and better throughput. These findings demonstrate the effectiveness of SU-MIMO configurations in optimizing network performance in dense, multi-user environments.

Time Intervals	Number of connected UEs	Approximate Throughput
[0.68 s - 25.6 s]	3 UEs	300 Mbps
[25.6 s - 84.7 s]	4 UEs	175 Mbps
[84.7 s - 100 s]	3 UEs	300 Mbps

TABLE 5.1: Correlation between the number of UEs at the serving cell and the throughput in Mbps for the no SU-MIMO configuration.

Time Intervals	Number of connected UEs	Approximate Throughput
[0.68 s - 12.7 s]	3 UEs	600 Mbps
[12.7 s - 33.6 s]	4 UEs	500 Mbps
[33.6 s - 41.9 s]	mostly 3 UEs	700 Mbps
[41.9 s - 47.1 s]	4 UEs	500 Mbps
[47.1 s - 61.8 s]	mostly 3 UEs	700 Mbps
[61.8 s - 80.6 s]	4 UEs	500 Mbps
[80.6 s - 100 s]	3 UEs	700 Mbps

TABLE 5.2: Correlation between the number of UEs at the serving cell and the throughput in Mbps for the polarization configuration.

5.2.2 Port

This section compares the no SU-MIMO configuration with the port configuration, both utilizing flexRLM. The analysis starts by examining the link quality and throughput differences across all UEs in both configurations. To gain a more detailed understanding of the variations affecting specific UEs, the performance of UE 9 is further analyzed in terms of beam management decisions, instantaneous SINR, and throughput.

5.2.2.1 Link Quality

The link quality, in terms of experienced SINR for the different UEs, is compared based on the mean instantaneous SINR. Overall, the changes between the no SU-MIMO and the port configuration appear ambiguous. Most UEs, including UE 2, UE 6, UE 8, UE 9, and UE 10, experience a slight decrease in their mean SINR by less than a few dB. UE 3, UE 5, and UE 10 even see significant drops, with UE 3 losing 16 dB, and UE 5 and UE 10 falling from above to below the maximum threshold. Only UE 1 and UE 4 show slight improvements of 1 dB and 2 dB, respectively. However, UE 1 and UE 4 remain below the maximum threshold for most of the simulation time in both configurations, meaning their SINR is not high enough to use rank two. The use of rank one with digital precoding can slightly enhance the experienced SINR, possibly explaining the slight improvements for UE 1 and UE 4. In contrast, using rank two splits the transmit energy into two streams, potentially worsening the instantaneous SINR. This might explain why UEs with a high overall SINR in the no SU-MIMO simulation, like UE 3, UE 6, UE 8, UE 9, and UE 10, experience a drop in SINR when using the port configuration, which enables them to use rank two most of the time. For UE 5, different serving cells between 8.3 s to 25.54 s and 84.57 s to 100 s could account for the variations in mean SINR between configurations. In both simulations, UE 1, UE 2, UE 4, and UE 7 remain below the maximum threshold without ever changing their cell. The lack of handovers is due to discrepancies between the estimated and experienced SINR, preventing the coordinator from initiating any beam management events.

5.2.2.2 Throughput

The throughput of the different UEs is compared between the no SU-MIMO and port configurations based on the mean throughput in Mbps depicted in Fig. 5.13. Overall, every UE exhibits a throughput improvement when the port configuration is used. The most significant improvement is observed in UE 6, where the mean throughput increases from 203.3 Mbps to 400 Mbps. The combined mean throughput of all ten UEs in the port configuration is 2.5 Gbps, which is 720 Mbps higher than the 1.76 Gbps achieved with the no SU-MIMO configuration. Similar to the polarization configuration, the maximum throughput capacity of the four gNBs is not reached due to the poor SINR experienced by some UEs. Additionally, as with the polarization configuration, the blue boxes representing the IQR have widened for UEs 2 to 9, indicating more varied throughput values. This variability is a result of using rank two, which allows for higher throughput rates.

In summary, the port configuration can potentially increase SINR through digital precoding when rank one is used. However, enabling rank two often results in a decrease in SINR due to the split of transmission power between two streams without the additional antenna gain seen in the polarization configuration. Despite this, the overall throughput significantly benefits from the use of SU-MIMO with rank two, enabling the ability of the port configuration to utilize two streams simultaneously. The port configuration's performance aligns closely with the polarization configuration, which also demonstrated substantial throughput gains due to the increased antenna array gain. Both configurations showcase the advantages of SU-MIMO in boosting network throughput, though the impact on SINR can vary based on specific UE conditions and configurations.

5.2.2.3 UE 9

To better understand what happens in the multi-user simulation, UE 9 was selected to analyse and compare its SINR and throughput graphs in the no SU-MIMO and port configuration. UE 9 is particularly interesting because its mean SINR is close to the maximum threshold, suggesting that both rank one and rank two will be used during the simulation. Its mean SINR slightly deteriorates from 32 dB to 28 dB, similar to most other UEs in the simulation. Despite the worsened SINR, the throughput increases by 15.7 Mbps in the port configuration. Fig. 5.20 shows the instantaneous SINR, cell ID, and triggered beam management events over time for the port and no

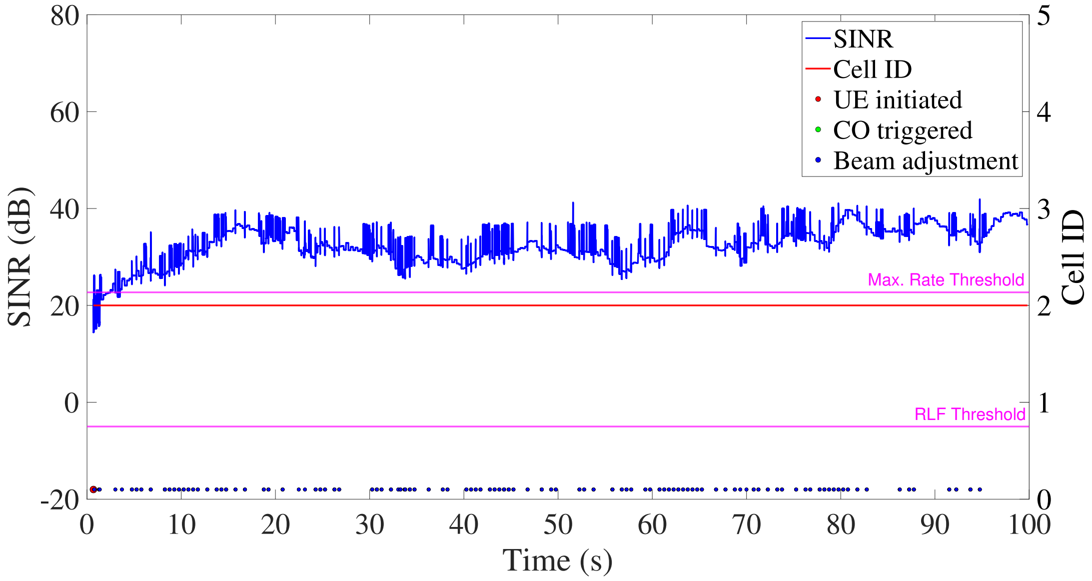

(a) No SU-MIMO

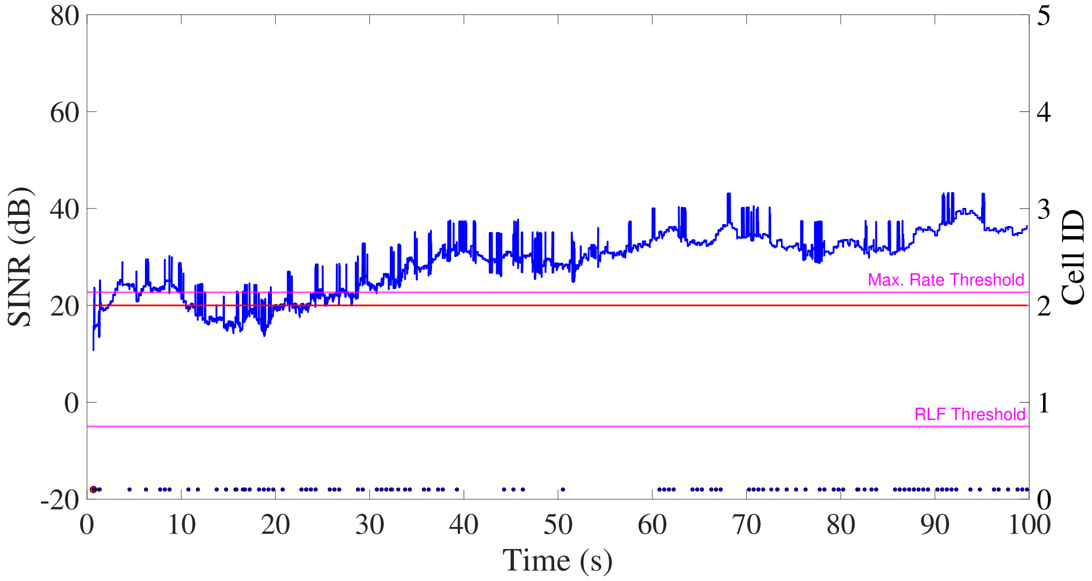

(b) Port

FIGURE 5.20: Instantaneous SINR graphs of UE 9 for (a) no SU-MIMO and (b) port configuration with 2 Gbps requested and flexRLM.

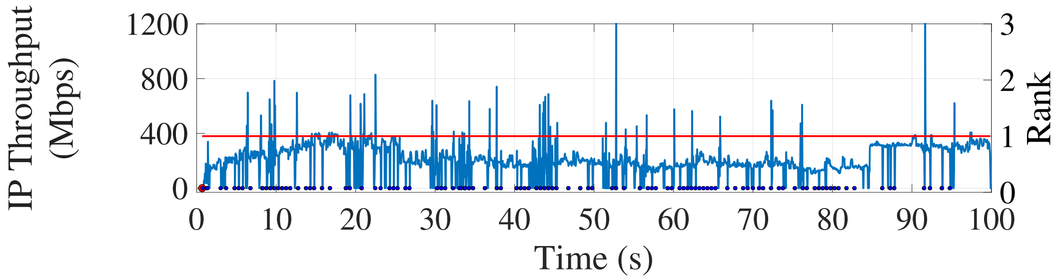

(a) No SU-MIMO

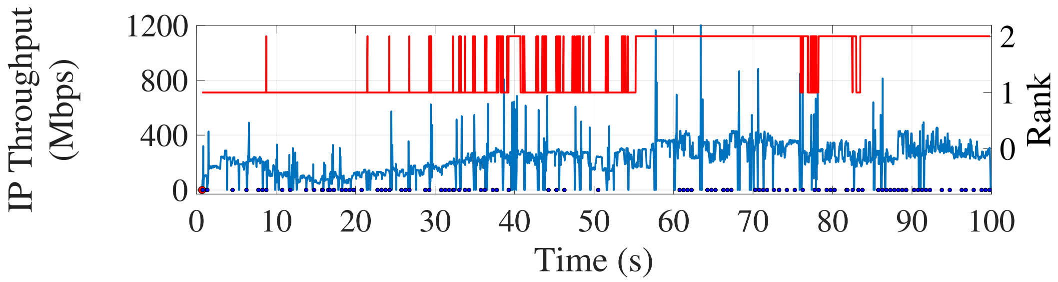

(b) Port

FIGURE 5.21: IP throughput graphs of UE 9 for (a) no SU-MIMO and (b) port configuration with 2 Gbps requested and flexRLM.

SU-MIMO configurations for UE 9. Fig. 5.21 illustrates the throughput in Mbps, rank, and triggered beam management events over time for the same configurations for UE 9.

In both configurations, UE 9 remains connected to cell 2 throughout the simulation. A beam sweep is initiated only for the initial access procedure. Both the no SU-MIMO and port configurations perform a high number of beam switches. In the no SU-MIMO simulation, the SINR remains above the maximum threshold, around 30 dB, for most of the simulation period. In contrast, in the port simulation, the SINR drops below the maximum threshold early on, particularly from 9.8 s to 23 s. After this initial drop, the SINR rises above the threshold and stabilizes around 30 dB.

The throughput graphs in Fig. 5.21, clearly show that SINR levels strongly influence throughput, as their trends are closely aligned. As observed with UE 6 in the polarization configuration, the number of UEs connected to the serving gNB significantly impacts throughput. In the no SU-MIMO configuration, from 0.9 s to 25.5 s and from 84.7 s to 100 s, three UEs are connected to UE 9's serving cell, as shown in Fig.5.11a. During these periods, the average throughput is higher, around 300 Mbps. Between these intervals, cell 2 serves four UEs, and the throughput drops to approximately 200 Mbps. In the port configuration, only between 0.8 s and 8.3 s are three UEs connected to cell 2, as seen in Fig.5.11c. During this interval, the SINR is below the maximum rate threshold, resulting in a throughput of around 200 Mbps. However, after a fourth UE registers to cell 2 at 8.3 s, the throughput drops to about 100 Mbps and only recovers after the SINR rises above the maximum threshold at 28.5 s. From the start of the simulation until 28.5 s, the rank remains at one due to the low SINR.

Between 28.5 s to 55 s, the SINR fluctuates between 23 dB and 31 dB, causing the rank to jump between one and two. Finally, once the SINR crosses the 31 dB mark and stays consistently above it, the use of rank two becomes stable. This results in a throughput of around 300 Mbps, similar to the level observed when three UEs were connected in the no SU-MIMO case. Despite UE 9 sharing its serving cell with three other UEs for most of the simulation time in the port configuration, the use of SU-MIMO allows it to achieve throughput levels comparable to having only two other connected UEs in the no SU-MIMO case.

In conclusion, the analysis of UE 9's performance highlights the significant benefits of using SU-MIMO in a multi-user environment. Despite a slight deterioration in SINR, caused by the split of the transmission power, the port configuration's ability to utilize rank two transmissions enhances overall throughput. The improvements in throughput achieved with SU-MIMO demonstrate its capability to maintain higher data rates even when multiple UEs are connected to the same cell. The ability to leverage multiple streams simultaneously enables the network to handle increased traffic loads, mitigating the impact of congestion and ensuring better overall performance for all users.

5.2.3 Beam Management

This section compares the two different beam management strategies: flexRLM and default 5G-NR RLM. The instantaneous SINR and throughput boxplots of both strategies with the no SU-MIMO and port configurations are compared. Fig. 5.12 and Fig. 5.13, already introduced at the beginning of Section 5.2, show the SINR and throughput boxplots for the polarization, port, and no SU-MIMO configuration with flexRLM. In contrast, Fig. 5.23 and Fig. 5.24 present the SINR and throughput boxplots for the port and no SU-MIMO configuration with default 5G-NR RLM. Finally, Fig. 5.11 and Fig. 5.22 illustrate the cell ID to which each UE is connected throughout the simulation for both flexRLM and default 5G-NR RLM strategies.

A first glance at at Fig. 5.23 and Fig. 5.24 reveals that the observations made in Section 5.2.3.1 regarding the comparison between the no SU-MIMO configuration and the port configuration are consistent with default 5G-NR RLM. Specifically, UE 1, UE 2, UE 4, UE 5, and UE 7 all show improvements in their mean SINR when moving from the no SU-MIMO to the port configuration. These UEs have a mean SINR below the maximum rate threshold in the no SU-MIMO configuration, confirming that digital precoding of rank one enhances the SINR. Conversely, UEs such as UE 3, UE 6, and UE 8, which have a SINR comfortably above the maximum rate threshold in the no SU-MIMO configuration, exhibit a lower mean SINR in the port configuration. This reduction occurs because rank two is used throughout the simulation, splitting the transmit energy into two streams and thereby worsening the SINR. UE 9 and UE 10 are borderline cases, experiencing a mean SINR increase and decrease, respectively. In terms of throughput, the results are clear: all UEs in the port configuration experience an increase compared to the no SU-MIMO configuration. This improvement is due to either the SINR enhancement through digital precoding or the use of rank two, which permits the transmission of two streams simultaneously. As observed before, the blue boxes representing the IQR of the throughput expand in the port configuration

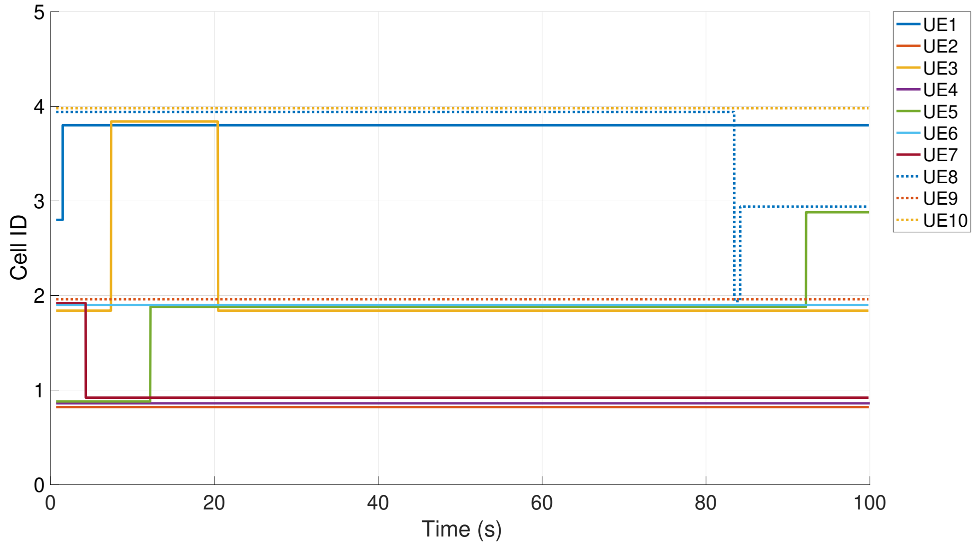

(a) No SU-MIMO

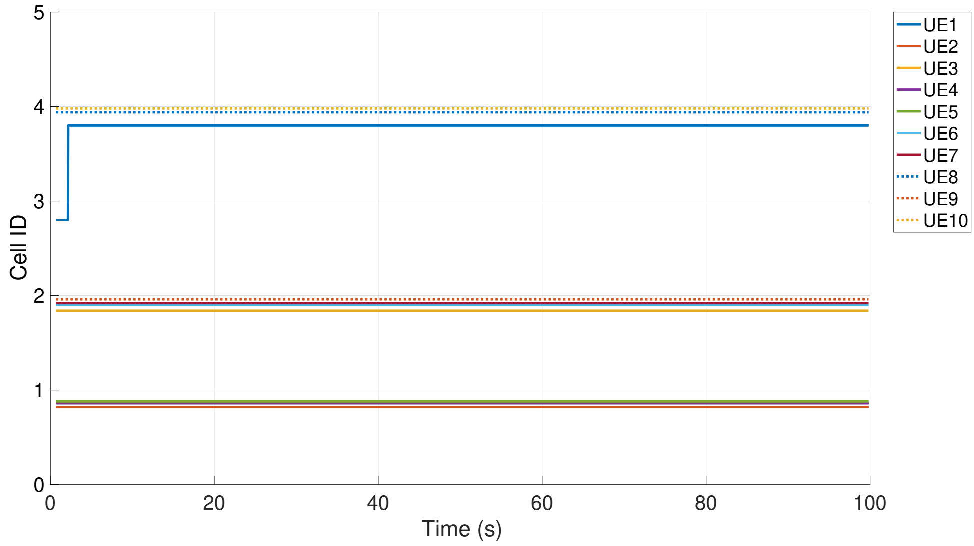

(b) Port

FIGURE 5.22: Cell ID graphs of the simulated UEs for (a) no SU-MIMO, and (b) port configuration with 2 Gbps requested and default 5G-NR RLM.

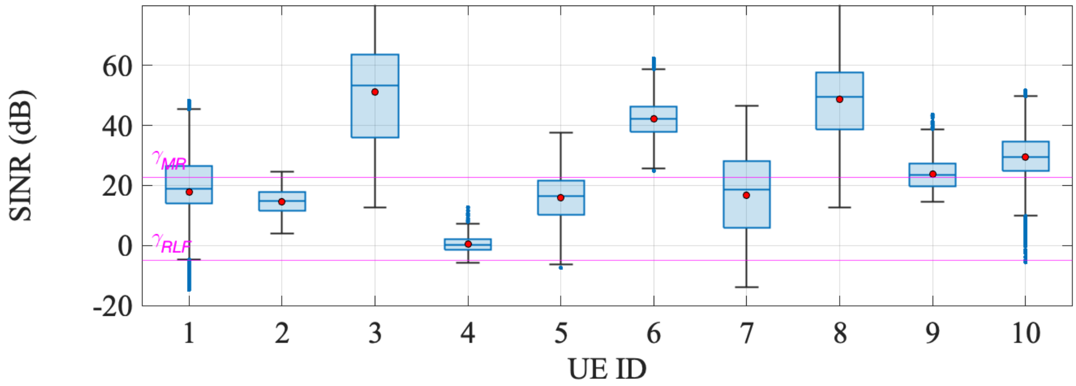

(a) No SU-MIMO

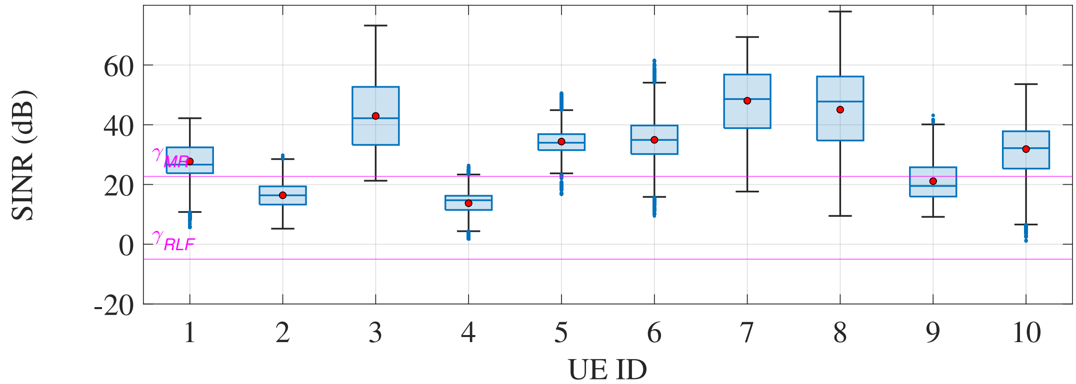

(b) Port

FIGURE 5.23: SINR boxplots of the simulated UEs for (a) no SU-MIMO, and (b) port configuration with 2 Gbps requested and default 5G-NR RLM.

compared to the no SU-MIMO configuration, indicating that SU-MIMO broadens the range of possible throughput values.

Next, Section 5.2.4.1 will compare the default 5G-NR RLM with flexRLM for the no SU-MIMO configuration, analyzing throughput and SINR for 10 UEs, each requesting 1 Gbps. Section 5.2.4.2 will then conduct the same comparison for the port configuration.

5.2.3.1 No SU-MIMO

The comparison of SINR between the default 5G-NR RLM and flexRLM configurations shows ambiguous results. The mean SINR worsens for UE 1, UE 3, UE 6, and UE 8, while it improves for UE 2, UE 4, UE 5, UE 7, UE 9, and UE 10. This variation can be attributed to differences in the propagation model, stemming from the randomness in the channel model. However, the throughput results present a clearer trend. All UEs, except UE 6 and UE 10, exhibit a throughput improvement in the flexRLM simulation. The improvements for UE 2, UE 4, UE 5, UE 7, and UE 9 correlate with their SINR improvements. For UE 1, UE 3, and UE 8, the throughput improvement can be attributed to reduced congestion in their serving gNBs, as observed when

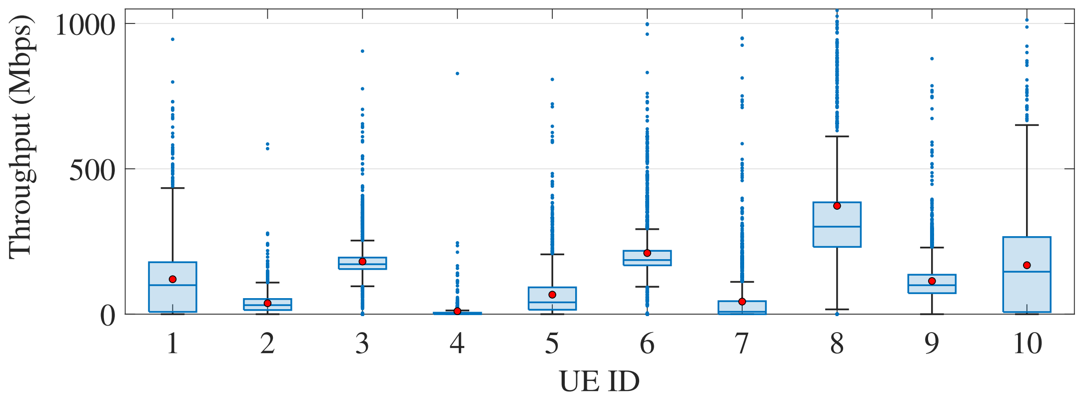

(a) No SU-MIMO

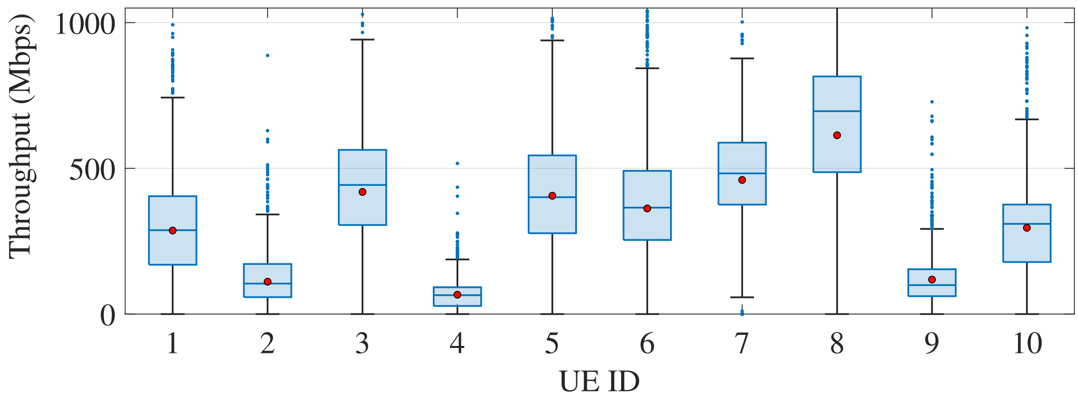

(b) Port

FIGURE 5.24: IP throughput boxplots of the simulated UEs for (a) no SU-MIMO, and (b) port configuration with 2 Gbps requested and default 5G-NR RLM.

comparing the cell ID graphs in Fig. 5.11a and Fig. 5.22a. For instance, the average number of users in UE 1's serving cells decreases from 3 in the default 5G-NR RLM to 2.5 in flexRLM. Similar reductions are noted for UE 3 (3.9 to 3.6) and UE 8 (2.9 to 1.9). These changes result from different beam management decisions, with UE 3, UE 5, and UE 8 switching cells between simulations. For example, UE 3 stays connected to cell 2 throughout the flexRLM simulation but experiences handovers in the default 5G-NR simulation. These differences in handovers arise from variations in the estimated SINR, not the beam management strategies. Therefore, drawing conclusive comparisons between the two simulations is challenging due to the inaccuracies in the estimated SINR.

5.2.3.2 Port

To further confirm the observations, the instantaneous SINR and throughput boxplots of both strategies with the port configurations are compared. Similar to the no SU-MIMO case, the SINR development between default 5G-NR RLM and flexRLM shows ambiguous results. The mean SINR of UE 2, UE 4, UE 6, and UE 9 improves, while the SINR of UE 1, UE 3, UE 5, UE 7, UE 8, and UE 10 worsens. This variation can be attributed to differences in the propagation model resulting from the randomness in the channel model. The throughput exhibits the same ambiguous trends. UEs experiencing a SINR downgrade also see a drop in throughput, while those with an improved SINR experience a rise in throughput. This correlation is logical because a worse SINR leads to more transmission errors and the use of lower MCS. When comparing the cell ID graphs in Fig. 5.11c and Fig. 5.22b, it is noticeable that only three UEs, UE 5, UE 7, and UE 8 make different handover decisions between the default 5G-NR RLM and flexRLM. However, this is not due to the difference in the RLM strategy; it is because the estimated SINR deviates between the two simulations, initiating different beam management events. Most notably, UE 5 and UE 7, who are connected to different cells throughout most of the simulation between default 5G-NR RLM and flexRLM, exhibit the biggest difference in SINR, with 15 dB and 33 dB respectively, and in throughput with 251.5 Mbps and 300 Mbps respectively.

In conclusion, the comparison between default 5G-NR RLM and flexRLM reveals that the variations in SINR and throughput are largely influenced by the inherent randomness in the channel model rather than the beam management strategies themselves. While the mean SINR improved for some UEs and worsened for others, this did not correlate directly with the different RLM strategies. Similarly, throughput showed ambiguous results, with improvements for UEs that experienced SINR gains and reductions for those with SINR losses. The cell ID graphs indicated that only a few UEs made different handover decisions between the two RLM strategies, primarily due to deviations in the estimated SINR. Overall, the findings suggest that to accurately compare the effectiveness of different RLM strategies, it is crucial to address the discrepancies in SINR estimation. Accurate SINR estimation would ensure that beam management decisions are consistent and reliable, providing a clearer assessment of each strategy's performance.

6

Conclusions and Further Work

In this thesis, a comprehensive study of end-to-end network performance of a 5G-NR non-standalone millimeter wave network in a multi-gNB environment with different SU-MIMO configurations and realistic beam management was conducted. To achieve this, a ns-3 framework was created that combines realistic beam management with a general SU-MIMO implementation. This framework is based on two extensions of the CTTC NR module [41] and [47], which were combined and adapted to ensure compatibility. The simulation setup was designed to replicate an urban area east of the main train station in Frankfurt am Main. Using the commercial pedestrian flow simulator Viswalk, realistic user walk paths were generated to reflect typical pedestrian movement. The in the CTTC NR module included statistical 3GPP compliant network model was used for the simulations. The network configuration was based on an NSA-DL system with dual-connectivity support, where handover management and handling of RLFs were managed by a central LTE coordinator. Two different SU-MIMO configurations were simulated: port and polarization, and these were compared to a reference scenario where no SU-MIMO was used. Additionally, the simulations included two beam management strategies: flexRLM and default 5G-NR RLM. These configurations and strategies were simulated to enable direct comparisons of their performance and interactions within the network.

In the first scenario, a single UE was simulated for 100 seconds with separate simulations conducted for the UE requesting both 1 Gbps and 2 Gbps. In the 1 Gbps case, the requested throughput can be achieved using a single stream if the experienced SINR is high enough, leading to no significant throughput improvements when using SU-MIMO in this simulation. However, the SINR significantly improves in the polarization case due to the doubling of the antenna elements, resulting in a higher antenna gain. When the requested data rate increases to 2 Gbps, surpassing the hard limit of 1.2 Gbps that a single gNB can provide without SU-MIMO, the advantages of using multiple streams in the same time instance become evident. Both SU-MIMO configurations show a significant improvement in throughput compared to the reference case. The use of two streams simultaneously raises the maximum throughput rate from 1.2 Gbps to 1.7 Gbps, underlining SU-MIMO's ability to deliver high throughput to UEs with substantial data demands and a stable link.

In the second scenario, 10 UEs are simulated over 100 seconds, each requesting 1 Gbps. This aims to simulate a highly loaded network with four gNBs providing a maximum of 4.8 Gbps in total without using SU-MIMO, serving 10 UEs with a total of 10 Gbps requested. Both SU-MIMO configurations show significant throughput improvement across all UEs. The limited resources of the gNBs must be split among the UEs, but using two streams simultaneously maximizes the possible throughput, counteracting network congestion. Observing individual UEs clearly shows how congestion at the serving gNB influences throughput and how SU-MIMO balances this degradation. Similar to the first scenario, the polarization configuration significantly improves SINR through higher antenna gain, which also enhances throughput due to fewer transmission errors, independent of using two streams. In the port configuration, UEs with comparatively worse SINR experience improvement through digital precoding when using a single stream. However, UEs with high enough SINR for two streams experience SINR degradation because the available transmit energy is split between the two streams.

In both scenarios, the two beam management strategies were compared, but no definitive evaluation could be made due to significant discrepancies between the estimated SINR used for beam management decisions and the experienced SINR. As a result, both flexRLM and default 5G-NR could not operate correctly, making a comparison impossible. In the multi-user simulations, some UEs remained below the maximum rate threshold throughout the entire simulation period without any beam management events being scheduled because the estimated SINR stayed above this threshold. Conversely, in other cases, beam management events were scheduled even though the experienced SINR was well above the maximum rate threshold. In the single-user scenario, a comparison suggested that flexRLM has some advantages due to its ability to conduct faster handovers through monitored BPLs from candidate gNBs, but a decisive conclusion remains unclear.

To conclude, SU-MIMO can significantly improve throughput for UEs requesting data rates higher than those achievable with a single stream. Additionally, in a multi-user environment, SU-MIMO configurations can effectively balance throughput degradation from congested gNBs. This is achieved by increasing the maximum achievable data rate per gNB through the use of two streams simultaneously. A comparison between flexRLM and default 5G-NR RLM yields no conclusive results due to discrepancies between the estimated SINR, which is essential for beam management decisions, and the experienced SINR. To compare beam management strategies in future work, this discrepancy needs to be eliminated. Additionally, it would be interesting to implement a framework that incorporates MU-MIMO on top of SU-MIMO, allowing multiple users to be served within the same time slot. A comparison between MU-MIMO and SU-MIMO in a loaded multi-user environment would provide valuable insights into how the ability to reach multiple UEs with the streams affects overall network performance.

A

ABBREVIATIONS

3GPP 3rd Generation Partnership Project

SNR signal to noise ratio

SINR signal-to-interference-plus-noise ratio

IoT internet of things

UE user equipment

5G fifth generation of cellular networks

eMBB enhanced mobile broadband

URLLC ultra-reliable and low latency communications

mMTC massive machine type communication

ITU International Telecommunication Union

SU-MIMO single-user multiple input, multiple output

MU-MIMO multi-user multiple input, multiple output

V2X vehicle-to-everything

FR2 frequency range 2

FR1 frequency range 1

TDMA time division multiple-access

FDMA frequency division multiple-access

SM spatial multiplexing

SDMA spatial division multiple-access

MIMO multiple input multiple output

DAC digital-to-analog converter

ADC analog-to-digital converter

RF radio frequency

OFDMA orthogonal frequency division multiple-access

OFDM orthogonal frequency division multiplexing

SSB synchronization signal block

PSS primary synchronization signal

SSS secondary synchronization signal

PBCH physical broadcast channel

DMRS demodulation reference signal

SS burst synchronization signal burst

CSI-RS channel state information - reference signal

CSI channel state information

CQI channel quality information

BPL beam pair link

SRS sound reference signal

LTE Long Term Evolution

NSA non-standalone

SA standalone

UL uplink

DL downlink

SA-DL standalone-downlink

NSA-DL non-standalone-downlink

NSA-UL non-standalone-uplink

RACH random access channel

RA random access

RAN radio access network

RLF radio link failure

WLAN wireless local area network

NYU New York University

CTTC Centre Tecnologic de Telecommunicacions de Catalunya

PHY physical layer

MAC media access control

SAP service access point

LOS line of sight

NLOS non line of sight

SGW service gateway

CP cyclic prefix

SCS sub-carrier spacing

RB resource block

RLC radio link control

API application programming interface

BSR buffer status report

TTI Transmission Time Interval

DCI downlink control information

RBG resource block group

BWP band width part

UPA uniform planar array

AoA angle of arrival

AoD angle of departure

PSD power spectral density

PMI precoding matrix indicator

RI rank indicator

SISO single input single output

RNTI radio network temporary identifier

MMSE-IRC minimum mean-squared error interference rejection combining

MSE mean square error

TB transport block

SVD singular value decomposition

RLM radio link monitoring

BFV beamforming vector

RSRP reference signal receive power

IMSI international mobile subscriber identity

RRC radio resource control

UMa urban macrocell

UMi urban microcell

V2V vehicle-to-vehicle

UDP user datagram protocol

CBR constant bit rate

EPC evolved packet core

MCS modulation and coding scheme

IA initial access

IQR interquartile range

LIST OF FIGURES

List of Tables

BIBLIOGRAPHY

[1] M. Series, "Minimum requirements related to technical performance for IMT-2020 radio interface (s)," *Report*, vol. 2410, pp. 2410–2017, 2017.

[2] N. Patriciello, S. Lagen, B. Bojovic, and L. Giupponi, "An E2E simulator for 5G NR networks," *Simulation Modelling Practice and Theory*, vol. 96, p. 101933, 2019.

[3] F. Tariq, M. R. A. Khandaker, K.-K. Wong, M. A. Imran, M. Bennis, and M. Debbah, "A Speculative Study on 6G," *IEEE Wireless Communications*, vol. 27, no. 4, pp. 118–125, 2020.

[4] M. Shafi, A. F. Molisch, P. J. Smith, T. Haustein, P. Zhu, P. De Silva, F. Tufvesson, A. Benjebbour, and G. Wunder, "5G: A tutorial overview of standards, trials, challenges, deployment, and practice," *IEEE journal on selected areas in communications*, vol. 35, no. 6, pp. 1201–1221, 2017.

[5] M. Boban, A. Kousaridas, K. Manolakis, J. Eichinger, and W. Xu, "Connected roads of the future: Use cases, requirements, and design considerations for vehicle-to-everything communications," *IEEE vehicular technology magazine*, vol. 13, no. 3, pp. 110–123, 2018.

[6] M. Xiao, S. Mumtaz, Y. Huang, L. Dai, Y. Li, M. Matthaiou, G. K. Karagiannidis, E. Björnson, K. Yang, I. Chih-Lin *et al.*, "Millimeter wave communications for future mobile networks," *IEEE Journal on Selected Areas in Communications*, vol. 35, no. 9, pp. 1909–1935, 2017.

[7] 3GPP, "NR; User Equipment (UE) radio transmission and reception; Part 1: Range 1 Standalone," 3rd Generation Partnership Project (3GPP), Technical Specification (TS) 38.101-1, 04 2024, version 18.5.0. [Online]. Available: https://portal.3gpp.org/desktopmodules/Specifications/SpecificationDetails.aspx?specificationId=3283

[8] H. T. Friis, "A note on a simple transmission formula," *Proceedings of the IRE*, vol. 34, no. 5, pp. 254–256, 1946.

[9] T. S. Rappaport, *Wireless Communications: Principles and Practice*. Prentice Hall, 2002, ch. 4, pp. 107–110.

[10] P. Nagaraj, "Impact of atmospheric impairments on mmwave based outdoor communication," *arXiv preprint arXiv:1806.05176*, 2018.

[11] J. Wells, "Faster than fiber: The future of multi-G/s wireless," *IEEE Microwave Magazine*, vol. 10, no. 3, pp. 104–112, 2009.

[12] J. Navarro-Ortiz, P. Romero-Diaz, S. Sendra, P. Ameigeiras, J. J. Ramos-Munoz, and J. M. Lopez-Soler, "A survey on 5G usage scenarios and traffic models," *IEEE Communications Surveys & Tutorials*, vol. 22, no. 2, pp. 905–929, 2020.

[13] S. Singh, F. Ziliotto, U. Madhow, E. Belding, and M. Rodwell, "Blockage and directivity in 60 GHz wireless personal area networks: From cross-layer model to multihop MAC design," *IEEE Journal on Selected Areas in Communications*, vol. 27, no. 8, pp. 1400–1413, 2009.

[14] M. Heino, C. Icheln, and K. Haneda, "Self-user shadowing effects of millimeter-wave mobile phone antennas in a browsing mode," in *2019 13th European Conference on Antennas and Propagation (EuCAP)*. IEEE, 2019, pp. 1–5.

[15] T. S. Rappaport, S. Sun, R. Mayzus, H. Zhao, Y. Azar, K. Wang, G. N. Wong, J. K. Schulz, M. Samimi, and F. Gutierrez, "Millimeter wave mobile communications for 5G cellular: It will work!" *IEEE access*, vol. 1, pp. 335–349, 2013.

[16] W. Roh, J.-Y. Seol, J. Park, B. Lee, J. Lee, Y. Kim, J. Cho, K. Cheun, and F. Aryanfar, "Millimeter-wave beamforming as an enabling technology for 5G cellular communications: Theoretical feasibility and prototype results," *IEEE communications magazine*, vol. 52, no. 2, pp. 106–113, 2014.

[17] S. Kutty and D. Sen, "Beamforming for millimeter wave communications: An inclusive survey," *IEEE communications surveys & tutorials*, vol. 18, no. 2, pp. 949–973, 2015.

[18] F. W. Vook, A. Ghosh, and T. A. Thomas, "MIMO and beamforming solutions for 5G technology. In 2014 IEEE MTT-S International Microwave Symposium (IMS2014)," 2014.

[19] E. Dahlman, S. Parkvall, and J. Skold, *4G, LTE-advanced Pro and the Road to 5G*. Academic Press, 2016.

[20] S. Sun, T. S. Rappaport, R. W. Heath, A. Nix, and S. Rangan, "MIMO for millimeter-wave wireless communications: Beamforming, spatial multiplexing, or both?" *IEEE Communications Magazine*, vol. 52, no. 12, pp. 110–121, 2014.

[21] M. Giordani, M. Mezzavilla, and M. Zorzi, "Initial access in 5G mmWave cellular networks," *IEEE communications Magazine*, vol. 54, no. 11, pp. 40–47, 2016.

[22] M. Giordani and M. Zorzi, "Improved user tracking in 5G millimeter wave mobile networks via refinement operations," in *2017 16th Annual Mediterranean Ad Hoc Networking Workshop (Med-Hoc-Net)*. IEEE, 2017, pp. 1–8.

[23] M. Giordani, M. Polese, A. Roy, D. Castor, and M. Zorzi, "A tutorial on beam management for 3GPP NR at mmWave frequencies," *IEEE Communications Surveys & Tutorials*, vol. 21, no. 1, pp. 173–196, 2018.

[24] A. Ichkov, O. Atasoy, P. Mähönen, and L. Simić, "Full-stack ns-3 framework for the evaluation of 5G-NR beam management in non-standalone downlink millimeter-wave networks," in *2022 IEEE 23rd International Symposium on a World of Wireless, Mobile and Multimedia Networks (WoWMoM)*. IEEE, 2022, pp. 40–49.

[25] 3GPP, "NR; Physical channels and modulation," 3rd Generation Partnership Project (3GPP), Technical Specification (TS) 38.211, 03 2024, version 18.2.0. [Online]. Available: https://portal.3gpp.org/desktopmodules/Specifications/SpecificationDetails.aspx?specificationId=3213

[26] A. Omri, M. Shaqfeh, A. Ali, and H. Alnuweiri, "Synchronization procedure in 5G NR systems," *IEEE Access*, vol. 7, pp. 41 286–41 295, 2019.

[27] 3GPP, "NR; Radio Resource Control (RRC); Protocol specification," 3rd Generation Partnership Project (3GPP), Technical Specification (TS) 38.331, 04 2024, version 18.1.0. [Online]. Available: https://portal.3gpp.org/desktopmodules/Specifications/SpecificationDetails.aspx?specificationId=3197

[28] M. Giordani, M. Polese, A. Roy, D. Castor, and M. Zorzi, "Standalone and non-standalone beam management for 3GPP NR at mmWaves," *IEEE Communications Magazine*, vol. 57, no. 4, pp. 123–129, 2019.

[29] 3GPP, "Study on New Radio (NR) access technology," 3rd Generation Partnership Project (3GPP), Technical report (TR) 38.912, 04 2024, version 18.0.0. [Online]. Available: https://portal.3gpp.org/desktopmodules/Specifications/SpecificationDetails.aspx?specificationId=3059

[30] M. Giordani, M. Mezzavilla, S. Rangan, and M. Zorzi, "Multi-connectivity in 5G mmWave cellular networks," in *2016 Mediterranean Ad Hoc Networking Workshop (Med-Hoc-Net)*. IEEE, 2016, pp. 1–7.

[31] ——, "An efficient uplink multi-connectivity scheme for 5G millimeter-wave control plane applications," *IEEE Transactions on Wireless Communications*, vol. 17, no. 10, pp. 6806–6821, 2018.

[32] R. L. Patel, M. J. Pathak, and A. J. Nayak, "Survey on network simulators," *International Journal of Computer Applications*, vol. 182, no. 21, pp. 23–30, 2018.

[33] M. Mezzavilla, M. Zhang, M. Polese, R. Ford, S. Dutta, S. Rangan, and M. Zorzi, "End-to-end simulation of 5G mmWave networks," *IEEE Communications Surveys & Tutorials*, vol. 20, no. 3, pp. 2237–2263, 2018.

[34] G. Piro, N. Baldo, and M. Miozzo, "An LTE module for the ns-3 network simulator." in *SimuTools*, 2011, pp. 415–422.

[35] 3GPP, "NR; NR and NG-RAN Overall description; Stage-2," 3rd Generation Partnership Project (3GPP), Technical Specification (TS) 38.300, 09 2018, version 15.3.0. [Online]. Available: https://portal.3gpp.org/desktopmodules/Specifications/SpecificationDetails.aspx?specificationId=3191

[36] ——, "Study on channel model for frequency spectrum above 6 GHz," 3rd Generation Partnership Project (3GPP), Technical Report (TR) 38.900, 06 2018, version 15.0.0. [Online]. Available: https://portal.3gpp.org/desktopmodules/Specifications/SpecificationDetails.aspx?specificationId=2991

[37] N. Patriciello, S. Lagen, L. Giupponi, and B. Bojovic, "5G new radio numerologies and their impact on the end-to-end latency," in *2018 IEEE 23rd international workshop on computer aided modeling and design of communication links and networks (CAMAD)*. IEEE, 2018, pp. 1–6.

[38] P. J. Mateo, C. Fiandrino, and J. Widmer, "Analysis of TCP performance in 5G mm-wave mobile networks," in *ICC 2019-2019 IEEE International Conference on Communications (ICC)*. IEEE, 2019, pp. 1–7.

[39] M. Polese, M. Mezzavilla, S. Rangan, and M. Zorzi, "Mobility management for TCP in mmWave networks," in *Proceedings of the 1st ACM Workshop on Millimeter-Wave Networks and Sensing Systems 2017*, 2017, pp. 11–16.

[40] C. Herranz, M. Zhang, M. Mezzavilla, D. Martin-Sacristán, S. Rangan, and J. F. Monserrat, "A 3GPP NR compliant beam management framework to simulate end-to-end mmWave networks," in *Proceedings of the 21st ACM International Conference on Modeling, Analysis and Simulation of Wireless and Mobile Systems*, 2018, pp. 119–125.

[41] A. Ichkov, A. Schott, P. Mähönen, and L. Simić, "flexRLM: Flexible Radio Link Monitoring for Multi-User Downlink Millimeter-Wave Networks," in *IEEE INFOCOM 2023-IEEE Conference on Computer Communications*. IEEE, 2023, pp. 1–10.

[42] Q. Xue, X. Fang, and C.-X. Wang, "Beamspace SU-MIMO for future millimeter wave wireless communications," *IEEE Journal on Selected Areas in Communications*, vol. 35, no. 7, pp. 1564–1575, 2017.

[43] F. Gómez-Cuba, T. Zugno, J. Kim, M. Polese, S. Bahk, and M. Zorzi, "Hybrid beamforming in 5G mmWave networks: A full-stack perspective," *IEEE Transactions on Wireless Communications*, vol. 21, no. 2, pp. 1288–1303, 2021.

[44] H. Assasa, N. Grosheva, T. Ropitault, S. Blandino, N. Golmie, and J. Widmer, "Implementation and evaluation of a WLAN IEEE 802.11 ay model in network simulator ns-3," in *Proceedings of the 2021 Workshop on ns-3*, 2021, pp. 9–16.

[45] H. Assasa, J. Widmer, J. Wang, T. Ropitault, and N. Golmie, "An Implementation Proposal for IEEE 802.11 ay SU/MU-MIMO Communication in ns-3," in *Proceedings of the 2019 Workshop on Next-Generation Wireless with ns-3*, 2019, pp. 26–29.

[46] B. Bojovic, Z. Ali, and S. Lagen, "Ns-3 and 5G-LENA extensions to support dual-polarized MIMO," in *Proceedings of the 2022 Workshop on ns-3*, 2022, pp. 1–9.

[47] B. Bojovic and S. Lagén, "MIMO in network simulators: Design, implementation and evaluation of single-user MIMO in ns-3 5G-LENA," *arXiv preprint arXiv:2404.17472*, 2024.

[48] G. Guennebaud, B. Jacob *et al.*, "Eigen v3," http://eigen.tuxfamily.org, 2010.

[49] 3GPP, "Study on channel model for frequencies from 0.5 to 100 GHz," 3rd Generation Partnership Project (3GPP), Technical report (TR) 38.901, 04 2024, version 18.0.0. [Online]. Available: https://portal.3gpp.org/desktopmodules/Specifications/SpecificationDetails.aspx?specificationId=3173

Zentrales Prüfungsamt/Central Examination Office

Eidesstattliche Versicherung
Statutory Declaration in Lieu of an Oath

___________________________ ___________________________

Name, Vorname/Last Name, First Name

Matrikelnummer (freiwillige Angabe)
Matriculation No. (optional)

Ich versichere hiermit an Eides Statt, dass ich die vorliegende Arbeit/Bachelorarbeit/ Masterarbeit* mit dem Titel

I hereby declare in lieu of an oath that I have completed the present paper/Bachelor thesis/Master thesis* entitled

____

____

____

selbstständig und ohne unzulässige fremde Hilfe (insbes. akademisches Ghostwriting) erbracht habe. Ich habe keine anderen als die angegebenen Quellen und Hilfsmittel benutzt. Für den Fall, dass die Arbeit zusätzlich auf einem Datenträger eingereicht wird, erkläre ich, dass die schriftliche und die elektronische Form vollständig übereinstimmen. Die Arbeit hat in gleicher oder ähnlicher Form noch keiner Prüfungsbehörde vorgelegen.

independently and without illegitimate assistance from third parties (such as academic ghostwriters). I have used no other than the specified sources and aids. In case that the thesis is additionally submitted in an electronic format, I declare that the written and electronic versions are fully identical. The thesis has not been submitted to any examination body in this, or similar, form.

___________________________ ___________________________

Ort, Datum/City, Date

Unterschrift/Signature

*Nichtzutreffendes bitte streichen

*Please delete as appropriate

Belehrung:
Official Notification:

§ 156 StGB: Falsche Versicherung an Eides Statt

Wer vor einer zur Abnahme einer Versicherung an Eides Statt zuständigen Behörde eine solche Versicherung falsch abgibt oder unter Berufung auf eine solche Versicherung falsch aussagt, wird mit Freiheitsstrafe bis zu drei Jahren oder mit Geldstrafe bestraft.

Para. 156 StGB (German Criminal Code): False Statutory Declarations

Whoever before a public authority competent to administer statutory declarations falsely makes such a declaration or falsely testifies while referring to such a declaration shall be liable to imprisonment not exceeding three years or a fine.

§ 161 StGB: Fahrlässiger Falscheid; fahrlässige falsche Versicherung an Eides Statt

(1) Wenn eine der in den §§ 154 bis 156 bezeichneten Handlungen aus Fahrlässigkeit begangen worden ist, so tritt Freiheitsstrafe bis zu einem Jahr oder Geldstrafe ein.

(2) Straflosigkeit tritt ein, wenn der Täter die falsche Angabe rechtzeitig berichtigt. Die Vorschriften des § 158 Abs. 2 und 3 gelten entsprechend.

Para. 161 StGB (German Criminal Code): False Statutory Declarations Due to Negligence

(1) If a person commits one of the offences listed in sections 154 through 156 negligently the penalty shall be imprisonment not exceeding one year or a fine.

(2) The offender shall be exempt from liability if he or she corrects their false testimony in time. The provisions of section 158 (2) and (3) shall apply accordingly.

Die vorstehende Belehrung habe ich zur Kenntnis genommen:
I have read and understood the above official notification:

___________________________ ___________________________

Ort, Datum/City, Date

Unterschrift/Signature